DISS. ETH NO. 26057

THE DEVELOPMENT OF ALVEOLAR AND IRON-RECYCLING MACROPHAGES

A thesis submitted to attain the degree of

DOCTOR OF SCIENCES of ETH ZURICH

(Dr. sc. ETH Zurich)

presented by

KATARZYNA MARIA OKRĘGLICKA

M.Sc., Jagiellonian University in Kraków

born on 05.04.1989

citizen of Poland

accepted on the recommendation of

Prof. Dr. Manfred Kopf; examiner

Prof. Dr. Florent Ginhoux; co-examiner

Prof. Dr. Gerald Schwank; co-examiner

2019

1 Table of Contents

2 Summary

Tissue resident macrophages are cells of the immune system which develop from fetal progenitors and are able to self-renew in adulthood with minimal contribution of monocytes. They are distributed throughout the body in order to provide immediate response to invading pathogens or danger. In addition, they perform important tissue-specific functions sustaining homeostasis. Tissue-specific development of macrophage subsets and their functions are determined by transcriptional programs that are induced locally by environmental cues. Recently, a few cytokines and metabolites produced specifically in certain tissues and the transcription factors induced in macrophages have been identified.

The transcription factors PPARγ and Spi-C have been identified as main drivers of alveolar macrophage (AM) and red pulp macrophage (RPM) development, respectively. GM-CSF produced by alveolar epithelial cells induces PPARγ in fetal lung monocytes, which drives development and function of AM by activation of many downstream target genes. Most of them are related to lipid metabolism and allow effective surfactant clearance, necessary for proper function of the lung. RPM are responsible for scavenging senescent red blood cells (RBCs) and iron-recycling. Heme, an intermediate product of hemoglobin degradation, indirectly activates Spi-C and animals lacking this transcription factor display strikingly decreased numbers of RPM and VCAM1$_+$ bone marrow erythroid island macrophages (BMEIM). Similarly, characterization of macrophages in various tissues of conditional knockouts lacking *Pparg* in the hematopoietic cells revealed a requirement of *Pparg* for development of RPM and BMEIM, in addition to AM. Interestingly, while absence of *Pparg* abrogated RPM development already in neonates, analysis of *Spic*$_{-/-}$ mice revealed that RPM were lacking in adults but not in neonates. Nonetheless, RPM present in neonatal *Spic*$_{-/-}$ mice differed significantly from the wild-type (WT) controls at the transcriptome level. Expression of many genes related to iron metabolism was decreased, indicating that Spi-C controls RPM function but not development in neonates. Moreover, PPARγ protein and mRNA expression were reduced in *Spic*-deficient RPM. Comparison of RPM transcriptomes from *Vav1-Cre/Pparg*$_{fl/fl}$ and WT mice provided insights on genes regulated by PPARγ during RPM development. Despite strongly reduced numbers, remaining RPM from *Vav1-Cre/Pparg*$_{fl/fl}$ mice were able to phagocytose RBCs and had only slightly reduced expression of genes related to

iron metabolism. A small fraction of genes known as PPARγ targets were down, while genes involved in migration and chemotaxis were up. Our study provided an evidence for a new role of PPARγ during cell development, not connected to well-studied metabolic processes but rather to cell mobility and positioning of the progenitor in an environment supposedly providing survival and further signals allowing final differentiation steps.

Previous studies addressing tissue resident macrophage development and function relied on generation of M-CSF-derived bone marrow macrophages. However, considering the enormous heterogeneity of tissue resident macrophages, it is unclear how well these *in vitro*-generated cells recapitulate function and phenotype of *bona fide* tissue macrophages. More recent studies provided evidence of effective AM differentiation from bone marrow derived macrophages (BMM) or induced pluripotent stem cell-derived macrophages (iMac) upon transfer to AM-deficient mice (i.e. *Csf2ra*$^{-/-}$ mice). Nonetheless, besides tissue-specific programming, the crucial influence of macrophage origin must be considered in order to produce the most relevant model for each tissue resident subset. We have established a protocol for efficient reconstitution of AM development in AM-deficient neonates by intranasal transfer of fetal monocytes. Specifically, we have isolated fetal liver or lung monocytes, the true AM progenitors, and optimized culture conditions allowing expansion and maintenance *in vitro* for several weeks. We noticed that cells expanded nicely in medium supplemented with GM-CSF and acquired AM-like phenotype within two weeks of culturing. After initial expansion, cells stopped proliferating but could be cultured for several months and maintained the capacity to reconstitute AM development upon transfer to AM-deficient recipients. The fetal monocyte-derived AM were able to prevent development of alveolar proteinosis and self-renew for at least one year after transfer. Moreover, cells could be transduced with retroviral vectors becoming a desired model to study AM function and development. Unfortunately, we have failed to establish CRISPR/Cas9-based gene editing in these cells. However, using another approach consisting of overexpression of HoxB4 in bone marrow cells (BMCs), we succeeded to establish long-lived and highly proliferative cells that have the capacity to differentiate to AM upon transfer to AM-deficient mice. Transient overexpression of Cas9 with guide RNA targeting GM-CSF receptor in HoxB4^{+} BMCs prevented the cell differentiation to AM following transfer, as expected. This proof of concept experiment assured us that this approach offers a good basis for a gene-screening platform identifying new genes involved in AM development and function.

Together, this study provides novel insight into RPM development and identifies new function of PPARγ involving migration and cell retention rather than lipid metabolism. Moreover, it describes novel *in vitro* models for gene manipulation and editing in fetal monocytes and BMC-derived progenitors, which will allow future high-throughput screening for genes involved in AM differentiation and function.

3 Zusammenfassung

Gewebe-residente Makrophagen sind Zellen des Immunsystems, die sich aus fötalen Vorläufern entwickeln und sich im Erwachsenenalter mit minimalem Beitrag an Monozyten selbst erneuern können. Sie sind im ganzen Körper verteilt, um sofort auf eindringende Krankheitserreger oder Gefahren reagieren zu können. Darüber hinaus erfüllen sie wichtige gewebespezifische Funktionen, die die Homöostase aufrechterhalten. Die gewebespezifische Entwicklung von spezifischen Makrophagen und ihre Funktionen werden durch Transkriptionsprogramme bestimmt, die lokal durch Umwelteinflüsse induziert werden. Kürzlich konnten einige Cytokine und Metaboliten, die spezifisch in bestimmten Geweben produziert werden, sowie Transkriptionsfaktoren, die Makrophagen induzierten, identifiziert werden.

Die Transkriptionsfaktoren PPARγ und Spi-C wurden als Haupttreiber für die Entwicklung von Alveolarmakrophagen (AM) bzw. die Makrophagen der roten Pulpa (RPM) identifiziert. GM-CSF, das von alveolären Epithelzellen produziert wird, induziert PPARγ in fötalen Lungenmonozyten, was die Entwicklung und Funktion von AM durch Aktivierung vieler nachgeschalteter Zielgene antreibt. Die meisten von ihnen stehen im Zusammenhang mit dem Fettstoffwechsel und ermöglichen eine wirksame Surfactant-Beseitigung, die für die ordnungsgemäße Funktion der Lunge erforderlich ist. RPM sind für das Abfangen alternder roter Blutkörperchen und das Eisenrecycling verantwortlich. Häm, ein Zwischenprodukt des Hämoglobinabbaus, aktiviert indirekt Spi-C, und Tiere, denen dieser Transkriptionsfaktor fehlt, zeigen eine auffallend reduzierte Zahl an RPM sowie eine reduzierte Zahl an einer Untergruppe von VCAM1+ Knochenmark-Erythroiden-Makrophagen (BMEIM). In ähnlicher Weise zeigte die Charakterisierung von Makrophagen in verschiedenen Geweben des bedingten Gen-Knockouts, denen *Pparg* in den hämatopoetischen Zellen fehlt, einen Bedarf an *Pparg* für die Entwicklung von RPM und BMEIM zusätzlich zu AM. Während das Fehlen von *Pparg* die RPM-Entwicklung bereits bei Neugeborenen verhindert, ergab die Analyse von *Spic*$^{-/-}$ Mäusen interessanterweise, dass RPM bei Erwachsenen fehlten, nicht jedoch bei Neugeborenen. Nichtsdestotrotz unterschieden sich die in neonatalen *Spic*$^{-/-}$ Mäusen vorhandenen RPM signifikant von den Wildtyp-Kontrollen auf Transkriptomebene. Die Expression vieler Gene, die mit dem Eisenstoffwechsel zusammenhängen, war verringert, was darauf hinweist, dass Spi-C die RPM-Funktion steuert, nicht aber deren Entwicklung in

Neugeborenen. Darüber hinaus waren die Expression von PPARγ-Protein und mRNA in RPM mit Spi-C Mangel reduziert. Ein Vergleich von RPM-Transkriptomen aus *Vav1-Cre/Pparg$^{fl/fl}$* und Wildtyp-Mäusen lieferte Einblicke in Gene, die während der RPM-Entwicklung durch PPARγ reguliert wurden. Trotz stark reduzierter Zahlen konnten die verbleibenden RPM von *Vav1-Cre/Pparg$^{fl/fl}$* -Mäusen rote Blutzellen phagozytieren und hatte nur eine geringfügig reduzierte Expression von Genen, die mit dem Eisenstoffwechsel zusammenhängen. Ein kleiner Teil von Genen, die als PPARγ-Ziele bekannt sind waren reduziert, während Gene, die an Migration und Chemotaxis beteiligt sind, erhöht waren. Unsere Forschung lieferte einen Beweis für eine neue Rolle von PPARγ während der Zellentwicklung, die nicht mit gut untersuchten Stoffwechselprozessen zusammenhängt, sondern eher mit Zellmobilität und der Positionierung der Vorläuferzellen in einer Umgebung, die angeblich Überleben- und weitere Signale bietet, die abschließende Differenzierungsschritte ermöglichen.

Frühere Studien, die sich mit der Entwicklung und Funktion von residenten Makrophagen beschäftigten, stützten sich auf die Generierung von mit M-CSF generierten Knochenmarkmakrophagen. Angesichts der enormen Heterogenität von gewebe-spezifischen Makrophagen ist es jedoch unklar, wie gut diese *in vitro* erzeugten Zellen die Funktion und den Phänotyp von bona-fiden Gewebemakrophagen widerspiegeln. Neuere Studien lieferten den Nachweis einer wirksamen AM-Differenzierung von aus Knochenmark stammenden Makrophagen (BMM) oder induzierten aus pluripotenten Stammzellen stammenden Makrophagen (iMac) bei der Übertragung auf AM-defiziente Mäuse (d. h. Csf2ra$^{-/-}$ Mäuse). Abgesehen von der gewebespezifischen Programmierung muss jedoch der entscheidende Einfluss des Makrophagenursprungs berücksichtigt werden, um das relevanteste Modell für jede gewebespezifische Population zu erstellen. Wir haben ein Protokoll für die effiziente Rekonstitution der AM-Entwicklung bei dem AM-defizienten Neugeborenen, durch intranasalen Transfer fötaler Monozyten, entwickelt. Insbesondere haben wir fötale Leber- oder Lungenmonozyten isoliert, die echten AM-Vorläufer, sowie Kulturbedingungen optimiert, die eine Expansion und Erhaltung *in vitro* für mehrere Wochen ermöglichen. Wir haben festgestellt, dass sich die Zellen in mit GM-CSF angereichertem Medium gut ausdehnten und innerhalb von zwei Wochen nach der Kultivierung einen AM-ähnlichen Phänotyp erlangten. Nach der anfänglichen Expansion hörten die Zellen auf zu proliferieren, konnten jedoch für mehrere Monate kultiviert werden und behielten die Fähigkeit bei, die AM-Entwicklung

nach der Übertragung an AM-defiziente Empfänger wiederherzustellen. Die aus fötalen Monozyten abstammenden AM konnten die Entwicklung einer Alveolarproteinose verhindern und sich mindestens ein Jahr nach der Übertragung selbst erneuern. Darüber hinaus konnten Zellen mit retroviralen Vektoren transduziert werden, um sie zu einem gewünschten Modell für die Untersuchung der AM-Funktion und Entwicklung werden zu lassen. Leider konnten wir keine CRISPR/Cas9-basierte Genbearbeitung in diesen Zellen etablieren. Mit einem anderen Ansatz, der aus der Überexpression von HoxB4 in Knochenmarkzellen (BMCs) besteht, gelang es jedoch, langlebige und stark proliferative Zellen zu etablieren, die bei der Übertragung in AM-defiziente Mäuse die Fähigkeit haben, sich zu AM zu differenzieren. Eine vorübergehende Überexpression von Cas9 mit Führungs-RNA, die auf den GM-CSF-Rezeptor in HoxB4+ BMCs abzielt, verhinderte wie erwartet die Fähigkeit zur Differenzierung zu AM nach der Übertragung. Dieses Proof-of-Concept-Experiment hat uns versichert, dass dieser Ansatz eine gute Grundlage für eine Gen-Screening-Plattform bietet, die neue Gene identifiziert, die an der AM-Entwicklung und -Funktion beteiligt sind.

Zusammenfassend bietet diese Studie neue Einblicke in die RPM-Entwicklung und identifiziert neue Funktionen von PPARγ, die Migration und Zellretention anstelle des Lipidmetabolismus einschließen. Darüber hinaus werden neue *In-vitro*-Modelle für die Genmanipulation und -bearbeitung in fötalen Monozyten und von BMC abgeleiteten Vorläufern beschrieben, die zukünftig High-throughput Screenings für Gene, die an der AM-Differenzierung und -Funktion beteiligt sind, ermöglichen.

4 Introduction

4.1 Immune system

Throughout life, our body is exposed to potential invaders. This constant threat of infection led to development of resistance mechanisms, found in most living creatures. Prokaryotes protect themselves from phages by innate response based on diversity-generating retroelements and phase variation mechanisms. They are also capable to integrate short DNA fragments of infectious agent in order to use it as a guide sequence allowing them to target and degrade foreign genomic elements in case of recurrent attack. This bacterial adaptive mechanism has been extensively used nowadays in gene editing [1, 2]. The immune system of animals on the other hand, is an interactive network of specialized cells, molecules, and lymphoid organs. Its two main fundamentally different components can be distinguished by the speed and precision of the reaction. The rapid and nonspecific innate response is the first part and more abundant form of the immunity, whereas highly selective but slower to develop adaptive immune response constitutes the second line of defense and is confined to vertebrae. The innate immunity relies mainly on phagocytic cells which can recognize conserved features of pathogens and provide immediate response [3-5]. Acquired immune response is involved in elimination of pathogens in later stages of infection and characterizes with memory, which enables the host to mount more vigorous response against the pathogen upon subsequent exposure. It relies on antigen-specific B and T lymphocytes which are activated within lymphoid organs upon binding on their surface an antigen. Their receptors are encoded by sets of gene segments, which are rearranged and assembled during development in order to create a vast repertoire of receptor specificities able to efficiently discriminate any non-self from self-proteins [6]. Even though these two parts of immune response are very distinct, they collaborate in effective response. Innate effector cells can be recruited by antigen-specific lymphocytes in order to enhance the defense, whereas activation of the aforementioned cells is mediated by so called antigen-presenting cells (APCs), inherent part of the innate immune system.

4.2 Innate immunity

In order to establish an infection, attacking microbes must cross surface barriers generated by epithelial cells that produce anti-microbial peptides and are covered with a layer of carbohydrate-rich mucus that prevents their attachment. If the pathogen manages to pass such barrier, the defense mediated by innate and adaptive immune cells kicks in. They get activated and unite their efforts in defeating the intruder [5]. The innate immune response is mounted within hours post-invasion and relies on macrophages, dendritic cells (DCs), mast cells, neutrophils, eosinophils and natural killer (NK) cells. Additionally, innate immunity is equipped with extracellular soluble proteins, such as complement proteins, lipopolysaccharide (LPS)-binding protein, C-reactive protein, collectins, and pentraxins, augmenting the response [7]. Unlike receptors of antigen-specific lymphocytes, the innate immune recognition is hardwired with genetically predetermined germline-encoded receptors that recognize highly conserved molecular structures expressed by various microbes. These structures, so called pathogen-associated molecular patterns (PAMPs), are crucial for microbial virulence or survival and therefore less prone to mutation. Pattern-recognition receptors (PRRs) are constitutively expressed mainly by myeloid cells allowing them to sense danger in form of PAMPs and to switch on effector defense pathways without the need to proliferate prior to action [8, 9]. Another strategy of the immune system to detect danger is recognition of damage-associated molecular patterns (DAMPs) that may be released by stressed or dying cells. Also, 'missing-self' signal, when commonly expressed surface marker is absent on infected cell or microbe, can induce a response [10]. Host cells express major histocompatibility complex (MHC) class I, which engages inhibitory receptors on NK cells. When the levels of MHCI are lowered or missing, the net balance of inhibitory and stimulatory signals tips the balance towards activation of NK cell and subsequent killing of targeted cell [11].

Immune cells constantly scan the body to detect danger in form of tissue damage and to ward off invaders. Every organ is equipped with subsets of resident macrophages that are adapted to the tissue-specific environment and participate in homeostasis in addition to first line defense. They phagocytose not only invading microbes but also cell debris during inflammation and infection in order to reinstate the equilibrium and accelerate

healing. Tissue resident macrophages are the main focus of this thesis and will be discussed more thoroughly in next paragraphs.

4.3 Tissue resident macrophages

Phagocytic mononuclear cells have been first observed in the late 19th century by Elie Metchnikoff, who coined the term macrophages and macrophage system [12]. Studies showing heterogeneity among phagocytic mononuclear cells, Aschoff and Volterra later proposed the term reticulo-endothelial system and reticulo-histiocyte system, respectively [13, 14]. In the late sixties of the last century, a group of researchers around van Furth proposed the mononuclear phagocyte system (MPS), as a new classification for macrophages, monocytes, and their precursors, basically suggesting that phagocytic tissue macrophage differentiate from circulating blood monocytes which originate from committed bone marrow precursors [15]. Again, this classification was put into question when new studies identified macrophages in the yolk sac much before the onset of primitive hematopoiesis as well as their capability to self-renew [16-18]. Fate-mapping studies allowed to trace embryonic progenitors and proved that they give rise to most of tissue resident macrophages which are able to persist into adulthood during homeostasis [19, 20].

Macrophages have a central role in innate and adaptive immunity due to their extreme versatility. They fulfil all the requirements for an antigen-presenting cell (APC). They are able to efficiently engulf soluble and particulate antigens, process and present them to T cells. Moreover, macrophages produce tremendous amounts of toxic metabolites and pro-inflammatory cytokines upon activation in order to kill microbes and tumor cells. They contribute to wound healing and tissue repair but most of all they patrol the host body in order to eliminate any cellular debris or apoptotic cells and support homeostasis [21]. These homeostatic clearance processes are performed without production of cell signaling mediators or cell activation [22]. Macrophages sense extraneous cellular material with use of multiple receptors like scavenger receptors (SR-A, CD36, AI, CD163, CD68), phosphatidyl serine receptors, the thrombospondin receptor, integrin (CR3) and complement receptors (huCRIg) [23]. However, cellular debris of necrotic cells are able to induce physiological changes and macrophage activation. This is due to endogenous DAMPs connected to necrosis, like heat-shock proteins, nuclear proteins, histones and DNA [24]. DAMPs are recognized by macrophages with set of Toll-

like receptors (TLRs) and intracellular PRRs and lead to production of cytokines and pro-inflammatory mediators in consequence alerting the system about danger. Similarly, macrophages, due to their distribution throughout the body, are extremely efficient in sensing invading pathogens. PRRs can be divided into TLRs, NOD-like receptors (NLRs), RIG-I-like receptors (RLRs), C-type lectin receptors (CLRs), AIM2-like receptors (ALRs), and intracellular DNA sensors such as cGAS [8, 25]. TLRs were first to be described and are composed of an ectodomain of leucine-rich repeats (LRRs) responsible for PAMPs recognition, a transmembrane domain, and a cytoplasmic Toll/IL-1 receptor (TIR) domain which initiates downstream signaling commonly through nuclear factor kappa-light-chain-enhancer of activated B cells (NF-κB), mitogen-activated protein kinase (MAPK) and type I interferons [26]. The family comprises of 12 members (in mouse) which localize to the cell membrane as well as to intracellular compartments (ER, endosome, lysosome, endolysosome). Additionally, RLRs, NLRs and ALRs are distributed in cytosol. Together, they recognize distinct or overlapping PAMPs such as bacterial cell wall components (peptidoglycan, LPS, flagellin, lipoproteins), fungal carbohydrates, virus-derived dsRNA and viral or bacterial ssRNA [27].

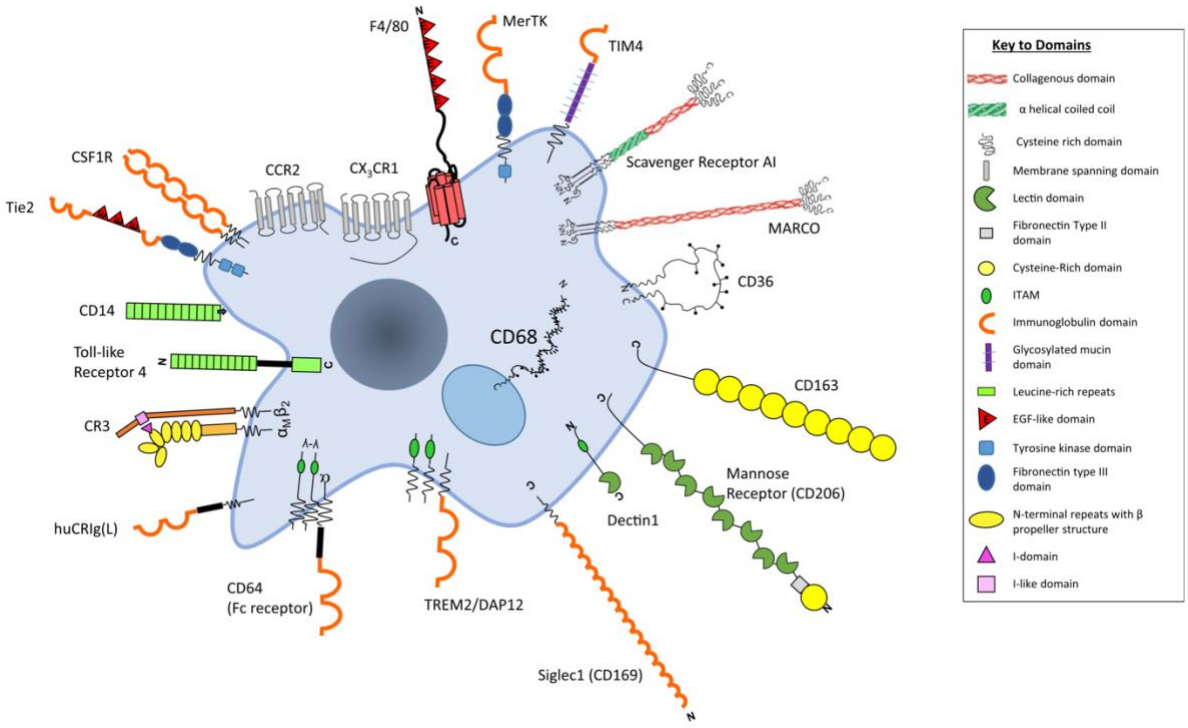

Figure 1. Membrane receptors mediating recognition of microbial and host-derived ligands commonly expressed by macrophages. Adapted from [28] .

Members of this large repertoire of membrane receptors have been illustrated in Figure 1. Many of them serve as useful markers for immunohistochemistry or flow cytometry (F4/80, CD64, MerTK, or CD68). Notably, besides commonly expressed receptors and mentioned responsibilities, macrophages handle tissue-imposed functions which lead to their unique specialization and explain population heterogeneity.

4.4 Development of tissue resident macrophages

Hematopoiesis describes the development of all types of blood cells during embryonic development and in adult life. The first wave of this process, called primitive hematopoiesis, starts during early gestation (E6.5-E8.5) and gives rise only to erythrocytes and macrophages [29]. These erythroid progenitors appear in blood islands in the extraembryonic yolk sac (YS) and have no renewal capacity explaining transient characteristics of the primitive wave. Subsequently, transient definitive hematopoiesis starts around E8.5 generating multipotent hematopoietic progenitors, called erythro-myeloid precursors (EMPs), which are able to give rise to erythroid and myeloid but not lymphoid lineages. EMPs derive from the YS hemogenic endothelium and after establishment of circulation (around E8.5), they migrate to fetal liver which becomes the primary site of hematopoiesis. Fetal definitive hematopoiesis starts in the aorta, gonads and mesonephros (AGM) regions at E10.5 by generation of fetal hematopoietic stem cells (HSCs) that migrate to the fetal liver and give rise to all types of mature cells during embryogenesis and perinatally [30-32]. After birth, adult HSCs are generated in the bone marrow (BM) and rise to common myeloid and lymphoid precursors (MP and LP, respectively). Successive commitment steps in common myeloid precursors then generate monocyte and DC precursors (MDP), from which common DC precursors (CDP) and monocytes derive [33]. More recent studies have identified common monocyte progenitor (cMOP) as MDP-derived monocyte-restricted precursor in the BM, which is no longer able to give rise to classical and plasmacytoid DCs (cDCs and pDCs, respectively) but differs from monocytes by lack of phagocytic activity [34]. Monocytes then leave the BM and upon inflammation can differentiate into monocyte-derived DCs (moDCs) [35]. For many years, monocytes were thought to constantly replenish tissue resident macrophage pools but this dogma has been challenged by identification of a potent self-renewal capacity of mature tissue resident macrophages.

Genetic fate-mapping studies, complemented with parabiotic and adoptive-transfer experiments, allowed to discern the relationship between circulating blood monocytes and macrophages. Induction of Cre in *Cx3cr1*^{Cre}*/R26-yfp* transgenic mice over 4 weeks, failed to provide evidence that tested macrophage populations (Kupffer cells, Langerhans cells, peritoneal, splenic or alveolar macrophages) could derive from monocytes [36]. Further evidence for limited if any requirement of monocytes in adult macrophage population maintenance comes with studies conducted on parabiotic mice. While lymphocytes and monocytes reached an equilibrium in the circulation of these mice, chimerism of tissue resident macrophages in the peritoneum, spleen and brain was very low, even after five months of parabiosis [37]. Taken together, these experiments provide strong evidence that tissue resident macrophages do not require monocytic contribution at steady-state. However, this is not true for every tissue. An important exception includes fetal monocyte-derived intestinal macrophages, which are short-lived and replenished by BM-derived Ly6C-positive monocytes [38-40] within the first week after birth, possibly due to constant exposure to the gut microbiota. Other examples are macrophages residing in the skin and heart, which are maintained partially by contribution of circulating monocytes [41, 42]. Also, adoptive transfers of WT monocytes to liver X receptor (*Lxra*)-deficient mice, which lack splenic marginal zone macrophages, provided evidence that this population could originate from circulating monocytes [43]. It seems that monocytes contribute minimally to homeostatic maintenance of macrophages unless there is an inflammatory incident or some other insults that result in loss of tissue macrophages and infiltration of blood monocytes that differentiate into macrophages [44]. It has been proposed that macrophage niche itself can control local macrophage development [45]. In that case, a sudden differentiation of monocytes to macrophages is driven by niche availability and accessibility as well as precursor plasticity. Temporary niche availability due to infection or injury leads to efficient engraftment of monocyte-derived macrophages, which share the expression profiles and ability to self-renew with their embryonic counterparts. Possibly, a mechanism preventing long-term self-maintenance, could explain a necessity of monocyte differentiation into macrophages in skin, heart, and intestine as the niche would be constitutively available. Interestingly, this niche model distinguishes steady-state from inflammatory niches giving possible explanation to reduced persistence of monocyte-derived macrophages. It has been shown previously that monocytes could engraft liver

after injection of aged erythrocytes and supported erythrocyte clearance, but they disappeared three months after insult coinciding with return of Kupffer cells [46]. Together, compelling evidence for non-monocytic origin of most tissue resident macrophages and their ability to self-renew induced further research in order to understand the true origin of these cells.

Fate-mapping method which utilizes the principle of genetic recombination and allows tracing labelled cells into adulthood was exploited extensively in recent years. Fate-mappers express Cre either constitutively or upon tamoxifen injection (CreERT2) and recombine a floxed STOP cassette upstream of a reporter gene and thereby driving its expression. Reporter genes, like yellow or green fluorescent proteins (YFP and GFP, respectively), are under control of constitutive promoter (like Rosa26) and permanently label cells and all their progenies as early as during embryonic development. First model used to trace embryonic contribution to adult tissue resident macrophages was based on inducible runt-related transcription factor 1 (*Runx1*^{CreER}), which is expressed in YS cells between E7.0 and E8.0 prior to the development of definitive hematopoiesis while definitive hematopoietic precursors start to express Runx1 around E8.5 [47]. Single tamoxifen injection into pregnant mothers at E7.0 allowed tracing YS progenitor-derived cells showing that labelled primitive macrophages seed all embryonic tissues around E10 and E13. However, in adult mice a considerable proportion of labelled cells was only found in the brain indicating that the YS-derived primitive macrophages in the other tissues were replaced by fetal monocytes during embryogenesis. Tamoxifen administration at E8.0 tagged more efficiently most of tissue resident macrophage subsets and monocytes, while the relative amount of labelled microglia was dramatically decreased, indicating again that microglia only derive from Runx1$_+$ YS progenitors with little contribution of definitive hematopoietic precursors and their progenies [19]. A study of Schulz *et al.* confirmed these findings by utilizing colony-stimulating factor 1 receptor (*Csf1r*^{CreER})-based fate-mapping [48]. Additionally, the group showed dependence of most of hematopoietic cells on transcription factor c-Myb, while fetal F4/80$_{hi}$ macrophages are intact in *Myb*-deficient embryos, concluding that macrophages derive from a c-Myb-independent lineage in YS. With use of fms-like tyrosine kinase 3 (Flt3), which is expressed by pluripotent hematopoietic progenitors, the group observed that most of adult F4/80$_{hi}$ macrophages develop independently of this factor in *Flt3*^{Cre} reporter mice, suggesting that adult macrophages are largely independent of adult

definitive HSCs. Subsequent study from the same group with *Tie2*-based fate-mapping proposed YS-derived EMPs as main precursors of adult macrophages [49]. More precise analyses of *Runx1*$_{CreER}$ and *Csf1r*$_{CreER}$ reporter mice and cell death analysis showed for most organs a gradual dilution of YS macrophages by non-labelled cells, hypothetically fetal monocytes. Comparative gene expression analysis between fetal liver monocytes and YS macrophages allowed to create a new monocyte-specific fate-mapping system based on exclusive expression of S100a4 (FSP1) by fetal monocytes. In this model, monocytes from *S100a4*$_{Cre}$ reporter embryos (at E10.5) were efficiently labelled with reporter protein (EYFP), while YS macrophages, EMPs and other leukocytes were labelled to much lower extent. Already during embryonic development, frequency of EYFP$_+$ macrophages exceeded the percentage of poorly labelled YS macrophages and microglia and gradually increased with time, implicating dominant role of fetal monocytes as a source of adult macrophages. This study proposed existence of two waves of EMP separated only by 1-2 days. "Early" EMPs emerging at E7 give rise to primitive macrophages in the YS and other tissues including the brain. In the second wave, "late" EMPs emerge at E8.5 and migrate to the fetal liver starting at E9.5, where they differentiate to fetal monocytes that seed all tissues, except the brain, and replace the pool of primitive macrophages. They also confirmed low contribution of Flt3-dependent MDPs to fetal monocytes and macrophages [50]. Notably, another report proposed yet another model according to which all tissue resident macrophages are derived from fetal definitive HSCs. The group used *c-Kit*-based fate-mapping system and tamoxifen administration at E7.5 efficiently labelled microglia and partially tagged Langerhans cells in the skin of adult mice. Injection of tamoxifen one day later labelled all adult HSC-derived leukocytes and macrophages suggesting HSC-derived origin of the latter [51]. However, late EMPs and fetal HSCs cannot be distinguished in this model due to equal labeling of E10.5 EMPs and AGM-derived multipotent progenitors derived from *Kit*$_{CreER}$ reporter embryos treated with tamoxifen at E8.5. Therefore, contribution of EMPs in macrophage development cannot be excluded. In summary, they all agree that microglia and to some extent Langerhans cells derive from primitive macrophages, which develop in YS and self-renew in adulthood with little contribution of later progenitors. It should be noted that different fate-mapping models have been employed, which are affected by their intrinsic limitations, what needs to be taken into consideration when interpreting the data.

The contribution of adult HSCs to the tissue resident macrophage pool can occur but molecular mechanisms standing behind macrophage turnover or their repopulation by monocytes are still not well understood. Tissue resident macrophages in the intestine and dermis have been shown to be maintained by monocytes in CCR2-dependent manner [40, 41, 52, 53]. In case of adult cardiac macrophages, circulating progenitors gradually replace fetal-derived pool [42, 54]. Kinetics of replacement of mentioned populations by monocytes differ in the steady-state. Macrophages in intestine and dermis have a rather fast turnover with estimated half-life of 4-6 weeks, while cardiac macrophages' half-life is predicted to be about 8-12 weeks. Therefore, studies analyzing monocytic contribution over extended periods of time would be required. Interestingly, a study concerning arterial macrophages shows that they develop immediately after birth from BM-derived monocytes, which are then maintained locally by self-renewal [55]. Similar finding was made for Kupffer cells [56]. Keeping in mind that these cells self-renew with no contribution of circulating progenitors in adulthood, it was proposed that these tissues are "open" only temporarily at birth. Microglia, Langerhans cells, alveolar macrophages do not require monocytic contribution in adulthood in steady-state providing examples of "closed" tissues [32]. These findings suggest tissue itself as a major controller of macrophage persistence and monocyte recruitment in order to replenish resident population.

4.5 Environmental imprinting of tissue resident macrophages

Tissue resident macrophages are distributed throughout the body and besides functions conserved across all organs they fulfil additional roles, which are tailored individually for each tissue in order to support local homeostasis. Therefore, macrophages exposed to different environments will significantly differ in surface phenotype, transcriptome and epigenome creating remarkable heterogeneity within the subset [57]. Joined efforts by the Immunological Genome Project Consortium (ImmGen.org) [58-60], based on comparative transcriptomics including a number of distinct tissue macrophage subsets, have formed a hypothesis of definable common tissue macrophage signature as well as signature characteristic for each tissue of residence. These designated signatures are undeniably associated with environmental signals. Isolated tissue resident macrophages lose their specific signature in culture whereas transplanted bone marrow cells into irradiated recipients acquire it [61, 62].

Collectively, local microenvironment imprints and maintains distinct tissue resident macrophage identities. The genome is identical among all cells, however regulatory modifications on chromatin level enable cell type specific functions [63-66]. Nucleosomes, the fundamental units of chromatin, consist of DNA wrapped around a histone core [67], which then undergoes modifications like methylation, phosphorylation, sumoylation or ubiquitination affecting gene regulation [68]. Some of the inactive genes in embryonic stem cells are marked by modifications of both activating (H3K4me3) and inhibitory (H3K27me3) nature on the same histones. These "poised" promoters are activated upon initiation of differentiation program leading to induction of lineage-specific gene expression [69]. A similar situation is observed for macrophage-specific enhancers. High number of poised enhancers allows to estimate that macrophages have a great potential to respond to local challenges [62]. Active enhancers are marked by H3K4me1 and H3K27ac modifications, whereas poised are H3K4me1$_+$ H3K27ac$_-$. Comparison of the enhancer landscapes of different tissue resident macrophage subsets revealed relatively small overlap of active enhancers within macrophage-specific enhancer pool. Interestingly, an *in vitro* exposure of isolated tissue resident macrophages to factors shaping unique identity of a subset derived from different organ or transfer to new microenvironment induces partial reprogramming and changes in chromatin landscapes. This finding demonstrates that instructive cues imposed by tissue are more critical than ontogenesis in establishing tissue resident macrophage identity [61, 62].

Macrophage colony-stimulating factor (M-CSF, Csf1) which signals through M-CSF receptor (M-CSFR, Csf1r) is one of the major factors required for macrophage lineage commitment. It is not only required for differentiation but also survival and self-renewal of most of tissue macrophages [70]. In case of microglia and Langerhans cells, these subsets have been shown to depend on IL-34, another ligand for M-CSFR with a distinct expression pattern from M-CSF that plays a complimentary rather than redundant role in lineage commitment [71]. Transcription factors which govern specific lineage fates are called "lineage-determining" or "pioneer" factors (LDTF) and are able to initiate transformation of silent chromatin into accessible state by either eviction of nucleosomes or introduction of activating histone modifications [72, 73]. Key player in macrophage lineage commitment is E26 transformation specific (Ets) family transcription factor (PU.1). Besides its pioneer factor activity, it regulates M-CSFR expression leading to

elevated receptor levels and increased sensitivity to the ligand [74]. Lineage determining factors belong to CCAAT/enhancer-binding protein (C/EBP) transcription factor family that, in collaboration with PU.1, have the potential to switch B cell-specific programming to macrophages by reshaping chromatin accessibility [75]. Comparison of enhancer landscapes of myeloid cell subsets revealed Maf transcription factors (c-Maf and MafB) as specific regulators of establishing macrophage-specific regulatory regions [62]. Previous studies indicated MafB involvement in exiting multipotent progenitor state promoting final macrophage differentiation and loss of c-Maf/MafB expression leads to cell immortalization [76, 77]. While LDTF maintain macrophage-specific regions in poised state and establish universal macrophage signature, supplementary transcription factors driven by environmental signals (signal-driven transcription factors, SDTF) are required in order to activate unique tissue-specific pattern of gene expression [78].

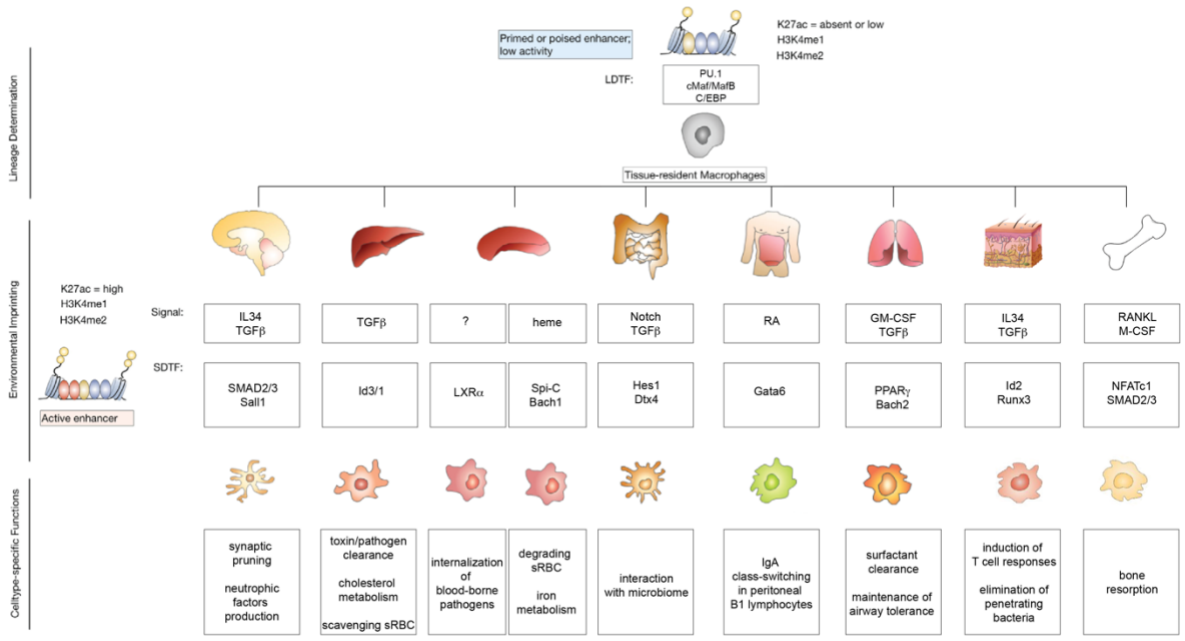

Figure 2. Environmental imprinting of tissue resident macrophages. Modified from [79].

Epigenetic and transcriptomic screens complemented with knockout studies shed some light on environmental triggers, responsive transcription factors, and genes which shape unique signature leading to functional specialization of committed macrophage. Microglia, the macrophages of the central nervous system, maintain central nervous system (CNS) homeostasis by supporting neuronal development and organization through neurotrophic factor production and synaptic pruning [80, 81]. They require IL-34 for their development and maintenance [71]. Transforming growth factor beta

(TGFβ)-mediated SMAD2/3 signaling was shown to keep microglia in an inactive state, which is necessary in order to support tissue homeostasis [82]. Additionally, gene expression profiling delivered another factor (Sall1) uniquely expressed by these macrophages [62]. Deletion of Sall1 led to activation of proinflammatory program confirming its critical role in maintenance of tissue-specific microglial identity [83]. The peritoneal cavity is colonized by two macrophage populations, which differ in terms of their origin, physiology and function [84]. Large peritoneal macrophages (LPM) have a F4/80$_{hi}$MHCII$_{low}$ phenotype and originate from fetal progenitors with ability to self-renew at steady-state [36]. In contrast, small peritoneal macrophages (SPM) are CCR2-dependent and have low expression of F4/80 and high MHCII levels. Their differentiation from monocytes relies on IRF4 [85]. Three groups independently reported Gata6 as a tissue-specific transcription factor for LPMs [86-88]. Activation of Gata6 is induced by retinoic acid (RA) and its expression is modulated by local pool of this metabolite. Osteoclasts reside in bones and specialize in bone resorption [89]. Their differentiation involves M-CSF and receptor activator of NFκB ligand (RANKL) binding [90], what leads to activation of NFATc1. Deficiency of either causes osteopetrosis, a condition where bones become abnormally dense due to dysbalanced bone remodeling [90, 91]. The biggest subset of tissue resident macrophages is located in the liver and supports homeostasis by toxin and pathogen clearance, bilirubin and cholesterol metabolism, scavenging of senescent or damaged RBCs and hepatocytes [92]. Not much is known about environmental cues governing functional specialization of Kupffer cells but one of Kupffer cell-specific transcriptional regulators (Id3) has been identified recently in unbiased RNAseq analysis [93]. The study shows that knocking out Id3 reduces the number of liver macrophages. Interestingly, loss of Id3 caused an increase in expression of Id1 suggesting that these proteins may have a redundant role in Kupffer cell development. Both factors are regulated in TGFβ-dependent manner [94] implicating this cytokine as a niche-specific inducer of differentiation. Functional similarity to red pulp macrophages (RPM) suggests that Kupffer cells might depend on the same factors as their splenic counterparts but there is no evidence to confirm this as liver population is intact in specific knockouts targeting these molecules. TGFβ is also important for development of macrophages in the skin (Langerhans cells) and in the colon. In the skin, it induces Id2 and Runx3, while in the colon it regulates genes connected to Notch signaling (Hes1 and Dtx4) [95-97]. Alveolar macrophages (AM) constantly patrol lungs and protect the

organism from inhaled pathogens. Also, they specialize in surfactant clearance and were shown to depend on GM-CSF signaling which induces peroxisome proliferator-activated receptor gamma (PPARγ) [98, 99]. Splenic macrophages are very heterogenic in terms of their function and localization. They rely on different transcription factors. Marginal zone macrophages (MZM) internalize blood-borne pathogens and induce tolerance to self-antigens [100]. LXRα was shown to be a major regulator of their development as the *Lxra*-deficient mice lack MZM [43]. Macrophages residing in the red pulp (RPM) specialize in breaking down senescent RBCs and recycling iron. An intermediate metabolite of hemoglobin degradation, heme, indirectly activates Spi-1/PU.1-related transcription factor (Spi-C) leading to final macrophage differentiation [101, 102]. As this study is focused mainly on AM and RPM, these two subsets will be discussed more thoroughly in next paragraphs. Summary of described pathways and differentiation steps are depicted in Figure 2.

4.6 Alveolar macrophages

4.6.1 Phenotype & Origin

Human respiratory tract is organized in a tree-like structure where lower airway includes the trachea, bronchi, bronchioles and alveoli. The thin-walled alveolar sacs are the terminal part of the airway that is surrounded by abundant capillaries. Together they are the functional unit where gas exchange occurs [103]. Millions of alveoli filter around $9x10^3$ liters of air daily and therefore are exposed to numerous pollutants, airborne microbes and dust. Inhaled particles are removed by AM and DCs in a tolerogenic manner (excluding pathogen clearance) [104]. Macrophages are found in several locations in homeostatic lung what constitutes the basis for their classification. Parenchymal space (interstitium) and bronchiolar submucosa are colonized by interstitial macrophages (IM), while the alveolar space is inhabited by AM. AM reside in the alveolar lumen and represent a major population (90-95%) found at this location in the steady-state [57]. Murine lungs contain one to two million of AM with an exceeding number of alveoli. In average, only every third alveolus is colonized by AM [105] but AM can move between adjacent sacs through the interalveolar pores of Kohn [106]. Exposure to the unique environment in the alveolar space produces a distinctive and AM-specific phenotype allowing their separation from IM and DCs by multiparameter flow cytometry. Similar to

other tissue resident macrophages, AM are MerTK^{+} CD64^{+} CD68^{+} CD206^{+} F4/80^{+} but they express low levels of CD11b and Cx3cr1 and are highly positive for CD11c and SiglecF [107].

Recent years brought new insight into macrophage ontogeny. It is generally accepted that most of tissue resident macrophage populations develop perinatally from fetal progenitors and self-renew in adulthood with low input from circulating monocytes in the steady-state [44, 108]. Fetal lungs contain populations of primitive macrophages (F4/80^{hi}CD11b^{int}) and fetal monocytes (F4/80^{lo}CD11b^{hi}) but only the latter undergo profound expansion between E17.5 and day 7 after birth. This process is accompanied with successive phenotypic changes leading to acquisition of mature AM characteristics [98, 99]. Adoptive transfers of two myeloid populations derived from E17.5 WT embryos to AM-deficient mice confirmed potential of fetal monocytes to give rise to AM while fetal macrophages could not reconstitute the population [99]. Interestingly, another study using similar transfer principle, showed potential of YS-derived macrophages (isolated at E12.5) to reconstitute AM population in deficient recipients. However, in competitive transfers monocytes (harvested from E15.5 embryos) outcompeted YS-derived macrophages and BM-derived monocytes in colonizing newborn lungs [109]. Under homeostatic conditions, circulating monocytes minimally contribute to adult AM pool [36, 37, 98, 110]. Nonetheless, in Flt3-based fate-mapping (labels all cells originating from HSCs) a fraction of AM become positive for fluorescent reporter implicating a role of definitive hematopoiesis in the AM renewal [49]. Certain circumstances like irradiation, inflammation or impaired self-renewal ability connected to aging could also induce monocyte infiltration and differentiation into macrophages [37, 54, 98, 111].

4.6.2 Function

AM maintain the alveolar space integrity through phagocytosis of senescent cells, removing of inhaled particles and creating first line of defense against invading pathogens [112]. Arguably, the most important role of AM in lung homeostasis is degradation of pulmonary surfactant, a complex of phospholipids and surfactant proteins (SP-A, SP-B, SP-C, SP-D) which reduces surface tension at the air-liquid interface and prevents alveolar collapse [113]. It also serves as a barrier to inhaled pathogens and due to its unique composition constitutes integral part of host defense [114]. SP-A and SP-D bind LPS and induce bacterial and fungal agglutination. SP-A mediates opsonization of *S.*

aureus and provides growth inhibitory signal for *Mycoplasma.* When bound to pathogens these collectins are able to stimulate phagocytosis in AM. Additionally, unbound SP-A and SP-D thorough binding to signal-regulatory protein alpha (SIRPα) suppress pro-inflammatory cytokine production by AM [114]. Therefore, any deviation from the homeostatic deposition of surfactant may lead to severe conditions. Decreased concentration can eventually lead to respiratory failure, while excessive accumulation of surfactant causes pulmonary alveolar proteinosis (PAP). There are three main categories of PAP including autoimmune, secondary and genetic PAP with autoimmune PAP representing 90% of all cases [115]. The main cause of this abundant form of PAP are autoantibodies against GM-CSF, a cytokine required for proper AM development [98, 99, 116]. Alveolar epithelial cells type 2 (AE2Cs) are the main producers of surfactant in the lung and are able to catabolize it too. However, AM are very well equipped to take up and catabolize lipoproteins and lipids and thereby largely contribute to clearing surfactant from the lung alveoli [117]. AM scavenge inhaled particles in a non-inflammatory manner. This hypo-responsiveness is maintained by various inhibitory receptors on AM

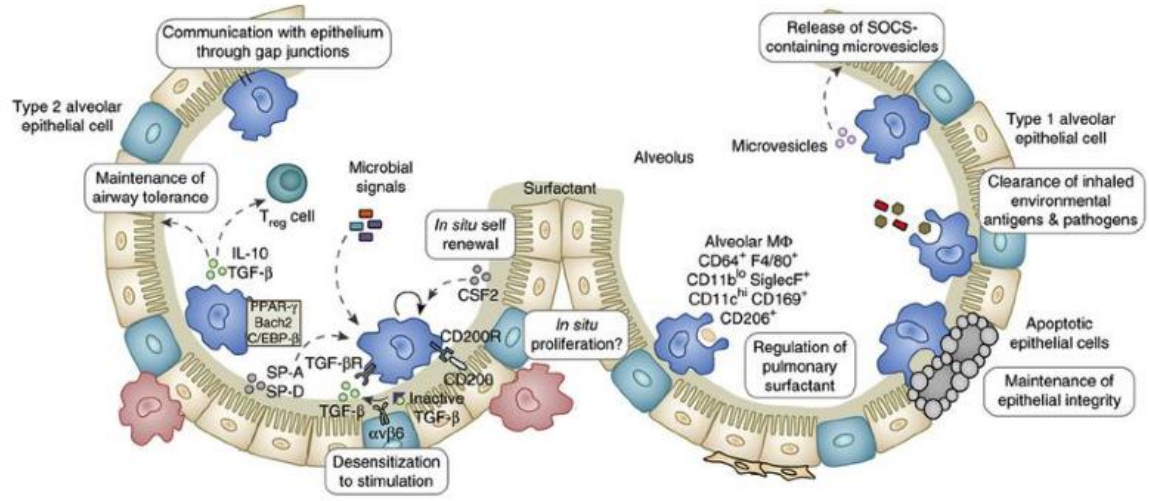

Figure 3. AM as key players in lung homeostasis. Adapted from [57].

surface, which are constantly stimulated by ligands expressed on AECs or present in the alveoli like aforementioned SP-A and SP-D. This SP-A/SP-D-regulated suppression of AM activation can be overcome by TLR4 stimulation, which controls SIRPα expression and leads to its downregulation [118]. Other inhibitory receptors include CD200R, IL-10R, and TGFβR [57]. AM can also regulate AEC reactivity by secretion into lung lining fluid suppressor of cytokine-signaling (SOCS) proteins in form of exosomes and microparticles. AEC then take up SOCS which translocate to nucleus and inhibit JAK-STAT

signaling pathway [119]. This continuous interaction between AM and AECs is crucial for proper function of the lungs during homeostasis and inflammation. Additionally, AM can promote development of regulatory T cells in order to induce protection to harmless antigens [120]. Figure 3 summarizes described functions and signals which enable AM to maintain homeostasis in the lung.

4.6.3 Signature genes

AM functional specialization imposed by environment makes the latter crucial supplier of factors inducing transcriptional adaptation of developing cell in order to fulfil tissue's needs and allow cell to survive in such a specific surrounding. Involvement of granulocyte-macrophage colony stimulating factor (GM-CSF) in promoting AM function was first observed in 1994 in transgenic mice lacking expression of this cytokine [121]. This finding was confirmed later in a study based in GM-CSF receptor beta subunit (*Csf2rb*)-deficient mice [122]. Both models reported abnormal function of AM upon loss of GM-CSF signaling and accumulation of surfactant in the lungs which resembled human condition known as pulmonary alveolar proteinosis (PAP). More recently, GM-CSF was shown to be critical for AM development from fetal liver monocytes [98, 99] while M-CSF signaling is dispensable [123]. Absence of GM-CSF abrogates differentiation of AM progenitors already at E17.0. It is secreted by AECs and acts on fetal lung monocytes leading to activation of PPARγ. This nuclear receptor modulates expression of multiple genes involved in lipid metabolism, transport, storage and degradation crucial for functional adaptation of AM to surfactant catabolism [99]. Although this GM-CSF/PPARγ axis is critical for lung homeostasis, additional signals and genes were described to be involved in AM development. Mice lacking transcriptional repressor BTB Domain and CNC homolog 2 (Bach2) develop PAP and their AM characterize with high lipid deposition [124], a phenotype similar to one detected in different ATP-binding cassette transporter (ABC1, ABCA1, and ABCG1) knockout mice [125-127]. ABCA1 and ABCG1 transporters mediate cholesterol efflux and are controlled by PPARγ [128]. Additionally, TGFβ was identified as another differentiation factor which controls AM development and their maintenance in autocrine manner [129]. Transition from pre-AM to AM in developing lung was demonstrated to depend on L-plastin which allows correct localization of AM in the alveoli [130]. Finally, a potential role of C/EBPβ in AM development was indicated

through a study based on *Cebpb*-deficient mice which characterize with reduced levels of adult AM [131].

4.7 Iron-recycling macrophages

4.7.1 Phenotype & Origin

The spleen is the largest secondary lymphatic organ in the body and contains around 25% of whole-body lymphocytes [132]. It comprises of two compartments called the white and the red pulp, which differ functionally and morphologically. The red pulp is a network of splenic cords (also called cords of Billroth) and venous sinuses, the latter being essentially blood-filled cavities. Splenic cords are composed of connective tissue and contain reticular cells and RPM. The primary function of the red pulp is to filter out damaged cells, debris, pathogens and senescent RBCs from the blood. The white pulp surrounds central arterioles and is responsible for initiation of immune responses to blood-borne antigens. It is subdivided into three regions: the periarteriolar lymphoid sheath (PALS) populated mainly by T lymphocytes and DCs, follicles containing B lymphocytes and marginal zone (MZ) [133].

A small population of macrophages was found in the germinal center of B cell follicles. These tangible body macrophages (TGM) express CD68 and milk fat globule-epidermal growth factor 8 (MFGE8), which promotes phagocytosis of apoptotic cells in a tolerogenic manner [134]. The MZ separates the red pulp from PALS and follicles. The inner circle of MZ consists of marginal zone metallophilic macrophages (MMM), which are characterized by expression of sialic-acid-binding immunoglobulin-like lectin 1 (Siglec-1). The second subset of macrophages, marginal zone macrophages (MZM), resides in the thick outer layer of MZ and can be visualized by staining against C-type lectin (SIGNR1) and scavenger receptor MARCO. These two subsets play an important role in processing blood-borne antigens [135]. RPM are the main phagocytes clearing senescent RBCs and recycling iron. They express F4/80, VCAM1, Dectin 2, and integrin $\alpha 9$ [136].

RPM self-maintain in the tissue with no contribution from circulating monocytes at steady-state [37]. They characterize with a long lifespan and slow turnover. As most of tissue resident macrophages, RPM were shown to develop perinatally from embryonic Cx3cr1-positive progenitors [36]. Conditional deletion of *Myb* gene in adult mice, which were subsequently reconstituted with WT cells, revealed that majority of RPM are

maintained independently of HSCs and Myb, suggesting possible development from *Myb*-independent YS progenitors [48]. Data provided by another research group suggested prenatal replacement of YS-derived splenic macrophages with fetal liver monocyte-derived RPM indicating fetal monocyte as the main progenitor of the RPM population which persists into adulthood [42].

4.7.2 Function

Iron-recycling macrophages include RPM, a small population of bone marrow macrophages and to some extent also Kupffer cells in the liver. Every day, they recycle over 25 mg of iron from senescent or damaged RBCs. Interestingly, only 1-2 mg of iron is absorbed in the gut. Recycled or collected iron is subsequently transported to the BM and used during erythropoiesis [137]. This process takes place in erythroblastic islands (EBIs) in the BM, where centrally positioned bone marrow erythroid island macrophages (BMEIM) are surrounded by developing erythroblasts [138]. Cells interact via integrin $\alpha4\beta1$ and ICAM4 expressed on erythroblasts and integrin αV, VCAM1, CD169 expressed on BMEIM allowing the latter to provide nutrients and signals regulating proliferation and differentiation to erythroblasts [138]. BMEIMs were also shown to phagocytose extruded nuclei from reticulocytes [139]. RPMs, localized in the splenic cords, examine condition of circulating RBCs. Macrophages are able to sense glycoprotein CD47 expressed on the surface by virtually every cell. CD47 interacts with SIRPα present on macrophage surface and inhibits induction of phagocytosis [140]. CD47 on aged erythrocytes undergoes conformational changes and thereby becomes an 'eat me' signal that activates erythrophagocytosis [141].

During erythrophagocytosis, RPM internalize RBCs, which get subsequently degraded by hydrolytic enzymes in the phagolysosome. An intermediate product of hemoglobin degradation, heme, is then translocated to the cytosol via heme transporter Hrg1 [142]. Almost $1.2x10^9$ of heme moieties are released from single RBC degradation and due to its high cytotoxicity, its synthesis and breakdown must be tightly regulated. Free heme induces expression of an enzyme, heme oxygenase 1 (HO1, gene name *Hmox1*) which degrades heme into iron, carbon monoxide (CO) and biliverdin [143]. Macrophages can also uptake hemoglobin or heme directly from circulation. Free hemoglobin or bound to the acute-phase protein haptoglobin is recognized by scavenger receptor CD163 [144]. Heme is sequestered by hemopexin in non-reactive form and

internalized via CD91 to be subsequently catabolized in the cytosol by HO1 [145]. Released iron can be then excreted from macrophages by transmembrane protein ferroportin-1 (Fpn1) [146] or stored by ferritin [147]. The described cycle of iron reuse is summarized graphically in Figure 4.

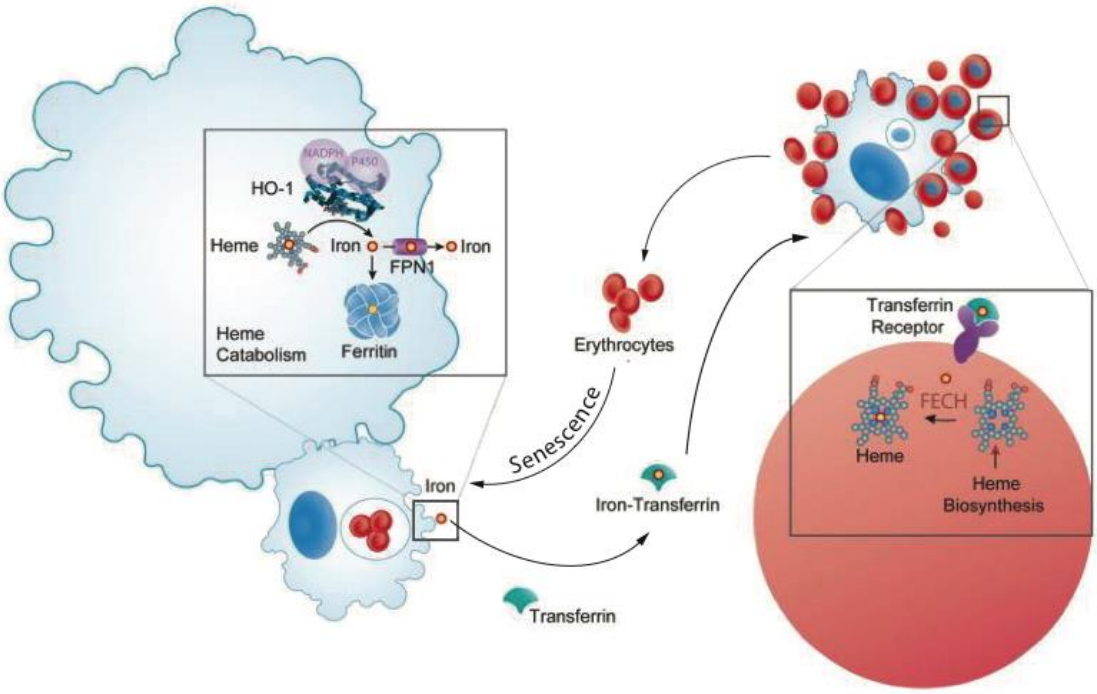

Figure 4. The cycle of iron reuse orchestrated by RPM and BMEIM. Modified from [148].

Heme-iron metabolism is tightly regulated and strongly influences macrophage function. CO produced during heme degradation for instance can bind iron of various hemoproteins and modulate their activity. NADPH oxidase 2 (NOX2) producing reactive oxygen species (ROS) could lead to oxidative stress during responses to pathogens or disassembling of dying cells but limited access to heme due to its catabolism inhibits ROS production [149]. Similarly, cyclooxygenases (COXs), which catalyze prostaglandin production during early PRR signaling and are associated with macrophage polarization can be inhibited in similar manner leading to modulated inflammatory response [150]. Additionally, accumulated ROS and reactive nitric species (RNS) can be sensed by Keap1 what leads to release of constitutively repressed nuclear factor E2-related factor-2 (Nrf2) which in a consequence triggers transcription of multiple genes involved in heme metabolism, like *Hmox1*, ferritin heavy chain (*Fth*), *Hrg1* and *Fpn1* [148]. Moreover, all mentioned Nrf2 target genes are repressed on transcription level by Bach1, which upon heme binding is destined for proteasomal degradation [148]. Macrophages could also

trigger responses restricting pathogens from heme-iron access [151]. Therefore, functional ability to recycle iron influences many additional processes autonomous to macrophage, like cell polarization, or systemic, including modulation of host defense.

4.7.3 Signature genes

Analysis of osteopetrotic (*op/op*) mice, which lack M-CSF, revealed a severe reduction in number of RPM and BMEIM [152]. This result was confirmed in M-CSFR silencing experiments. Together, these data demonstrate that M-CSF is critical for development of RPM and BMEIM [153]. HO1 is indispensable for heme degradation and therefore necessary for proper function of RPM. Enzyme deficiency leads to anemia and iron deposits [154] accompanied with loss of all iron-recycling macrophage subsets in older animals [155]. Therefore, expression of HO1 is critical for RPM and BMEIM survival. Both subsets have been shown to depend on Spi-C, a member of E26 transformation-specific (Ets) transcription factor family [101, 102]. *Spic*$^{-/-}$ mice characterize with severely reduced numbers of RPM and BMEIM accompanied with iron overload in the spleen. The defect is cell autonomous and could be reverted by retroviral overexpression of the transcription factor in BM cells. Spi-C is indirectly induced by heme, which promotes proteasomal degradation of transcriptional repressor Bach1, and in a consequence activates Spi-C expression and differentiation of iron-recycling macrophage from monocytic progenitor. One of the identified target genes of Spi-C is VCAM1, an adhesion molecule specifically expressed by the two macrophage subsets which mediates macrophage interactions with erythroblasts and HSCs [153, 156]. Interferon regulatory factor 8 (IRF8) is also strongly expressed by RPM. IRF8 is required for development of many myeloid cell subsets but inhibits neutrophil differentiation [157]. Interestingly, mice lacking IRF8 display a modest reduction of RPM and a strong defect in BMEIM development, while IRF8 and IRF4 double knockouts present a severe decrease in both subsets [158]. Mice lacking Trib1, an adaptor protein involved in protein degradation, have increased expression of C/EBPα in myeloid progenitors what results in defective macrophage differentiation. RPM and BMEIM are strongly affected but no abnormal iron deposition in spleens of deficient mice was observed [159].

4.8 Peroxisome proliferator-activated receptor gamma (PPARγ)

Peroxisome proliferator-activated receptor gamma (PPARγ) is a nuclear receptor and, together with two other members of PPAR subfamily (PPARα and PPARβ/δ), acts as ligand-inducible transcription factor. All three receptors dimerize with retinoid X receptor (RXR) for efficient DNA binding [160]. Each has been involved in regulation of distinct processes controlling energy metabolism [161]. First to be identified was PPARα and the family owes its name to the ability of this receptor to bind chemicals able to induce peroxisome proliferation [162]. It is predominantly expressed in the liver, heart, kidney and brown adipose tissue (BAT) and responds to poly-unsaturated fatty acids and leukotriene B4 as well as to lipid-lowering fibrate drugs regulating fatty acid oxidation and high-density lipoprotein cholesterol levels [163, 164]. PPARβ/δ is ubiquitously expressed contributing to activities governed by PPARα, it also activates intestinal lipid absorption and is the major regulator of fatty acid catabolism in muscles [164]. Saturated and unsaturated long-chain fatty acids, prostacyclin or phenoxyacetic acid derivatives can activate PPARβ/δ [164]. The last member of the family, PPARγ, exists in two variants formed by alternative splicing and differential promoter usage. Isoform 1 lacks 30 amino acids at N-terminus present in the second isoform (PPARγ1 and PPARγ2, respectively). PPARγ1 is broadly expressed in cell types and tissues including white adipose tissue (WAT) and BAT, liver, skeletal muscles, colon, bones, pancreatic β-cells, and macrophages while PPARγ2 is detected mainly in WAT and BAT at steady-state [165]. It responds poorly to native fatty acids but oxidized forms such as 9-HODE and 13-HODE (9/13-hydroxyoctadecadienoic acids) are efficient activators of the receptor in atherosclerotic lesions [166]. Also, certain prostanoids including 15-deoxy-Δ12,14-prostaglandin J2 (15-dPGJ2) were shown to activate PPARγ and promote adipocyte differentiation [167, 168]. However, best studied are possibly synthetic ligands of PPARγ, thiazolidinediones (TZDs), which are broadly used as anti-diabetic drugs [169-171].

All PPARs contain N-terminal domain (NTD) with ligand-independent activation function (AF1), highly conserved DNA-binding domain (DBD), flexible hinge region and ligand-binding domain (LBD) containing ligand-binding pocket and ligand-dependent activation function (AF2) [163]. Unliganded PPAR-RXR complex is bound to corepressor complex containing nuclear receptor corepressor (NCoR), silencing mediator of retinoid

and thyroid hormone receptor (SMRT) and Sin3 which facilitate recruitment of histone deacetylases (HDACs) and suppress target gene transcription [172, 173]. The engagement of an agonistic ligand causes structural changes in the C-terminal part of the protein what subsequently induces corepressor complex dissociation and generates hydrophobic cavity enabling docking of coactivators displaying LXXLL motif. Coactivator complexes facilitate transcriptional activation of target genes mainly by assembling into stable preinitiation complex on the target gene promoter with PPAR-responsive elements (PPRE). Potent histone acetyltransferases (HATs) like steroid receptor coactivator (p160/SRC) and CREB-binding protein (CBP) with its homologue p300 are recruited to the AF2 domain and acetylate histones. HAT complex is then linked to Mediator complex, which facilitates recruitment of TATA-box-binding protein (TBP) and associated factors which position RNA polymerase II over the transcription start site (TSS) of the target gene [174].

Expression of most of these coactivators seems not to be tightly regulated. Therefore, the activation of PPARs mainly depends on ligand binding. However, PPARγ coactivator 1 (PGC-1α) was shown to bind to PPARγ in ligand-independent manner and is strongly upregulated by exposure of human and mice to cold temperature. PGC-1α is highly overrepresented in BAT compared to WAT and induces expression of selected target genes specific to BAT [175]. Additionally, PPARγ was shown to undergo post-translational modifications like phosphorylation, sumoylation, acetylation and ubiquitination, what could contribute to modulation of its activity in various cell types or tissues [176]. Phosphorylation of Ser82 in PPARγ1 (Ser112 in PPARγ2) by MAPKs represses its activity by changing recruitment of cofactors and inhibits ligand binding. Surprisingly, the same modification performed by cyclin-dependent kinases Cdk7 and Cdk9 have a positive effect on PPARγ activation [177-179]. Additional Cdk5-mediated phosphorylation within LBD has rather negative effect on PPARγ activity and was linked to pathogenesis of insulin resistance [180]. Acetylation at Lys268 and Lys293 inhibits recruitment of PR/SET Domain 16 (PRDM16), which was shown to positively regulate BAT development and browning of WAT [181]. Sumoylation within AF1 of PPARγ leads to the repression of transcriptional activity most probably through promoting recruitment of corepressors [182]. In macrophages, sumoylated PPARγ is recruited to promoters of inflammatory genes and prevents their transcription through a mechanism

known as trans-repression [183]. PPARγ has rather short half-life (2 hours) and undergoes proteasomal degradation when polyubiquitinated. This modification was shown to be enhanced upon ligand binding [184].

PPARγ functions as a master regulator of adipogenesis [185]. It was shown that PPARγ over-expression in fibroblasts induces expression of adipose-associated genes and accumulation of lipid droplets [186]. Moreover, studies utilizing chimeric mice reconstituted with PPARγ-deficient cells confirmed a crucial role of this transcription factor in adipose tissue formation [187]. The mechanism of adipogenesis was further dissected by cell culture studies, where hormonal treatment of preadipocytes led to induction of C/EBPβ and δ, which in turn bind to PPARγ promoter leading to its increased expression [188, 189]. Liganded PPARγ induces many genes, including C/EBPα, which then maintains PPARγ expression and genes like adipocyte protein 2 (aP2), phosphoenolpyruvate carboxykinase (PEPCK), lipoprotein lipase (LPL), adiponectin, and glucose transporter type 4 (Glut4), connected to processes of lipogenesis and adipogenesis [190]. Adipocyte-specific deletion of PPARγ in mice results in severe insulin resistance, increased levels of plasma free fatty acids (FFA), and glucogenesis [191, 192]. These data confirmed previous discoveries linking TZDs activity, broadly used antidiabetic drugs, with induction of PPARγ [171]. Type 2 diabetes characterizes with inappropriate deposition of lipids in the liver or skeletal muscles, increased plasma levels of FFA and insulin resistance [193]. PPARγ activation enhances lipid uptake and storage in WAT, lowering their levels in other tissues mainly through activation of fatty acid translocase (CD36), aP2, LPL, fatty acid transport proteins (FATPs), PEPCK and glycerol transporter aquaporin 7 (AQP7) [190]. Simultaneously, it influences production of bioactive molecules by adipocytes (adipokines) impacting whole-body insulin sensitivity [194]. Obesity is associated with accumulation of pro-inflammatory macrophages in the fat, which has been shown to contribute to insulin resistance by production of TNFα and IL-6 [195]. The evidence outlining a role of PPARγ in differentiation of anti-inflammatory, alternatively-activated macrophages brought to light a new pathway governed by PPARγ directly linked to improved insulin sensitivity [196]. Moreover, this anti-inflammatory nature of PPARγ was further investigated in the context of cardiovascular disease. Fat deposits in arterial walls lead to recruitment of monocytes, which differentiate into macrophages and internalize modified low-density lipoproteins (LDL).

Excessive lipid accumulation trigger formation of macrophage foam cells, which are a hallmark of an early atherosclerotic lesion. An LDL receptor, CD36 was shown to contribute to the process while mice lacking CD36 expression were protected against the atherosclerotic lesion development [197]. Use of synthetic agonists of PPARγ was therefore speculated to induce lipid accumulation by upregulation of CD36, a well-established PPARγ target, which would accelerate foam cell formation [198]. However, data from mice and human studies did not confirm that theory. Interestingly, two groups described a PPARγ-ligand-activated pathway which contributed to efficient cholesterol excretion from macrophages. This positive effect was attributed to identification of a new target gene, namely LXRα which activates ABCA1 [199, 200]. Therefore, the lipid internalization and efflux within single cell should be well balanced in order to negatively regulate the progress of the lesion.

Many studies reported PPARγ as a potent regulator of immune responses, mainly through its activity in myeloid cells. PPARγ inhibits pro-inflammatory genes in macrophages [201, 202]. It does so indirectly, by mediating inhibition of other transcription factors (trans-repression) involved in induction of pro-inflammatory genes, namely NF-κB and activator protein 1 (AP-1) [203]. In DCs, PPARγ ligands have been suggested to regulate lipid antigen presentation to T cells through modulation of retinoid signaling [204], although our group could not confirm this finding. IL-4, the prototype Th2 cytokine, was shown to augment PPARγ expression and ligand-induced activity in both, macrophages and DCs. This effect was facilitated by signal transducer and activator of transcription 6 (STAT6) by cooperative binding of two transcription factors to promoters of target genes [205]. Moreover, more recent discoveries described PPARγ as a pro-inflammatory factor during lung inflammation by promoting DCs in priming T cell polarization and controlling Th2 effector functions [206]. PPARγ was shown to be crucial for AM development and its activation was fully dependent on GM-CSF [99]. Thus, PPARγ modulates many processes involved in cell metabolism, development and immunity.

5 Results

5.1 PPARγ and Spi-C drive unique programs required for the development of iron-recycling macrophages in spleen and bone marrow

Authors:

Katarzyna Okreglicka[1], Lea Pohlmeier[1], Lucas Onder[2], Michael Kurrer[3], Burkhard Ludewig[2], Peter Nielsen[1], Christoph Schneider[1], Manfred Kopf[1]

Affiliations:

[1]Institute of Molecular Health Sciences, Department of Biology, Swiss Federal Institute of Technology Zurich, Zurich, Switzerland

[2]Institute of Immunobiology, Kantonal Hospital St. Gallen, St. Gallen, Switzerland

[3]Pathology praxis, Zurich, Switzerland

Corresponding author:

Prof. Manfred Kopf, e-mail: manfred.kopf@biol.ethz.ch

Author contributions:

K.O. and M.Ko. designed the experiments; K.O. performed and analyzed most of the experiments; L.P., M.Ku., L.O. and C.S. performed and analyzed specific experiments; K.O., P.N., C.S, and M.Ko wrote the manuscript.

5.1.1 Abstract

Tissue resident macrophages play a crucial role in maintaining homeostasis. Recent studies show that macrophage progenitors migrate to tissues prenatally, where environmental cues shape their identity and unique functions. Here we present a novel key role for the nuclear transcription factor peroxisome proliferator-activated receptor gamma (PPARγ) in regulating the tissue-specific development of iron-recycling macrophages. We find that the developmental programs governed by PPARγ are different for the functionally distinct iron-recycling macrophages compared to alveolar macrophages, which have been previously reported to depend on this transcription factor. The absence of PPARγ leads to a strong reduction of red pulp macrophages (RPM) and bone marrow erythroid island macrophages (BMEIM) but the function of the few remaining cells seems not to be affected. Moreover, analysis of mice lacking Spi-C, another transcription factor indispensable for the maintenance of iron-recycling macrophages in adult mice, shows a minor role of this factor during the development of these cells. Although the RPM and BMEIM numbers are not changed upon Spi-C absence in young mice, the transcriptome is strongly affected. Similarities shared by *Pparg*- and *Spic*-deficient RPM allowed us to identify pathways, which rely on both factors. PPARγ and Spi-C collaborate in inducing transcriptional changes which could be required for progenitor retention in the tissue, allowing access to niche-related signals which finalize differentiation.

5.1.2 Introduction

Tissue resident macrophages are immune phagocytes present in almost all tissues [207-209]. In addition to general functions like pathogen clearance and tissue homeostasis (for a review, refer to [210, 211]), tissue resident macrophages are specialized to perform additional environment-imposed functions [212, 213]. The mechanisms underlying this adaptation to the tissue's needs are poorly understood. It has recently been discovered that macrophages develop from fetal progenitors and are able to homeostatically self-renew in adulthood [19, 36, 37, 48, 214]. Upon tissue seeding, which occurs before birth, progenitor cells receive environment-specific signals, such as cytokines or metabolites, which induce signaling cascades and a unique differentiation program leading to the development of specialized macrophages [58, 61, 62, 73, 215, 216]. PU.1 (encoded by the *Spi1* gene), a member of the ETS-domain containing family, has been shown to be an essential transcription factor for macrophage development [48]. It binds to both common and subset-specific genomic locations and is required for collaborative interactions with alternative sets of transcription factors induced by environmental triggers in each tissue-specific macrophage subset [61].

While fate-mapping studies have helped to understand the origin of macrophages, transcriptome and enhancer region analyses have provided crucial information about tissue-specific gene signatures [49, 50, 58, 61, 62]. For example, TGFβ-induced SMAD2/3 activation is crucial for microglia development [82, 217] while peritoneal macrophages depend on GATA6, which is induced by retinoic acid binding to the retinoic acid receptor beta (RARβ) [86]. Terminal differentiation of osteoclasts, a macrophage subset residing in bones and responsible for bone resorption, depends on NFATc1 activation via RANKL signaling [218]. In lungs, GM-CSF production by lung epithelial cells induces PPARγ, which is indispensable for alveolar macrophage (AM) differentiation from fetal monocytes [98, 99]. The spleen contains several macrophage subsets, including marginal zone macrophages (MZM), marginal metallophilic macrophages (MMM), and red pulp macrophages (RPM). MZM and MMM have been shown to be dependent on nuclear liver X receptor alpha (LXRα) that is activated by a so far unknown trigger [43]. RPM develop in a M-CSF dependent manner and rely on a PU.1-related factor (or Spi-C) [102, 136]. Similarly, Spi-C is needed for the development of a population of VCAM1-positive bone marrow macrophages [101], also known as bone marrow erythroid island macrophages

(BMEIM) due to their function in facilitating iron-recycling from senescent red blood cells (RBC), similar to RPM in the spleen [219]. Both RPM and BMEIM constitutively degrade hemoglobin and metabolize the highly oxidative intermediate product of this degradation – heme. The BTB domain And CNC Homolog 1 (Bach1) transcription regulator represses Spi-C expression in monocytes. It has been shown that heme can bind to Bach1, and heme-bound Bach1 is marked for proteasomal degradation. This results in Spi-C activation and macrophage differentiation [101].

In this study, we describe a previously unknown crucial role of PPARγ in RPM and BMEIM development. Surprisingly, although this factor is the main driver of perinatal alveolar macrophage differentiation, the programs induced by PPARγ in lung and spleen are distinct and in the case of the latter, are not related to lipid metabolism. Moreover, we show that upon tissue seeding, developing RPM downregulate migration-related markers and strongly upregulate integrin α_D, which is uniquely expressed by this macrophage subset and is correlated with cell retention [220].

5.1.3 Materials and methods

Mice

Spic^{tm1Kmm}*/J (Spic*$^{-/-}$*)* mice [102] (provided by Carsten Riether, University Bern) and *Pparg*$^{tm1.2Mtz}$*(Pparg*$^{fl/fl}$) mice [192] (originally provided by P. Chambon) were back-crossed for 8 generations to C57BL/6 before crossing to either *Lyz2Cre*$^{tm1(Cre)Ifo}$ *(LysM-Cre*) mice [221], *Tg(Itgax-cre)1-1Reiz (Cd11c-Cre*) mice [222], *B6.Cg-Tg(Vav1-Cre)A2Kio/J (Vav1-Cre*) mice [223], or *B6.Cg-Ndor1*$^{Tg(UBC-cre/ERT2)1Ejb}$*/2J (CreERT2*) [224] resulting in mice with PPARγ deficiency in myeloid cells (*LysM-Cre/Pparg*$^{fl/fl}$), CD11c^{+} cells (*Cd11c-Cre/Pparg*$^{fl/fl}$), hematopoietic cells (*Vav1-Cre/Pparg*$^{fl/fl}$), and all cells upon tamoxifen treatment (*CreERT2/Pparg*$^{fl/fl}$) were generated. For deletion of *Pparg* gene in *CreERT2/Pparg*$^{fl/fl}$ animals, 8-week old mice were injected with 2mg tamoxifen (Sigma-Aldrich) every other day for six times and analyzed four days later. *Gt(ROSA)26Sor*^{tm1Hjf} *(Rosa26-RFP*) mice, which contain Cre-inducible tdRFP [225], were crossed with *Vav1-Cre* in order to check the Cre activity. All animals were housed in individually ventilated cages under specific pathogen–free conditions at ETH Phenomic Center (EPIC, Zurich, Switzerland) and were used for experiments between 8 and 17 weeks of age unless otherwise stated. All animal experiments were approved

by the local animal ethics committee (cantonal veterinary office Zurich) and were performed according to local guidelines (Swiss Animal Protection Ordinance (TschV Zurich) and Swiss animal protection law (TschG)).

Cell suspensions

Mice were killed by CO_2 overdose. Organs were removed and cut into small pieces, then digested and passed through a 70-µm cell strainer. The spleens and fetal livers were digested for 30 min at 37 °C with 2 mg/ml of type IV collagenase (Worthington) and 50U/ml DNase I (Sigma-Aldrich). Adult livers were digested for 45 min at 37 °C with 2 mg/ml of type IV collagenase and 50U/ml DNase I. Liver cell suspensions were centrifuged at 20*g* for 5 min and the supernatants with reduced number of hepatocytes were resuspended in 30% Percoll (GE Healthcare) prior to density centrifugation at 2000 r.p.m. for 20 min at 25 °C, with low acceleration and no brake. Bone marrow was flushed from femur and tibia from mouse hindlimbs and passed through a 70-µm cell strainer. Erythrocytes were lysed with ACK (ammonium chloride–potassium bicarbonate) buffer.

Flow cytometry

The multiparameter analysis was performed with LSR Fortessa (BD), and followed by data analysis with FlowJo software (TreeStar). All fluorochrome-conjugated or biotinylated monoclonal antibodies used are listed in Supplemental Table 1. Dead cells were gated out using the viability marker eFluor780 (eBioscience). FcγIII/II receptors were blocked by incubation with anti-CD16/32 (2.4G2) purified from hybridoma supernatant (Swiss Federal Institute of Technology Zurich, Switzerland) before staining. PPARγ intracellular staining was performed using the Foxp3/Transcription Factor Staining Buffer Set according to the manufacturer's protocol (Thermo Fisher Scientific).

Cell sorting

Fetal liver cells were enriched for $CD45^+$ cells using MACS LS columns and anti-CD45 beads (both Miltenyi Biotec). Briefly, single cell suspensions were incubated with 10 µl of beads/10^7 cells for 15 min at 4°C followed by a wash with MACS buffer (PBS containing 1% BSA and 2mM EDTA [both from Sigma-Aldrich]). Pelleted cells were resuspended in 500µl of MACS buffer and loaded on equilibrated LS columns. Samples

were washed twice with gravity flow of 4ml MACS buffer and after removing columns from the magnetic field, the purified fraction was eluted. $CD45_+$ cells were later used for injections to *Vav1-Cre/Pparg$_{fl/fl}$* newborns in 10µl of PBS ($0.6x10_6$/newborn). Fluorescence-activated cell sorting of RPM/BMEIM for cytospins, RBC phagocytosis and RNAseq analysis was performed with a FACSAria IIIu (BD).

Quantitative real-time PCR

RNA was isolated with TRIzol reagent (Invitrogen) and reverse-transcribed with GoScript reverse transcriptase according to the manufacturer's instructions (Promega). The resulting cDNA was used for quantitative real-time PCR with KAPA SYBR FAST (Sigma-Aldrich) performed on an i-Cycler (Bio-Rad Laboratories). Expression was normalized to the house-keeping gene *G6PDX* expression and the values were calculated using the comparative threshold cycle method ($2^{-\Delta Ct}$). Primer sequences: *Spic* forward primer 5'-TCCGCAACCCAAGACTCTTCAA-3', reverse primer 5'-GGGTTCTCTGTGGGTGACATTCCAT-3'; for *Pparg* forward primer 5'-GTGATGGAAGACCACTCGCATT-3', reverse primer 5'- CCATGAGGGAGTTAGAAGGTTC-3'

Immunohistochemistry

Isolated spleens were fixed overnight in freshly prepared 4% PFA (MERCK Millipore) at 4°C under constant agitation. Fixed spleens were embedded in 4% agarose and cut with a vibratome (Leica VT-1200). 40µm sections were blocked with PBS supplemented with 10% FCS, 1 mg/ml anti-FcγR (BD Biosciences), and 0.1% Triton X-100 (Sigma-Aldrich) for 30 min at room temperature (RT). Next, a primary antibody mix containing anti-B220, anti-F4/80, anti-MOMA was added and samples were incubated in 4°C overnight. After washing with PBS supplemented with 2% FCS, 0.1% Triton X-100, secondary antibodies were applied for 1h, at RT. Stained sections were transferred onto slides and cover slips were mounted with Dako fluorescent mounting media (Dako). Microscopic analysis was performed using a confocal microscope (Zeiss LSM 710) and images were processed with ZEN 2010 software (Carl Zeiss Inc.).

RNA preparation and sequencing

1000 cells (RPM/BMEIM) were sorted directly into lysis buffer (0.2% Triton X-100, 2U/µl RNase inhibitor [New England Biolabs] in RNase-free water [Thermo Fisher Scientific]). RNA isolation and sequencing was performed as described before [226].

Briefly, oligo-dT primers and dNTPs were added to lysed cells and hybridization of the primer to poly(A) tails of all mRNA was performed at 72°C for 3 min. Next, samples were reverse transcribed with LNA-containing TSO primer (enabling template switching) and SuperScript II reverse transcriptase (Thermo Fisher Scientific) at 42°C for 90 min followed by ten cycles of 2 min intervals at 50°C and 42°C in order to increase efficiency and complete the reaction. cDNA was pre-amplified using ISPCR primers containing the matching sequence to the outer fragments of oligo-dT and TSO primers. Amplification was performed with 18 cycles of 20s denaturation at 98°C, 15s annealing at 67°C and 6min extension at 72°C with KAPA HiFi HotStart ReadyMix (Kapa Biosystems). PCR products were purified with AMPure XP beads (Beckman Coulter) and 1ng of the product was tagmented by using the Nextera XT DNA sample preparation kit (Illumina). Afterwards, the final enrichment with Index primers from the Nextera XT kit (Illumina) was performed for 8 cycles of 30s denaturation at 95°C, 30s annealing at 55°C and 30s extension at 72°C followed by purification with AMPure XP beads. Two nanomoles of each library were pooled for single-end DNA sequencing on a HiSeq4000 or NovaSeq instruments. Sequencing was performed at the Functional Genomics Center Zurich (FGCZ). The sequences were analyzed with SUSHI application [227]. In short, fragments were mapped to the ensemble mouse reference genome GRCm38 (Version25.06.2015) with the STAR aligner [228]. Values were then computed with the featureCounts function (Rsubread) [229] and differentially expressed genes were detected with the Bioconductor package edgeR [230]. For the volcano plot all genes with |log2 ratio| > 1.5 and FDR < 0.1 are presented as significant.

Gene Set Enrichment Analysis

Gene set enrichment analysis (GSEA) was performed with the GSEA v3.0 tool from Broad Institute [231, 232]. Gene Ontology (GO) gene sets for mouse were downloaded from http://baderlab.org/GeneSets (version from 2018-10-01). Only gene sets consisting of more than 3 genes were analyzed and the resulting enriched sets (with FDR q value <0.1) were visualized with Cytoscape 3.5.0 [233] with use of Enrichment Map plugin [234]. Clustering of gene sets was performed with AutoAnnotate 1.2.

Statistical analysis

All statistical analyses were performed with use of Prism software (GraphPad). Comparisons of two groups were calculated with unpaired two-tailed Student's t-tests. Differences with a p-value of <0.05 were considered significant.

5.1.4 Results

RPM numbers in Spic$^{-/-}$ mice are not affected early after birth

Spi-C is a signature transcription factor of RPM and adult mice lacking Spi-C are defective in development of RPM and also BMEIM, another important iron-recycling myeloid compartment that supports erythropoiesis as nurse cells and shares a transcriptional program with RPM [101]. However, since most resident macrophages develop perinatally from fetal precursors, we have revisited the role of Spi-C for RPM and compared newborn *Spic*$^{-/-}$ to wild-type (WT) counterparts. First, we confirmed strong reduction of RPM and BMEIM in adult *Spic*$^{-/-}$ mice (Figures 1A and S1A). To our surprise, the number of RPM and BMEIM in 7 days old animals were unaffected by the lack of Spi-C (Figures 1B and S1B). In order to understand why this population disappears in aged animals, we compared the transcriptomes of RPM derived from *Spic*$^{-/-}$ and WT mice. Spi-C deficiency changed the expression of 1447 genes more than 2.8-fold (Figure 1C). Genes whose expression was strongly reduced in *Spic*$^{-/-}$ RPM were particularly enriched for genes previously described to define RPM identity [58] (Figure 1D). Most of genes related to iron metabolism were also decreased in Spi-C-deficient RPM (Figure 1E), indicating a functional disability of the *Spic*-deficient RPM and a possible cause for their loss in adult mice. Interestingly, we noted a significant reduction in PPARγ mRNA expression, a transcription factor previously reported to be crucial for AM differentiation [99]. *Spic*-deficient RPM and BMEIM also showed a significant decrease in PPARγ protein expression (Figures 1F-G and S1C-D). These results suggest that Spi-C is not critical for early stages of RPM and BMEIM development but is required for their maintenance and functionality. However, reduced expression of PPARγ in RPM from neonatal Spi-C-deficient mice may indicate that this transcription factor is an important regulator of RPM differentiation.

Figure 1

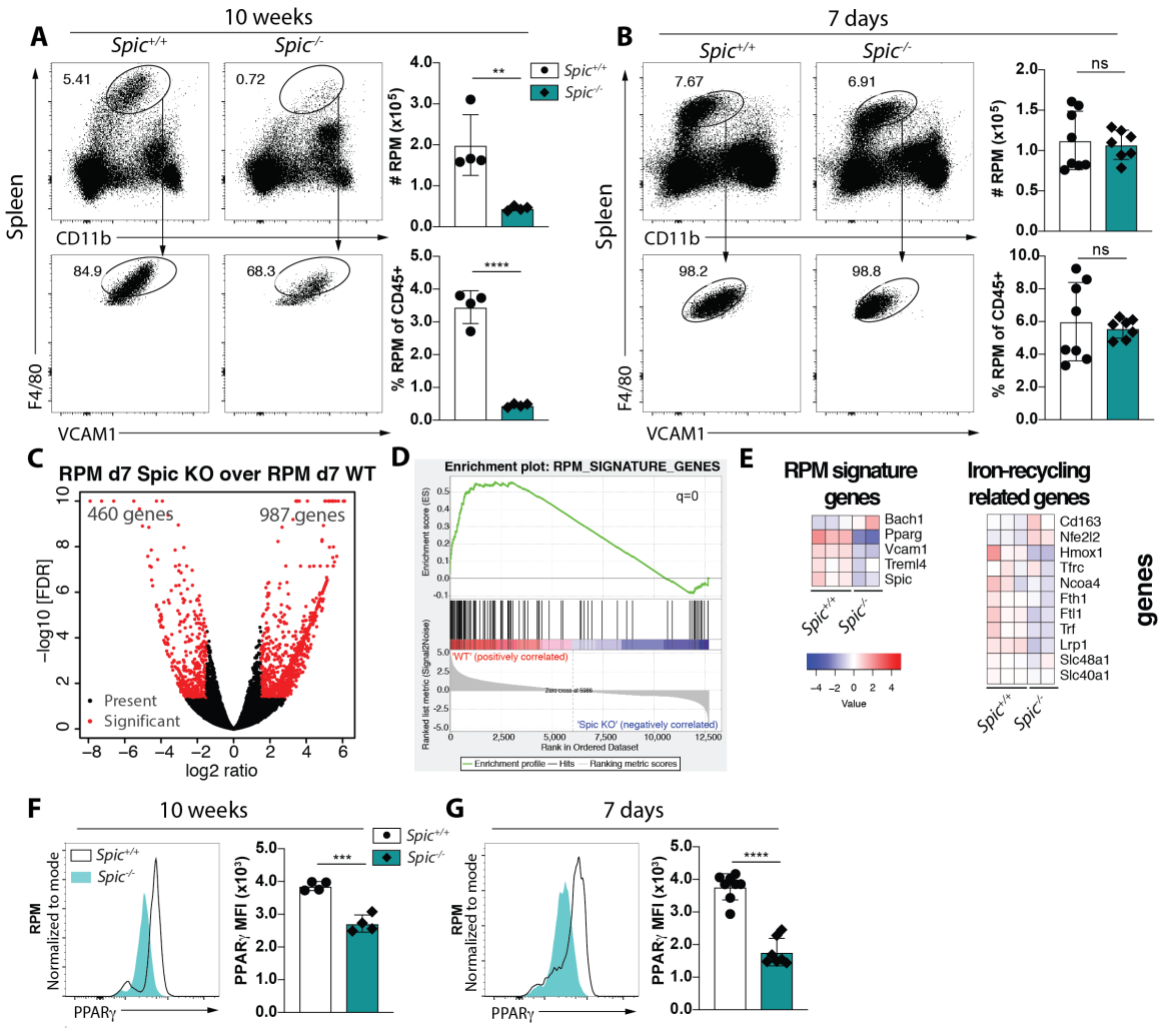

Figure 1. RPM numbers in *Spic*$_{-/-}$ mice are not affected early after birth. (A, B) Flow cytometry of spleen for 10 weeks old (A) and 5-7 days old (B) *Spic*$_{+/+}$ and *Spic*$_{-/-}$ mice; plots supplemented with bar graphs showing RPM counts and their frequencies of CD45$_{+}$ cells; RPM pregated as live CD45$_{+}$ cells. (C) Volcano plot showing differentially expressed genes between *Spic*$_{+/+}$ and *Spic*$_{-/-}$ RPM (|log2 ratio|>1.5; FDR<0.05); cells isolated from 7 days old animals. (D) Gene set enrichment plot for RPM gene signature; RPM gene signature list derives from Gautier *et al.* [58]; the false discovery rate (FDR) q value is shown in the top right corner of the plot. (E) Heat maps showing top RPM signature genes and genes related to iron-recycling. (F, G) Histograms and mean fluorescence intensity (MFI) of PPARγ expression in RPM derived from 10 weeks old (F) and 5-7 days old (G) *Spic*$_{+/+}$ and *Spic*$_{-/-}$ mice. Ns, not significant; *P<0.05; **P<0.01; ***P<0.001 (unpaired two-tailed Student's t-test). The presented data are from a single experiment (C-E) or pooled data from three independent experiments (A, B, F, G; mean and s.d. from four to eight mice per group).

PPARγ deficient animals lack iron-recycling macrophages

To test the hypothesis that PPARγ is important for RPM development, we used a *Vav1-Cre/Pparg$^{fl/fl}$* mouse line that efficiently deletes PPARγ in all hematopoietic cells, including differentiating fetal monocytes [99]. The development of RPM and BMEIM (characterized as F4/80^{+}CD11b^{int}VCAM1^{+} cells) is considerably impaired in *Vav1-Cre/Pparg$^{fl/fl}$* mice (Figure 2A and B). Notably, *CD11c-cre/Pparg$^{fl/fl}$* mice and *LysM-Cre/Pparg$^{fl/fl}$* mice showed no significant reduction of RPM and BMEIM (Figures S2A-S2C), most probably due to poor *CD11c* and *LysM* promoter-driven Cre recombinase expression and accordingly inefficient PPARγ deletion in macrophages. In contrast, *Vav1-Cre* expression in *ROSA26-RFP* reporter mice induced deletion of a loxP flanked stop cassette and RFP expression in >95% RPM without Cre toxicity (Figure S2D). Immunohistology of spleens confirmed the almost complete absence of F4/80^{+} cells in the red pulp of *Vav1-Cre/Pparg$^{fl/fl}$* mice, while CD169^{+} marginal metallophillic macrophages (MMM), localized at the interface of white pulp and red pulp, were unchanged from WT controls (Figure 2C). RPM are critical for phagocytosis of senescent red blood cells and iron-recycling. Consistent with the loss of RPM, *Vav1-Cre/Pparg$^{fl/fl}$* mice accumulated ferric iron in the spleen (Figure 2D). Nevertheless, red blood cell (RBC) and reticulocyte number, mean corpuscular volume (MCV), hematocrit (HCT), and hemoglobin (HGB) were unaffected in circulating blood of *Vav1-Cre/Pparg$^{fl/fl}$* mice (Figure 2E).

RPMs require PPARγ intrinsically for their development

Most tissue macrophages arise during perinatal development [32]. Indeed, we noted a 20-fold expansion of RPM between days 2 and 5 (Figure 3A). PPARγ expression was concomitantly upregulated (Figure 3B and C). To assess whether PPARγ regulates postnatal RPM development, we analyzed RPM populations in *Vav1-Cre/Pparg$^{fl/fl}$* mice and littermate controls at different days after birth. While the absence of PPARγ negatively influenced the postnatal expansion of RPM (Figure 3A and S3A), this reduction did not significantly affect the total number of splenocytes (Figure S3B). The frequency of Ly6C^{+} monocytes was increased in neonatal *Vav1-Cre/Pparg$^{fl/fl}$* mice and inversely corresponded to the decrease in RPM (Figure S3C and D). Although *Vav1-Cre/Pparg$^{fl/fl}$* mice lack PPARγ in all hematopoietic cells, the numbers of B cells, T cells, DC and other

myeloid subsets in spleen and blood were not changed in adult mice (Figure S4A and B), in support of a direct role of PPARγ for RPM differentiation.

Figure 2

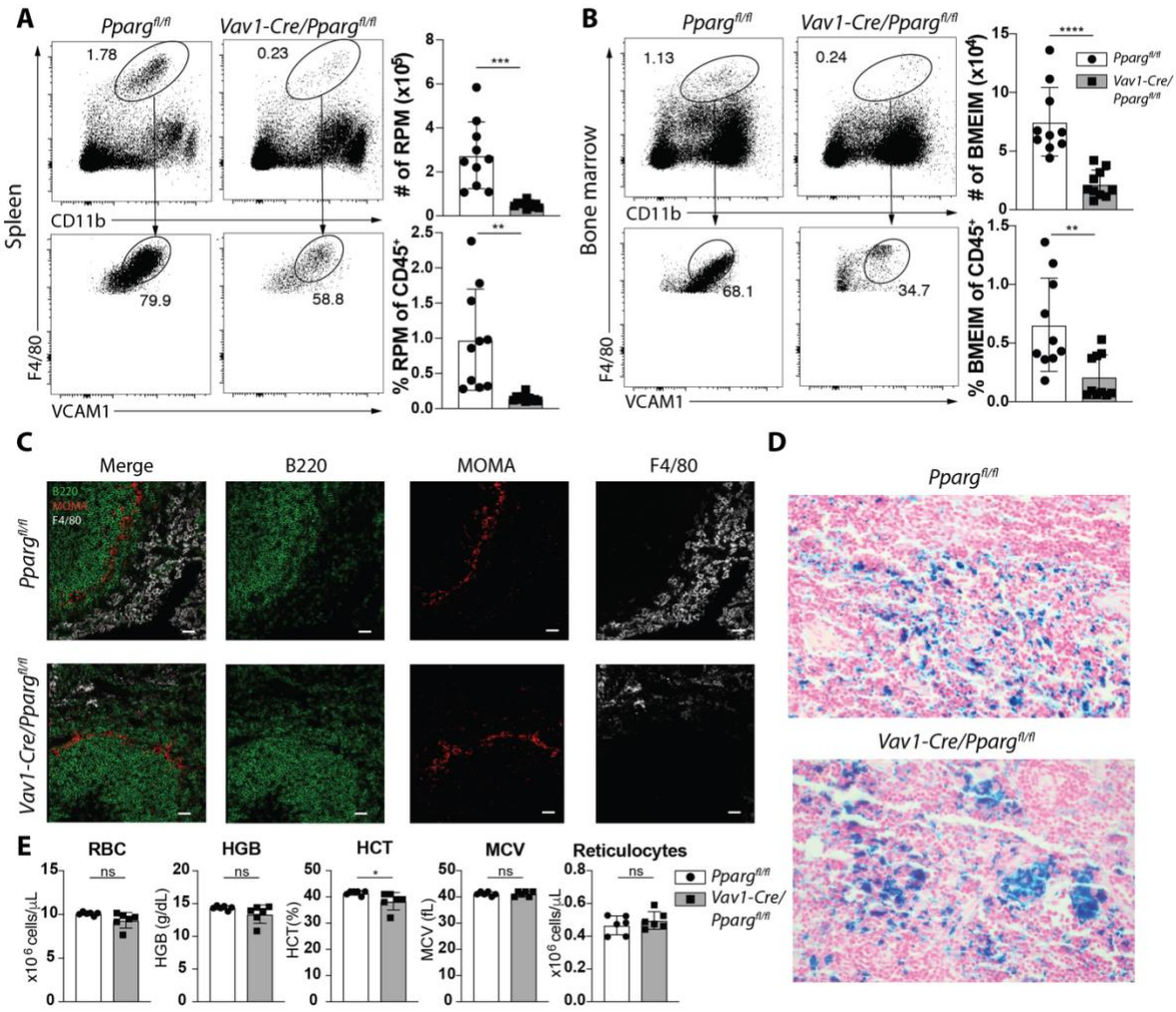

Figure 2. PPARγ deficient animals lack iron-recycling macrophages. (A, B) Flow cytometry plots of spleen (A) and BM (B) from *Pparg$_{fl/fl}$* and *Vav1-Cre/Pparg$_{fl/fl}$* animals and bar graphs showing RPM/BMEIM counts and their frequencies of CD45$_+$ cells; RPM/BMEIM pregated as live CD45$_+$ cells. (C) Images of immunohistochemistry staining of B220 (B cell marker), MOMA (metallophillic macrophage marker) and F4/80 (RPM marker) on splenic sections; white scale bars indicate 25 μm. (D) Representative microscopic images of splenic sections stained with Perls' Prussian Blue to demonstrate ferric iron deposits; the original magnification is 40x. (E) Comparison of the number of reticulocytes and red blood cells (RBC), hemoglobin (HGB), hematocrit (HCT), and mean corpuscular volume (MCV) of RBC from blood test of *Pparg$_{fl/fl}$* and *Vav1-Cre/Pparg$_{fl/fl}$* animals. **P<0.01, ***P<0.001 and ****P<0.0001 (unpaired two-tailed Student's t-test). The presented data are pooled from three independent experiments (A–B; mean and s.d. of ten mice per group) or are representative of three independent experiments (D; mean and s.d. of three to five mice per group).

The fetal liver contains progenitors with the capacity to give rise to multiple types of tissue macrophages [42]. To assess a cell autonomous requirement of PPARγ for RPM development, we sorted CD45+ cells from the fetal liver of E14.5 WT embryos (CD45.1) and injected them into newborn *Vav1-Cre/Pparg$^{fl/fl}$* and *Pparg$^{fl/fl}$* mice. Eight weeks later, RPM in *Vav1-Cre/Pparg$^{fl/fl}$* mice were completely restored with cells derived from transferred WT fetal precursors (Figure 3D-F). Notably, transferred cells did not contribute to macrophages in the liver (Figure S5A and B). Overall, our data demonstrate an intrinsic requirement for PPARγ in the perinatal development of RPM.

Figure 3

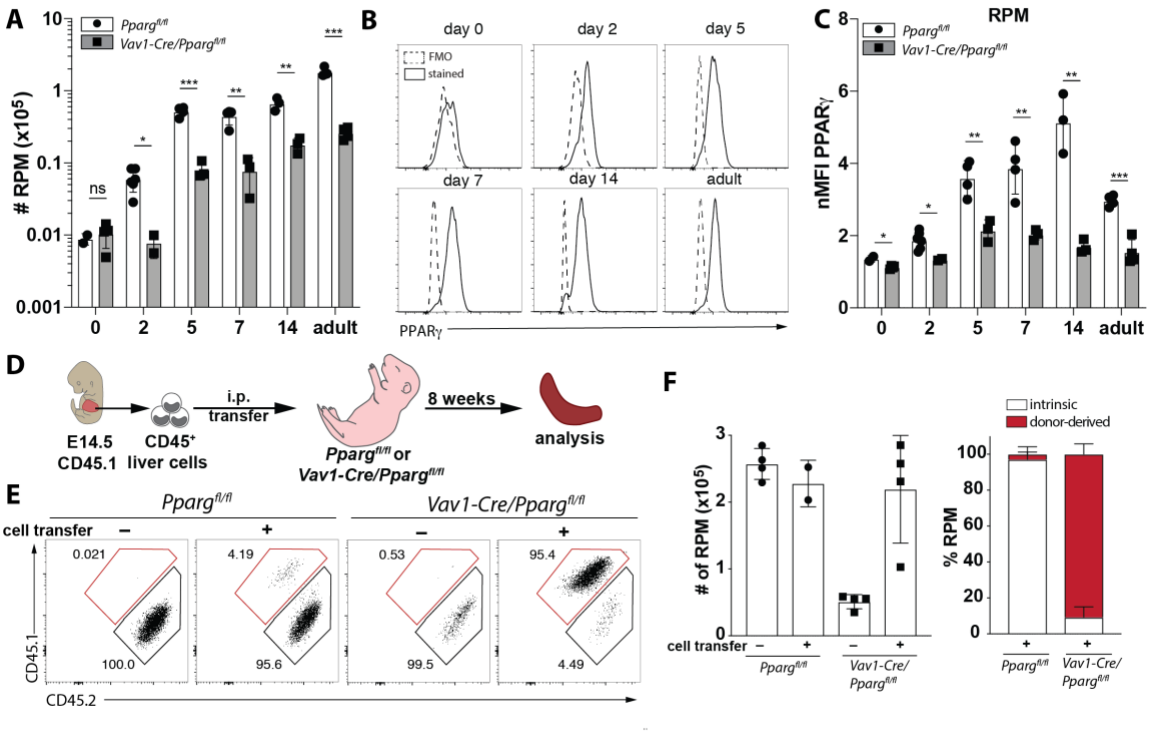

Figure 3. RPM require PPARγ intrinsically for their development. (A) Total cell counts of RPM from *Pparg$^{fl/fl}$* and *Vav1-Cre/Pparg$^{fl/fl}$* animals at different days after birth; gated as in Figure 2A. (B) Representative histograms of PPARγ expression by RPM from *Pparg$^{fl/fl}$* animals. (C) MFI of PPARγ expression by RPM at different days after birth, MFI normalized to fluorescence minus one (FMO) controls. (D) Graphical presentation of experiment designed to test the intrinsic requirement of PPARγ for RPM development; CD45+ cells were sorted from fetal livers of E14.5 embryos (CD45.1) and subsequently transferred to *Pparg$^{fl/fl}$* and *Vav1-Cre/Pparg$^{fl/fl}$* newborns, analysis of the RPM reconstitution was performed 8 weeks post-transfer. (E) Dot plots showing RPM origin in recipient mice 8 weeks post-transfer; RPM are gated as live CD11b^{int}F4/80+VCAM1+CD11c^{lo}; red gates indicate CD45.1+ RPM (derived from transferred fetal progenitors). (F) RPM counts supplemented with frequencies of donor-derived and

(legend continued on the next page)

intrinsic RPM for transferred animals. Ns, not significant; *P<0.05 **P<0.01 and ***P<0.001 (unpaired two-tailed Student's t-test). The presented data are from single experiments (A-F; mean and s.d. of two to five mice per group).

PPARγ is not required for proper function of RPM

Although RPM and BMEIM were drastically reduced in the absence of PPARγ, we noted a small remaining population with comparable surface marker expression (Figure 2A and B). To better characterize the transcriptional program that is regulated by PPARγ in RPM and BMEIM, we sorted the remaining F4/80^{hi}VCAM1^{+}CD11b^{int} population from the spleen and BM of 7 days old *Vav1-Cre/Pparg$^{fl/fl}$* mice and compared their transcriptome to *Pparg*-sufficient RPM and BMEIM from littermate controls using RNAseq (Figure 4A and S6A). Volcano plots in Figures 4B and S6B represent the expression fold-change and adjusted p-values of the dysregulated genes in RPM and BMEIM with 256 and 269 genes being downregulated in *Pparg*-deficient RPM (Figure 4B) and BMEIM (Figure S6B), respectively. In contrast, the expression of 229 and 108 genes was strongly elevated when compared to WT RPM (Figure 4B) and BMEIM (Figure S6B), respectively (|log2 ratio|>1.5, FDR<0.05). Despite many dysregulated genes, *Vav1-Cre/Pparg$^{fl/fl}$*-derived RPM did not differ morphologically from their WT counterparts (Figure 4C), although the cell size seems to be increased. GSEA analysis comparing genes with altered expression in the *Pparg*-deficient RPM with previously identified RPM signature genes [58] showed a strong overlap (Figure 4D), indicating that PPARγ signaling is crucial for establishing the RPM identity. However, *Spic*, *Vcam1* and *Treml4,* as well as genes related to iron metabolism, were either not changed or slightly decreased (Figure 4E). RNAseq data indicated increased levels of *Pparg* transcripts but real time PCR confirmed the efficient recombination of the *Pparg* locus in *Vav1-Cre/Pparg$^{fl/fl}$*-derived RPM (Figure 4F). We concluded that Cre-mediated deletion allowed production of a non-functional truncated transcript. Additionally, we checked *Spic* levels and confirmed a minor downregulation of its expression (Figure 4F). The ability of *Pparg*-deficient RPM-like cells to phagocytose labelled red blood cells (RBCs) *in vivo* (Figures S7A-D) and *in vitro* (Figure S7E) was comparable to WT counterparts, but due to fewer RPM in *Vav1-Cre/Pparg$^{fl/fl}$* mice, RBCs were cleared less efficiently (Figure S7A). Moreover, Kupffer cells (KCs), which should help in degrading damaged RBCs, were not more active in the *Vav1-Cre/Pparg$^{fl/fl}$* mice (Figure S7C and D). Thus, it appears that a few

RPM can develop independently of PPARγ but this is not sufficient to allow an efficient clearance of senescent RBCs and the reuse of iron.

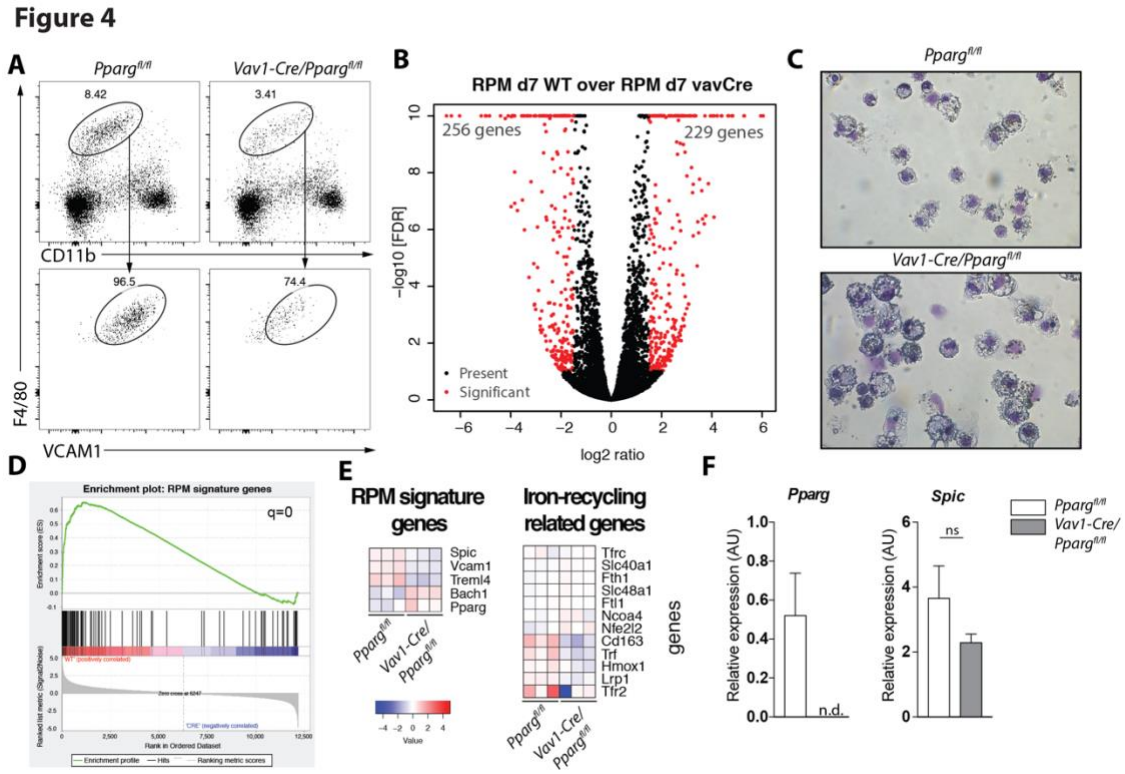

Figure 4. PPARγ is not required for RPM function. (A) Flow cytometry of spleens derived from 7 days old *Pparg*$_{fl/fl}$ and *Vav1-Cre/Pparg*$_{fl/fl}$ animals used for RNAseq analysis. (B) Volcano plot showing differentially expressed genes between *Pparg*$_{fl/fl}$ and in *Vav1-Cre/Pparg*$_{fl/fl}$ RPM (|log2 ratio|>1.5; FDR<0.05). (C) Cytospins of sorted RPM; original magnification 20x. (D) Gene set enrichment plots for the RPM gene signature; the RPM gene signature list is from Gautier *et al.* [58]; the FDR q value is shown in the top right corner of the plot. (E) Heat maps showing the top RPM signature genes and genes related to iron-recycling. (F) *Pparg* and *Spic* mRNA expression in sorted RPM from *Pparg*$_{fl/fl}$ and *Vav1-Cre/Pparg*$_{fl/fl}$ animals; values are normalized to a house-keeping gene (*G6PDX*). Ns, not significant (unpaired two-tailed Student's t-test). The presented data are from single experiments (B-E) or representative of three independent experiments (A, F; mean and s.d. of three to five mice per group).

PPARγ controls genes related to migration and chemotaxis

The literature provides experimentally validated PPARγ target genes, mainly from studies using PPARγ-driven adipocyte differentiation as a model [185, 187]. We used publicly available ChIPseq data for PPARγ (collected by Chip-Atlas.com) in order to test whether which known target genes are also affected in RPM upon loss of PPARγ expression. Using the 1000 top PPARγ target genes from all available ChIPseq data as a gene set of interest, GSEA analysis revealed a significant association with genes whose

Figure 5

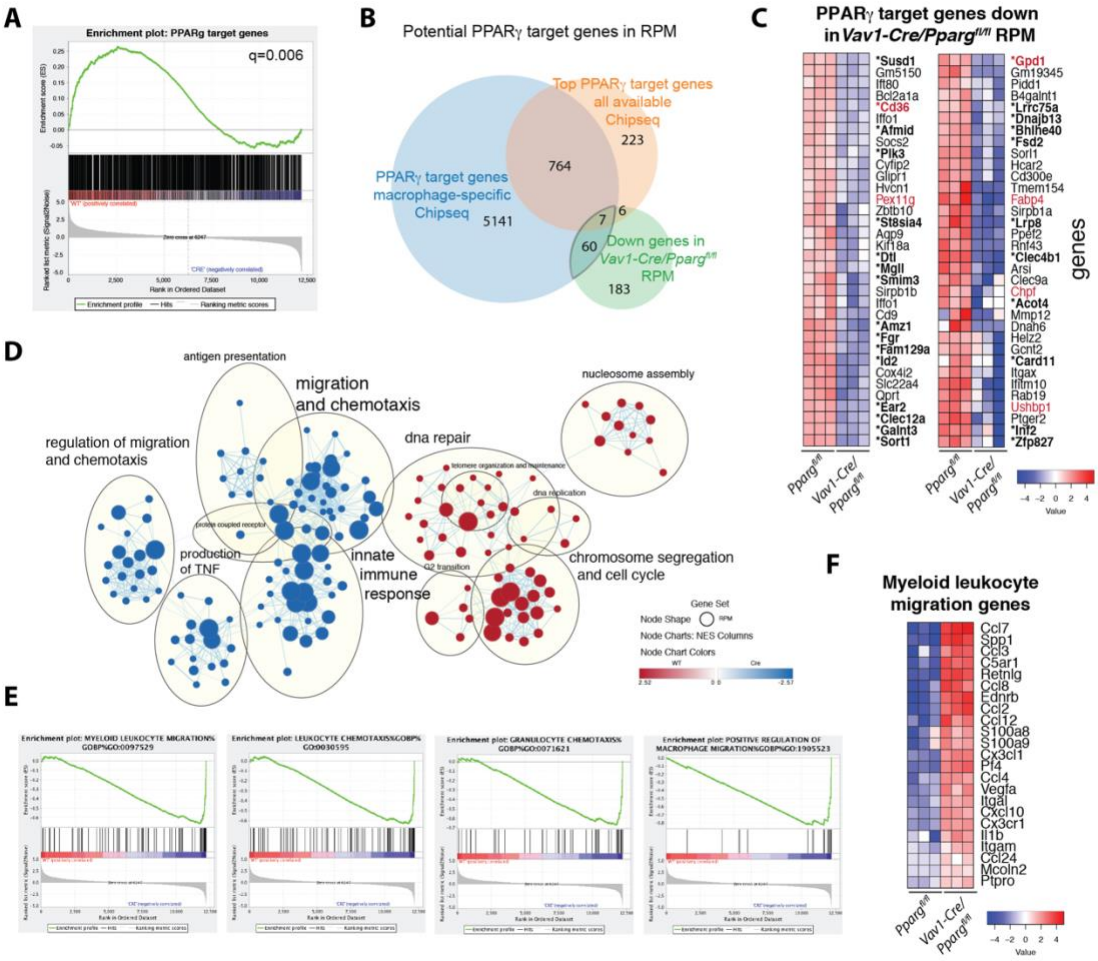

Figure 5. PPARγ deficiency leads to increased expression of genes related to migration and chemotaxis. (A) Gene set enrichment plots for PPARγ target genes; the PPARγ target genes are from Chip-Atlas.org/target-genes; 1000 top genes from all available data sets were used; the FDR q value is shown in the top right corner of the plot. (B) Venn diagram comparing the PPARγ target gene list (from Chip-Atlas.org/target-genes, 1000 top genes from all available data sets) with PPARγ target genes from macrophage-specific ChIPseq (from Chip-Atlas.org/target-genes, from experiment SRX769794) and with the genes downregulated in *Vav1-Cre/Pparg$^{fl/fl}$* RPM compared to *Pparg$^{fl/fl}$* (log2 ratio<-1.5; FDR<0.1). (C) Heat map showing macrophage-specific PPARγ target genes downregulated in *Vav1-Cre/Pparg$^{fl/fl}$* RPM; starred bold gene names are genes overlapping with PPARγ targets discovered in BMEIM, red gene names are the 7 genes overlapping between the genes downregulated in *Vav1-Cre/Pparg$^{fl/fl}$* RPM, the top 1000 targets, and all macrophage-specific ChIPseq target genes. (D) Gene Ontology (GO) term enrichment maps for Biological Process (BP) from *Pparg$^{fl/fl}$* and *Vav1-Cre/Pparg$^{fl/fl}$* RPM; the maps show the top enriched gene networks with the FDR q value <0.1; the line thickness connecting two gene set nodes corresponds to the number of genes overlapping between the two sets, red nodes – gene sets enriched within genes strongly reduced in *Vav1-Cre/Pparg$^{fl/fl}$* RPM, blue nodes – gene sets enriched within genes strongly upregulated in

(legend continued on the next page)

Vav1-Cre/Pparg$^{fl/fl}$ RPM compared to WT RPM. (E, F) Four top gene set enrichment plots for *Vav1-Cre/Pparg*$^{fl/fl}$ RPM (E) supplemented with heat map showing core genes from the myeloid leukocyte migration gene set (F). The presented data are from a single experiment with three mice per group.

expression was reduced in *Pparg*-deficient cells (Figure 5A and S6C). However, comparison of the significantly reduced genes in *Vav1-Cre/Pparg*$^{fl/fl}$–derived RPM and BMEIM (log2 ratio<-1.5; FDR<0.1) with the genes predicted to be directly regulated by PPARγ, based on the binding profiles of publicly available macrophage-specific ChIPseq data (genes with a positive score from ChIPseq experiment SRX769794 from Chip-Atlas.com) revealed 67 genes for RPM and 61 genes for BMEIM that are known to be PPARγ targets (Figures 5B and S6D). Twenty-seven of these genes were common for RPM and BMEIM (marked bold and with an asterisk in Figures 5C and S6E). Additionally, the experimentally confirmed PPARγ target gene set in macrophages encompasses 77% of the genes scored as top PPARγ targets among all available ChIPseq data, but only 7 genes were present in all compared sets (Figure 5B, S6D and marked red in Figure 5C and S6E). These data indicate that PPARγ may induce distinct signaling pathways and facilitate processes in these cells, not related to the functions known from the literature, such as lipid metabolism or fatty acid oxidation. Therefore, we performed GSEA on Gene Ontology (GO) gene sets and noticed that genes related to cell migration and chemotaxis, as well as to the innate immune response, were strongly enriched in *Pparg*-deficient RPM and BMEIM, whereas gene sets related to DNA repair, replication and recombination were significantly reduced (Figure 5D-F and S6F-G).

PPARγ maintains RPM identity throughout life

Although multiple macrophage markers, including *F4/80, Sirpa*, and *Mertk*, remained unchanged or were only slightly affected in mRNA expression in the absence of PPARγ, we noted a strong increase in the expression of *C5ar1, Cx3cr1*, *Itgam* and *Itgal* (Figure 6A). Notably, *Pparg*-deficient RPM expressed high surface levels of CD88 (encoded by the *C5ar1* gene). Similar effects were observed in BMEIM (Figure 6B and C). We further confirmed the correlation between high CD88 levels and PPARγ deficiency by crossing *Pparg*$^{fl/fl}$ mice with Ubc-Cre mice (*CreERT2/Pparg*$^{fl/fl}$) enabling temporally controlled deletion of PPARγ. Although, we did not observe a reduction of RPM and BMEIM numbers in tamoxifen-treated *CreERT2/Pparg*$^{fl/fl}$ mice (Figure 6D), CD88 upregulation was readily detectable four days after tamoxifen treatment (Figure 6E and F), which correlated with efficient recombination of the *Pparg* floxed allele (Figure S8A) and decrease in PPARγ

protein expression (Figure 6G). Interestingly, deletion of *Pparg* induced an influx of Ly6C- monocytes into the spleen (Figure S8B) but no change in this population was seen in the BM (Figure S8C).

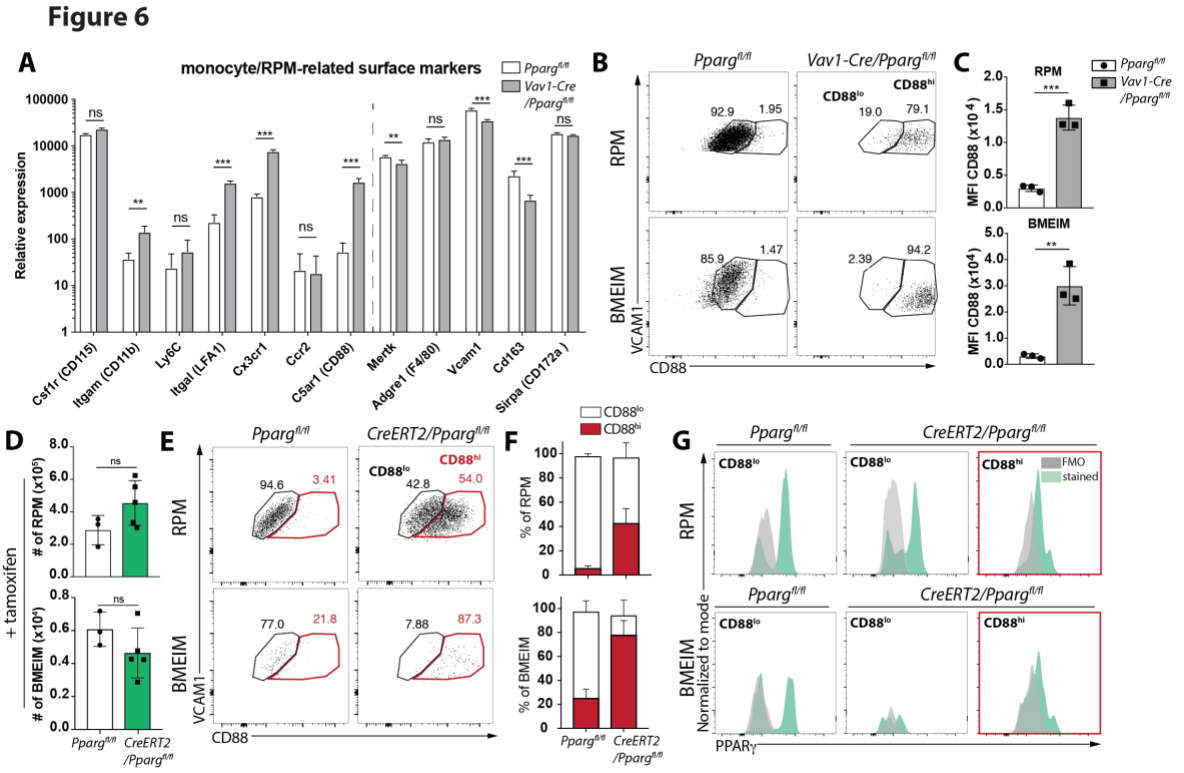

Figure 6. PPARγ is required to maintain RPM and BMEIM identity. (A) Relative expression of transcripts of the indicated surface markers characteristic for monocytes or macrophages. (B, C) Expression of CD88 on *Pparg*$^{fl/fl}$ and *Vav1-Cre/Pparg*$^{fl/fl}$-derived RPM and BMEIM detected by flow cytometry (B) and plotted as a mean fluorescence intensity (MFI) in graph (C). (D-G) 8 weeks old *Pparg*$^{fl/fl}$ and *CreERT2/Pparg*$^{fl/fl}$ mice were treated with tamoxifen every other day for 2 weeks and analyzed four days later, cell numbers of RPM and BMEIM (D), changes in CD88 expression (E), frequencies of CD88^{hi} and CD88^{lo} cells (F), and PPARγ expression (G) within the two populations are shown. For A: ns, not significant; *FDR<0.05 **FDR<0.01 ***FDR<0.001. Presented data are from a single experiment with three mice per group. For B-G: Ns, not significant; *P<0.05 **P<0.01 ***P<0.001 (unpaired two-tailed Student's t-test). The presented data are representative from three independent experiments (C, D, F; mean and s.d. from three to five mice per group).

RPM develop mainly from *Myb*-dependent progenitors, most likely fetal monocytes [36, 48]. Fetal monocytes and macrophages express high levels of CD88 (Figure S9A), while in the adult WT spleen, only neutrophils and Ly6C- monocytes are highly positive for this marker (Figure S9B). RPM and Ly6C+ monocytes express it to a lower extent, while DCs, B cells, and T cells are negative (Figure S9B). CD88 expression is very high on

different tissue macrophages (Figure S9C and D), implying that only some subsets downregulate CD88 at later stages of development. Taken together, these results indicate that loss of PPARγ expression might lead to RPM identity loss, apparent by the upregulation of CD88, or to the influx of new cell lineages which either do not depend on PPARγ expression or are partially blocked in development.

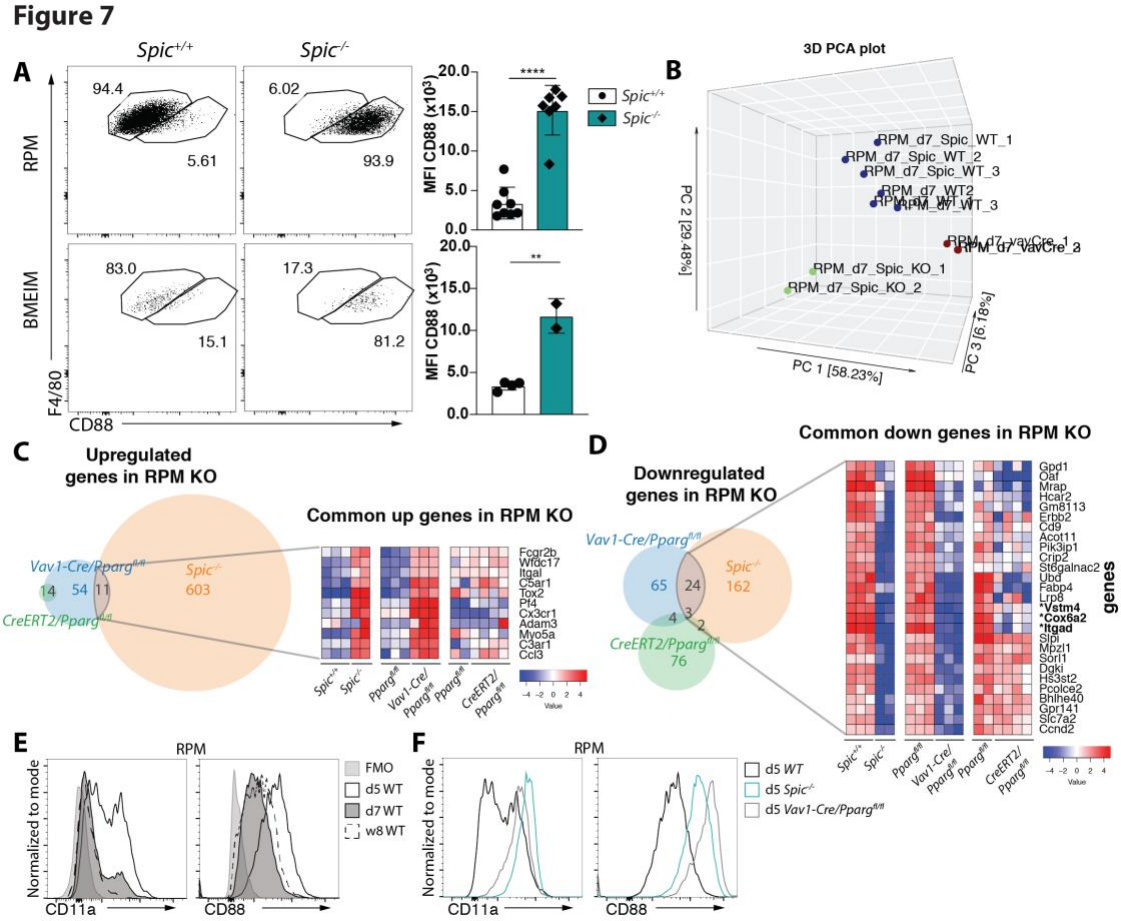

Figure 7. Co-expression of PPARγ and Spi-C is necessary for induction of the last differentiation steps during RPM development. (A) Representative dot plots of CD88 expression on RPM and BMEIM from *Spic+/+* and *Spic-/-* mice supplemented with mean fluorescence intensity (MFI) of CD88. (B) Principal component analysis of the four sorted populations (*Ppargfl/fl*, *Vav1-Cre/Ppargfl/fl*, *Spic+/+* and *Spic-/-*); colors were assigned to each cluster. (C, D) Venn diagrams comparing upregulated (C) or downregulated (D) genes in RPM derived from *Vav1-Cre/Ppargfl/fl*, *Spic-/-*, and *CreERT2/Ppargfl/fl* mice (after tamoxifen administration) when compared to WT counterparts (|log2 ratio|>2.5; FDR<0.05); the results are accompanied with heatmaps presenting 11 upregulated (C) or 27 downregulated genes (D) shared by *Vav1-Cre/Ppargfl/fl* and *Spic-/-* RPM with three gene names in bold (and starred) shared by all three deficient RPM populations. (E) Representative histograms of CD11a (gene name *Itgal*) and CD88 (gene name *C5ar1*) expression during WT RPM maturation (F) Representative histograms of CD11a and CD88 expression for

(legend continued on the next page)

RPM of indicated genotypes at day 5 post-birth. **P<0.01 ****P<0.0001 (unpaired two-tailed Student's t-test). The presented data are representative of two independent experiments (A; mean and s.d. from two to seven mice per group) or from a single experiment (B-F).

Co-expression of PPARγ and Spi-C is necessary to induce the last differentiation steps during RPM development

The dependence of RPM development on PPARγ and the consequences of its absence manifest similarly to the phenotype detected in adult *Spic*$^{-/-}$ mice. Given the decreased levels of PPARγ in RPM from young *Spic*-deficient mice, we speculated that these cells are somewhat similar to the ones detected in *Vav1-Cre/Pparg*$^{fl/fl}$ newborns. We confirmed high CD88 expression on *Spic*$^{-/-}$ RPM and BMEIM (Figure 7A). This similarity led us to compare RPM transcriptomes. Principle component analysis (PCA) assigned all RPM samples into three distinct clusters with all WT RPM in one cluster separated from *Spic*- and *Pparg*-deficient RPM along the first two components (Figure 7B). This analysis also revealed additional differences between knockout (KO) RPM, but we focused on similarities between the two. We examined the overlap between highly dysregulated genes (|log2 ratio|>2.5, FDR<0.05) from *Spic*- and *Pparg*-deficient RPM. We included genes derived from adult *CreERT2/Pparg*$^{fl/fl}$ CD88^{hi} RPM which appear after tamoxifen treatment (Figures 7C and D). Significantly upregulated genes shared between *Spic*$^{-/-}$ and *Vav1-Cre/Pparg*$^{fl/fl}$ RPM included *C5ar1, Itgal* and *Cx3cr1*, genes connected with a phenotype of patrolling monocytes (Figure 7C). Among downregulated genes, 27 were shared between the two sets (Figure 7D). The strongest gene reduction, common to all three cell subsets, was the gene encoding integrin α_D (*Itgad*). Interestingly, the *Itgad* promoter contains several predicted binding sites for PPARγ and could be a novel target of this transcription factor. We traced changes in CD88 and CD11a (encoded by *Itgal* gene) protein expression on WT RPM at different time points (Figure 7E). Indeed, both markers are downregulated between days 5 and 7 post-birth, while this downregulation is abrogated in both KO RPM (Figure 7F). Notably, *Spic*- and *Pparg*-deficient RPM express similar levels of CD11b and VCAM1 which are higher or lower, respectively, when compared to WT controls derived from age-matched littermate controls (Figure S10A).

5.1.5 Discussion

Recent studies have identified signature transcription factors important for the differentiation of a variety of cell types and have elucidated the mechanism by which

environmental signals trigger their expression [43, 82, 83, 86, 99, 235]. To our knowledge, we are the first to describe the dependency of different tissue resident macrophage subsets (iron-recycling macrophages and alveolar macrophages) on the same transcription factor (PPARγ), even though the macrophages have seemingly different functions.

Alveolar macrophages (AM) start to develop perinatally from yolk sac-derived fetal liver monocytes [98, 99]. Sensing of GM-CSF produced mainly by alveolar epithelial cells induces PPARγ activation and consequent transcriptional changes of target genes that orchestrate terminal differentiation and functional specialization. Deletion of *Pparg* at birth (induced by CD11c-cre), arrests AM development at the level of a dysfunctional pro-AM with defects in lipid metabolism [99]. The two other *Pparg*-dependent macrophage populations reported here, splenic red pulp macrophages (RPM) and bone marrow erythroid islands macrophages (BMEIM), share iron-recycling function. RPM derive from fetal liver monocytes and are long-lived [42]. Their development from monocytes has been shown previously to depend on another transcription factor, Spi-C [102]. Spi-C is constantly repressed in monocytes by Bach1 but is released upon increasing levels of heme, an intermediate product of hemoglobin degradation. Heme binds to Bach1 and marks the transcriptional repressor for proteasomal degradation [101]. Interestingly, we show that *Spic* is dispensable for RPM and BMEIM expansion that occurs in the first week after birth. Nonetheless, *Spic*$^{-/-}$ RPM differ significantly from their WT counterparts on the transcriptomic level. Expression of genes related to iron metabolism, like heme oxygenase 1 (*Hmox1*), ferritin (*Fth1, Ftl1*) and ferroportin (*Slc40a1*) is decreased, indicating compromised functionality of *Spic*$^{-/-}$ RPM. Similarly, *Hmox1*$^{-/-}$ mice lose iron-recycling macrophage populations with time, because they are unable to break down cytotoxic heme leading to elevated oxidative stress and cell death [155].

The lack of Spi-C or PPARγ expression leads to a similar phenotype in adult animals. Both *Spic*$^{-/-}$ and *Vav1-Cre/Pparg*$^{fl/fl}$ mice have strongly reduced RPM and BMEIM populations and accumulate iron in the spleen and the bone marrow, while their blood contains normal levels of erythrocytes. Also, the decrease in RPM does not influence the cellular composition of the spleen, indicating that deletion of PPARγ in other immune cells (driven by the Vav1-Cre) did not change the cell composition and indirectly cause

the loss of RPM. To definitely exclude this possibility, we experimentally confirmed that PPARγ is required intrinsically for RPM development.

PPARγ full knockout mice are embryonically lethal [236]. Using the Cre-loxP system, PPARγ deficiency has been studied in various cell subtypes and was identified as a master regulator of adipocyte differentiation [237]. Studies addressing the importance of PPARγ in the immune system show that this nuclear receptor is essential for alveolar macrophage development [99] and M2 macrophage polarization [196]. Also, PPARγ licenses DCs to prime Th2 cells and becomes the master regulator of pathogenic Th2 cells during allergic asthma [206]. PPARγ is highly expressed in alveolar and splenic macrophages but it is low in most of other hematopoietic cells in steady-state [238]. We show that PPARγ starts being expressed by RPM during the first few days after birth and persists at high levels in adulthood. This increasing expression within the first days of life correlates with an abrupt expansion of this subset and a marked defect in RPM counts when PPARγ is deleted prenatally. We confirmed that the RPM-like cells in *Vav1-Cre/Pparg*$^{fl/fl}$ mice have excised the floxed fragment in the *Pparg* gene and are therefore *Pparg*-independent. Interestingly, they maintain *Spic* expression and are able to phagocytose RBCs. For some reason they are not able to use the empty niche and support normal iron recycling.

PPARγ can act both as a transcriptional activator or a repressor. Many PPARγ target genes have been identified during adipogenesis, mainly connected with lipid metabolism, sequestration of fatty acids, and glucose uptake [165]. In immune system, the role of PPARγ was mainly studied during the induction of alternatively-activated macrophage differentiation and repression of transcription factors regulating the inflammatory phenotype [196, 201]. It has been shown that PPARγ expression in peritoneal macrophages is crucial for attenuating the inflammatory response and promoting tissue repair [238]. The comparison of transcriptomes of splenic and bone marrow macrophages from control and *Vav1-Cre/Pparg*$^{fl/fl}$ mice revealed many differentially expressed genes. We have compared these genes to available ChIPseq data for PPARγ. As mentioned above, PPARγ was mainly studied in the context of adipogenesis, therefore most of datasets derive from adipocytes or preadipocyte cell line. We found only two datasets from macrophages, in both cases from thioglycolate-elicited peritoneal macrophages [239, 240]. Few genes repressed in *Pparg*-deficient splenic or bone marrow

macrophages overlapped between PPARγ top target genes (derived from all available ChIPseq) and macrophage-specific PPARγ targets, including the well-studied *CD36* or *Fabp4*. Unfortunately, with these comparisons, we could not dissect the role of PPARγ during RPM development. Ideally, a control with primary macrophages expressing or devoid of PPARγ should be created. Gene ontology (GO) set enrichment analysis for dysregulated genes in RPM-like cells from *Vav1-Cre/Pparg$^{fl/fl}$* mice compared to WT counterparts confirmed the pro-inflammatory profile of *Pparg*-deficient RPM-like cells as early as seven days after birth. Gene sets connected to chemotaxis and cell migration were highly enriched while genes involved in DNA repair and cell cycle were strongly reduced.

Interestingly, *Spic*-deficient and *Vav1-Cre/Pparg$^{fl/fl}$*-derived RPM share many similarities. We showed that both subsets fail to downregulate CD11a and CD88 on the transcriptional, as well as on the protein level. We identified another member of the integrin family, integrin α_D (also called CD11d, gene name *Itgad*), to be strongly downregulated in deficient RPM. Importantly, integrin α_D expression is specific to RPM and, according to Immgen.org, is not expressed in any other tissue resident macrophage subset. Elevated levels of integrin α_D have been linked to increased cell adhesiveness and macrophage retention in vascular lesions [220, 241]. We speculate that both transcription factors Spi-C and PPARγ are upregulated when precursors enter the neonatal spleen and together induce changes in integrin expression, thereby docking progenitors in the niche and allowing the final steps of differentiation. Upon loss of either of the two factors, the potential progenitor cannot be retained in the tissue and possibly migrates out or dies due to displacement and/or lack of a niche factor. Collectively, the presented data unequivocally demonstrate PPARγ as a master regulator of iron-recycling macrophage development. The program triggered in the spleen and bone marrow seems to be very distinct from the program induced by the same factor in alveolar macrophage differentiation and includes novel pathways not related to lipid metabolism, possibly due to collaborative action of Spi-C and PPARγ on tissue-specific target gene expression.

Acknowledgements

We thank P. Chambon (Université Louis Pasteur, Paris, France) for *Pparg$^{fl/fl}$* mice and Carsten Riether (University of Bern, Bern, Switzerland) for *Spic$^{-/-}$* mice. We thank the Swiss National Science Foundation for funding of this project (310030-124922/1).

5.1.6 Supplementary material

Supplementary methods

RBC phagocytosis assay

In vivo. RBCs from whole blood were prepared as previously described [46]. In short, cells were washed with 3 volumes of PBS three times and centrifuged at 400*g*, 10 min and subsequently stressed by incubation at 48$_{o}$C for 20 min under continuous shaking. Next, stressed RBCs were resuspended in 1ml of Diluent C (Sigma-Aldrich) and incubated for 5 min at room temperature with an equal volume of 4µM PKH26 (Sigma-Aldrich) in the dark. Unbound particles were quenched with 2ml of 100% FBS and the sample was spun down (400*g*, 10min) and washed two times with quenching buffer (PBS with 10% FBS). Finally, RBCs were resuspended in PBS and approximately 0.8x10^{9} RBCs were injected into the tail vein of *Vav1-Cre/Ppargfl/fl* and control mice. Some of the mice were sacrificed 16 hours post-injection and spleens and livers were isolated for single cell suspension preparation. Blood samples were taken 20 min, 16h, 64h, 88h and 90h post-injection.

In vitro. Sorted RPM were plated on round glass cover slips in 24-well plate in RPMI 1640 + GlutaMAX, 10 % FCS, 100 U/mL penicillin, 100 µg/mL streptomycin, 50 µM β-mercaptoethanol (all Gibco) and left overnight to attach. The next day, red blood cells (RBCs) were isolated from 200 µl whole blood by several centrifugations with isotonic buffer (0.9% NaCl, 5mM Na_3PO_4, pH8) at low speed (600*g*, 10 min). Cells were then lysed with 1ml of hypotonic buffer (5mM Na_3PO_4, pH8) and spun down for 10 min at 12000*g*. The lysis and centrifugation were repeated until the pellet was white. Ghost RBCs were resuspended in 500 µl of PBS+0.1%BSA and incubated for 10 min at 37°C with an equal volume of 10µM CFSE (5-(and-6)-Carboxyfluorescein Diacetate, Succinimidyl Ester; Life Technologies). Unbound particles were quenched with 1ml of PBS with 10% FBS and the sample was spun down (12000*g*, 10min) and washed two times with quenching buffer. Finally, RBCs were resuspended in the same medium as RPM and incubated with cultured cells for 1h at 37°C. Afterwards, cells were washed twice with PBS to remove unbound RBCs and fixed with 4% paraformaldehyde (PFA, Sigma-Aldrich) for 15 min at room temperature. Glass cover slips were then washed with PBS and cells were perforated with PBS containing 10% FBS and 0.1% Triton X-100 for 1h

at room temperature. Next, cells were stained with FluoProbes-647-conjugated phalloidin (Interchim) for 1h room temperature. After extensive washing with PBS, cells were stained with DAPI (Sigma-Aldrich) and mounted on slides with Dako fluorescent mounting media (Dako). Samples were analyzed with the Zen 2 software (Zeiss) on a fluorescence microscope (Zeiss AxioImager M2).

Supplementary tables

Supplementary Table 1.

channel	name	dilution	company	clone
AF488	F4/80	300	Biolegend	BM8
FITC	VCAM1	200	eBioscience	429
PE	CD88	200	Biolegend	20/70
PE-Cy7	CD11c	1000	Biolegend	117318
PerCP-Cy5.5	CD11b	1000	Biolegend	M1/70
APC	CD45.1	200	Biolegend	A20
AF647	αrabbit IgG(H+L)-	1000	Thermo Fisher Scientific	polyclonal
BV421	CD64	200	Biolegend	X54-5/7.1
BV421	F4/80	300	Biolegend	BM8
BV510	MHCII	400	Biolegend	M5/114.15.2
FL9 (BV605)	CD11c	500	Biolegend	N418
BV785	CD45.2	100	Biolegend	104
BV785	CD45	1000	Biolegend	30-F11
BV711	Streptavidin	1000	BD Biosciences	
Biotinylated	Ly6C	2000	Biolegend	HK1.4
Biotinylated	CD11a	1000	Biolegend	M17/4
unlabelled	PPARγ	25	Cell Signaling Technology	81B8

Supplementary figures

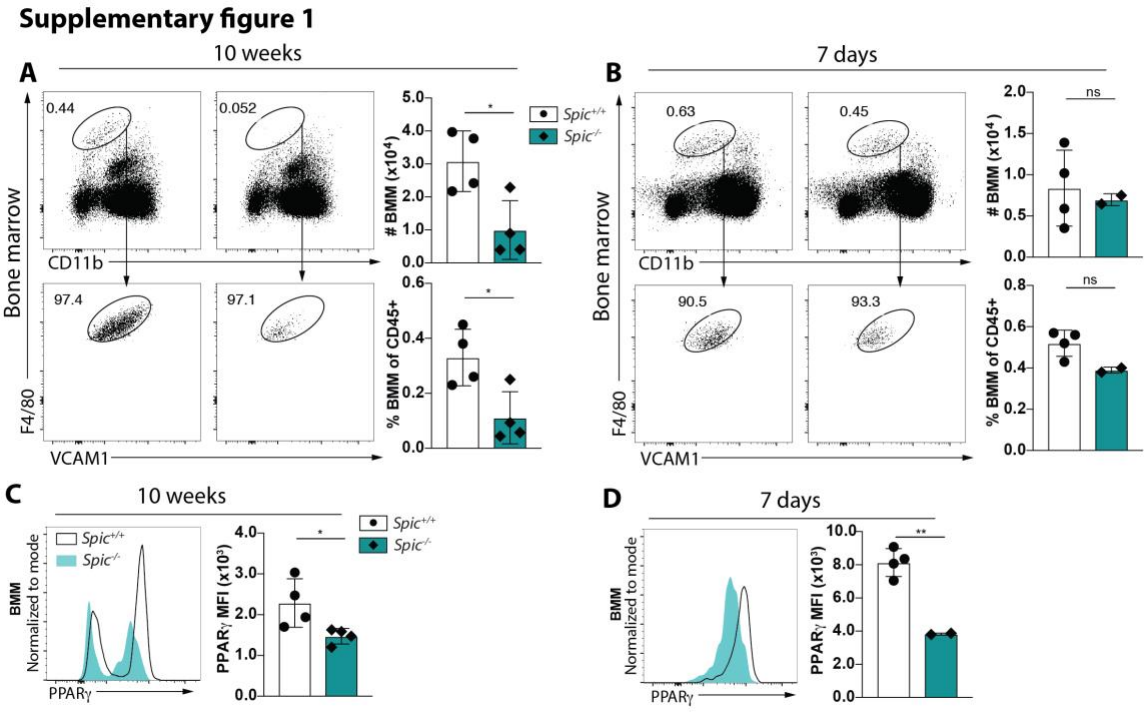

Supplementary figure 1. (A, B) Flow cytometry of BM from 10 weeks old (A) and 7 days old (B) *Spic*$_{+/+}$ and *Spic*$_{-/-}$ mice; plots supplemented with bar graphs showing BMEIM counts and their frequencies of CD45+ cells; BMEIM pregated as live CD45$_{+}$ single cells. (C, D) Histograms of PPARγ expression on BMEIM derived from 10 weeks old (C) and 7 days old (D) *Spic*$_{+/+}$ and *Spic*$_{-/-}$ mice; supplemented with mean fluorescence intensity (MFI) of PPARγ. Ns, not significant; *P<0.05; **P<0.01; ***P<0.001 (unpaired two-tailed Student's t-test). The presented data are from a single experiment (A-D; mean and s.d. from two to four mice per group).

Supplementary figure 2

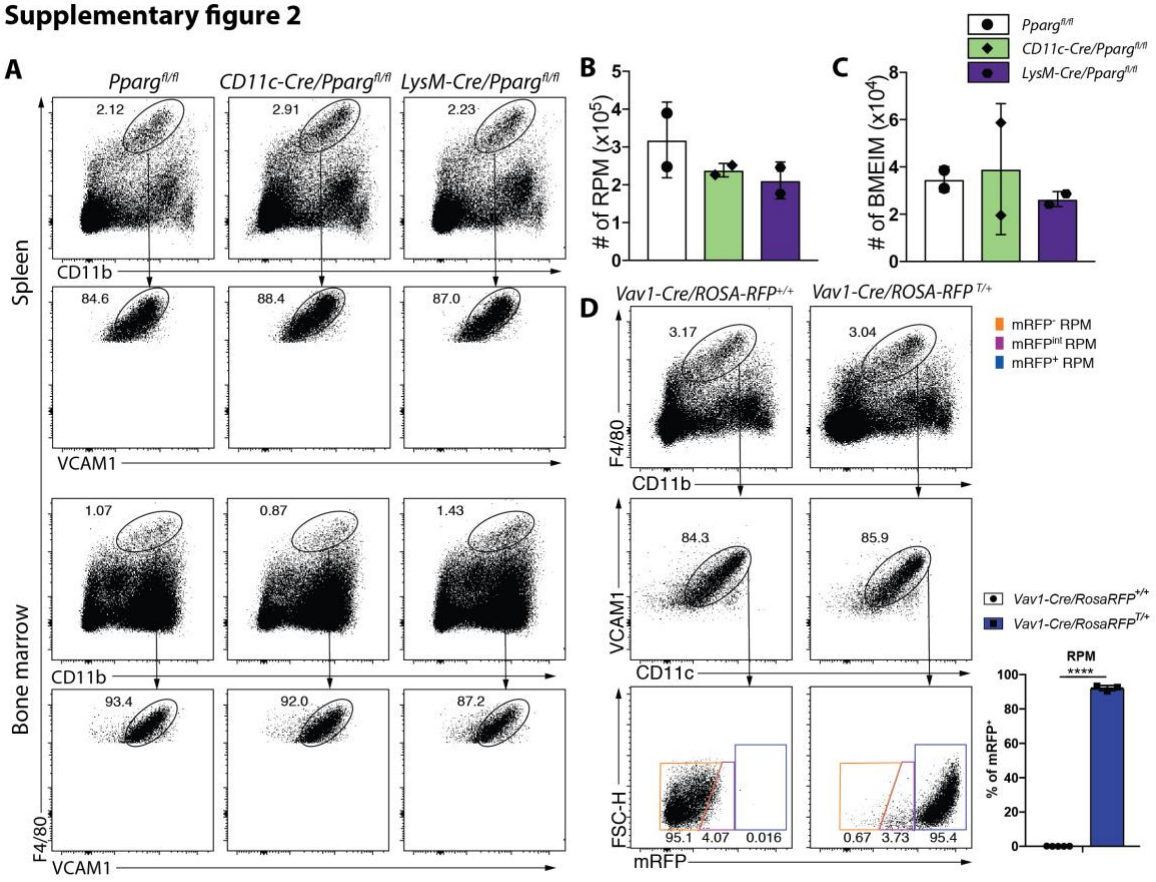

Supplementary figure 2. (A) Flow cytometry of spleen and bone marrow from *Pparg*$_{fl/fl}$, *CD11c-Cre/Pparg*$_{fl/fl}$ and *LysM-Cre/Pparg*$_{fl/fl}$ animals; gated on live cells. (B, C) Total cell count of RPM (B) and BMEIM (C), gated as in A. (D) Cre activity in RPM from *Vav1-Cre/ROSA-RFP* animals; RPM gated as depicted on representative flow cytometry plots; Cre activity in RPM is presented on the bar graph as RFP positive cells. No mark, not significant; ***P<0.0001 (unpaired two-tailed Student's t-test). The presented data are representative of two independent experiments (mean and s.d. of two to three mice per group).

Supplementary figure 3

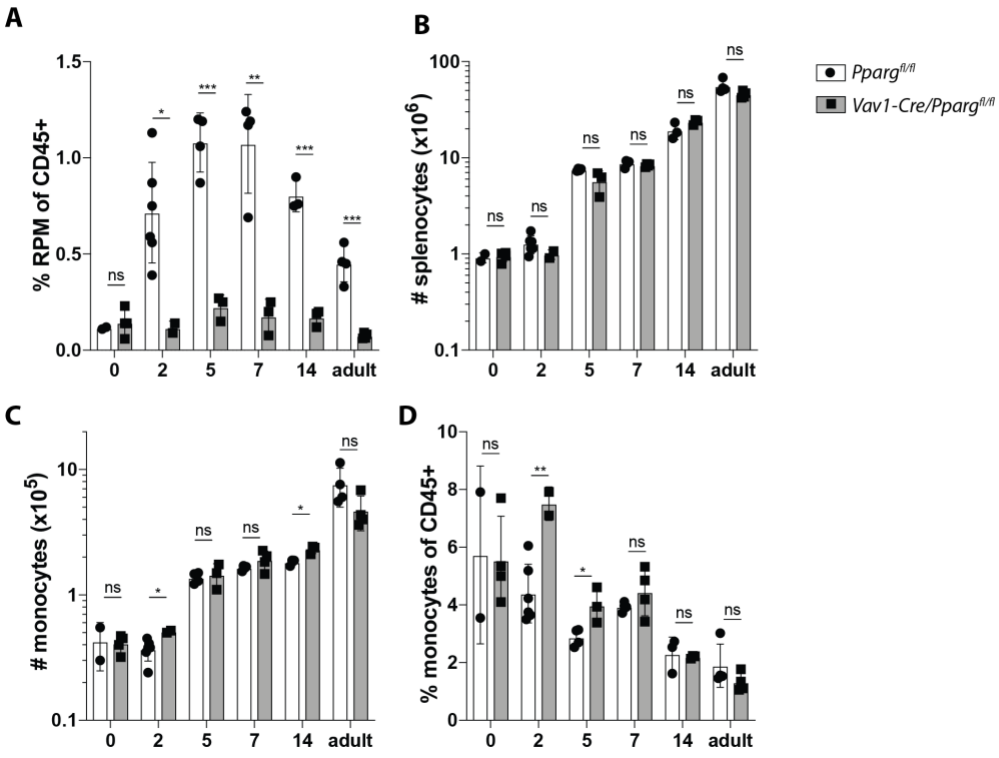

Supplementary figure 3. (A) RPM frequencies of CD45+ cells at different days after birth. (B) Total cell counts of all splenic cells from *Pparg*$^{fl/fl}$ and *Vav1-Cre/Pparg*$^{fl/fl}$ animals at different days after birth. (C-E) Total Ly6C+ monocyte count (C) and frequencies of CD45+ (D) at different days after birth, MFI normalized to fluorescence minus one (FMO) controls. Ns, not significant; *P<0.05 **P<0.01 and ***P<0.001 (unpaired two-tailed Student's t-test). The presented data are from a single experiment (A-D; mean and s.d. of two to five mice per group).

Supplementary figure 4

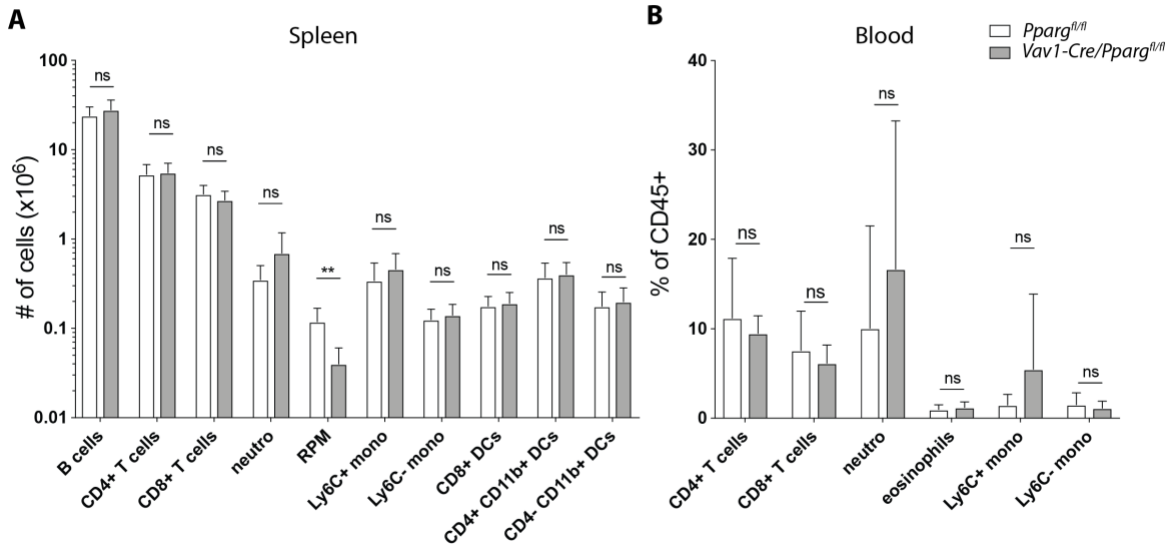

Supplementary figure 4. (A, B) Total counts and frequencies of the indicated cell subsets in the spleen (A) and blood (B), respectively, from *Pparg$^{fl/fl}$* and *Vav1-Cre/Pparg$^{fl/fl}$* animals at steady-state; The indicated subsets were gated as live CD45$^+$ cells: CD19$^+$ (B cells), TCRβ$^+$CD4$^+$ (CD4 T cells), TCRβ$^+$CD8$^+$ (CD8 T cells), CD11b^{hi}Ly6G$^+$ (neutrophils), SiglecF$^+$ (eosinophils), F4/80$^+$CD11b^{lo}VCAM1$^+$ (RPM), MHCII$^+$CD11c$^+$CD8$^+$ (CD8 DCs), MHCII$^+$CD11c$^+$CD11b$^+$CD4$^+$ or CD4$^-$ (CD11b DCs), MHCII$^-$CD11c$^-$CD11b^{hi}Ly6C$^+$ or Ly6C$^-$ (monocytes). Ns, not significant (unpaired two-tailed Student's t-test). The presented data are representative from three independent experiments (A, B; mean and s.d. of six mice per group).

Supplementary figure 5

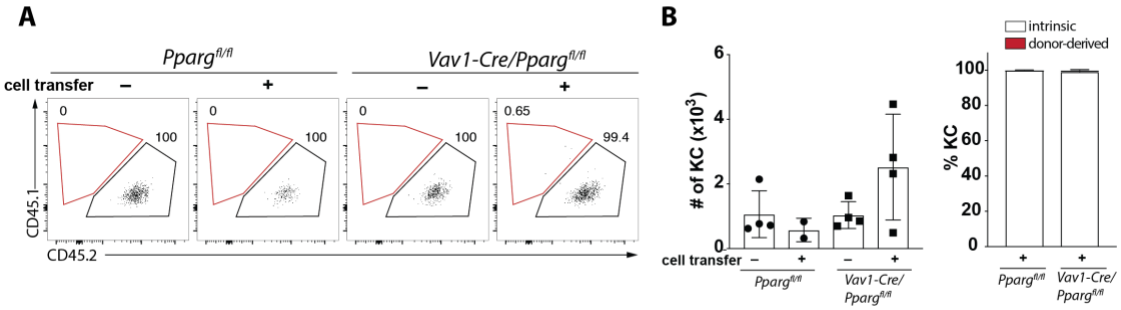

Supplementary figure 5. (A) Dot plots showing Kupffer cell (KC) origin in recipient mice; KC were gated as live CD11b^{int}F4/80$^+$CD64$^+$CD11c^{neg}; the red gates indicate CD45.1$^+$ KC (derived from transferred fetal progenitors). (B) KC counts supplemented with bar graph showing frequencies of donor-derived and intrinsic KC for transferred animals. The presented data are from a single experiment (B; mean and s.d. of two to five mice per group).

Supplementary figure 6

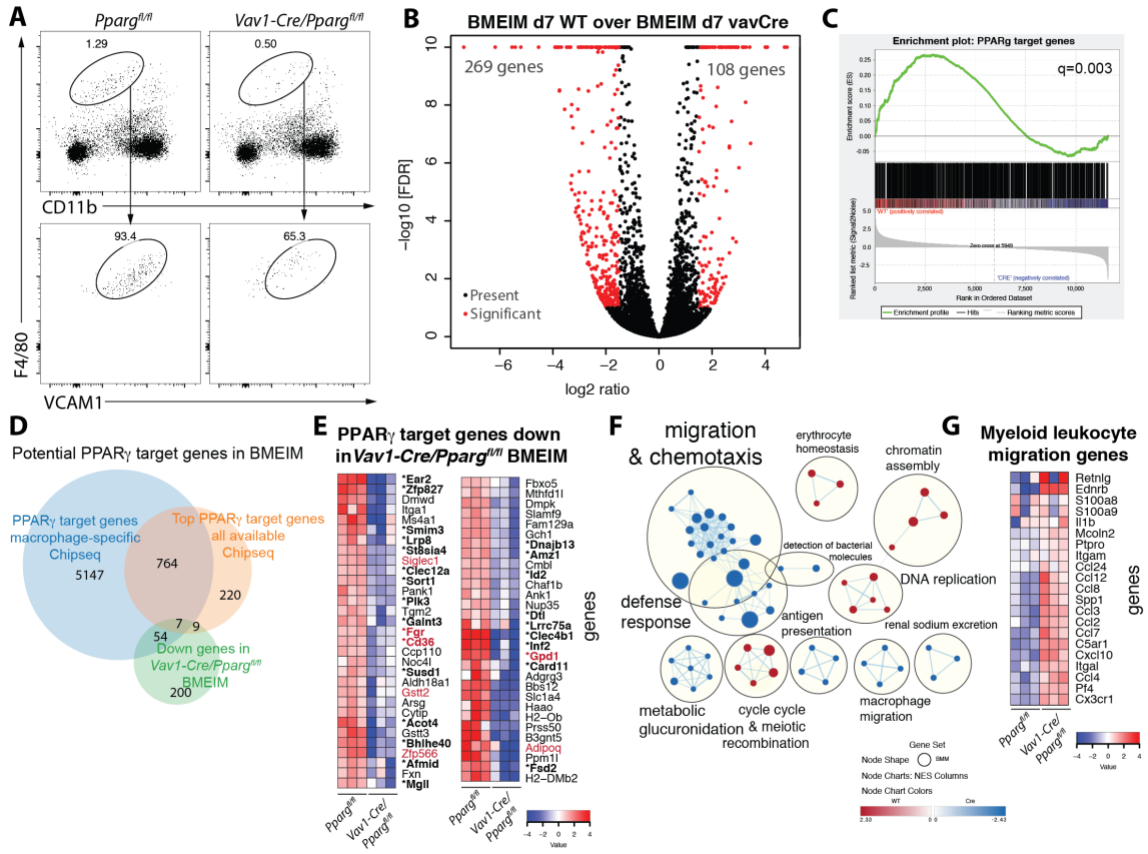

Supplementary figure 6. (A) Flow cytometry of BM from 7 days old *Pparg*$^{fl/fl}$ and *Vav1-Cre/Pparg*$^{fl/fl}$ animals used for RNAseq analysis. (B) Volcano plot showing differentially expressed genes between *Pparg*$^{fl/fl}$ and *Vav1-Cre/Pparg*$^{fl/fl}$ BMEIM (|log2 ratio|>1.5; FDR<0.05). (C) Gene set enrichment plots for PPARγ target genes; PPARγ target genes are from Chip-Atlas.org/target-genes; 1000 top genes from all available data sets were used; the FDR q value is shown in the top right corner of the plot. (D) Venn diagram comparing the PPARγ target gene list (derived from Chip-Atlas.org/target-genes, 1000 top genes from all available data sets) with the PPARγ target genes from macrophage-specific ChIPseq (from Chip-Atlas.org/target-genes, experiment SRX769794) and the downregulated genes in *Vav1-Cre/Pparg*$^{fl/fl}$ BMEIM when compared to *Pparg*$^{fl/fl}$ (log2 ratio<-1.5; FDR<0.1). (E) Heat map showing macrophage-specific PPARγ target genes downregulated in *Vav1-Cre/Pparg*$^{fl/fl}$ BMEIM; the starred bold gene names are genes overlapping with PPARγ targets discovered in RPM, the red gene names are the 7 genes overlapping between the genes downregulated in *Vav1-Cre/Pparg*$^{fl/fl}$ BMEIM, the top 1000, and all macrophage-specific ChIP target genes. (F) GO term enrichment maps for BP from *Pparg*$^{fl/fl}$ and *Vav1-Cre/Pparg*$^{fl/fl}$ BMEIM; the maps show the top enriched gene networks with the FDR q value <0.1; the line thickness connecting two gene set nodes corresponds to the number of genes overlapping between the two sets. (G) Heat map showing genes from the myeloid leukocyte migration gene set. The presented data are from a single experiment with three mice per group.

Supplementary figure 7

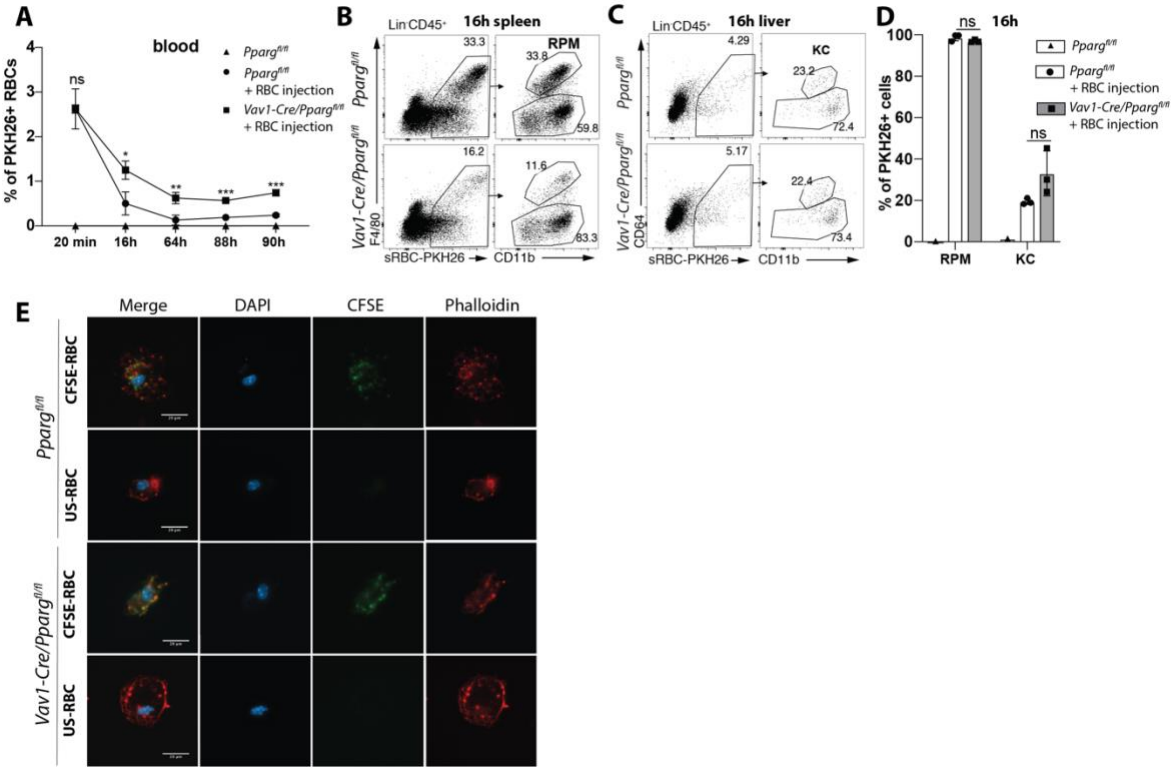

Supplementary figure 7. (A) Frequencies of PKH26-positive RBCs in the blood of *Pparg*$^{fl/fl}$ and *Vav1-Cre/Pparg*$^{fl/fl}$ animals; RBCs were stressed and labelled with the dye prior to injections and their clearance from the bloodstream was assessed at the indicated timepoints. (B, C) Flow cytometry showing the uptake of RBC-PKH26-positive RBCs in the spleen (B) and liver (C) by RPM and KCs (pregated as Lin$^-$ CD45$^+$) 16h post-injections. (D) Frequencies of RBC-PKH26-positive RPM and KCs illustrating their phagocytosing capacities 16h post-injection (E) Representative photographs of sorted RPMs from *Pparg*$^{fl/fl}$ and *Vav1-Cre/Pparg*$^{fl/fl}$ animals, which were co-incubated for 1h with CFSE-labelled or unstained (US) lysed RBCs followed by fixation and phalloidin staining. Ns, not significant; *P<0.05 **P<0.01 ***P<0.001 (unpaired two-tailed Student's t-test). The presented data are representative of two independent experiments (A-D; mean and s.d. from three mice per group).

Supplementary figure 8

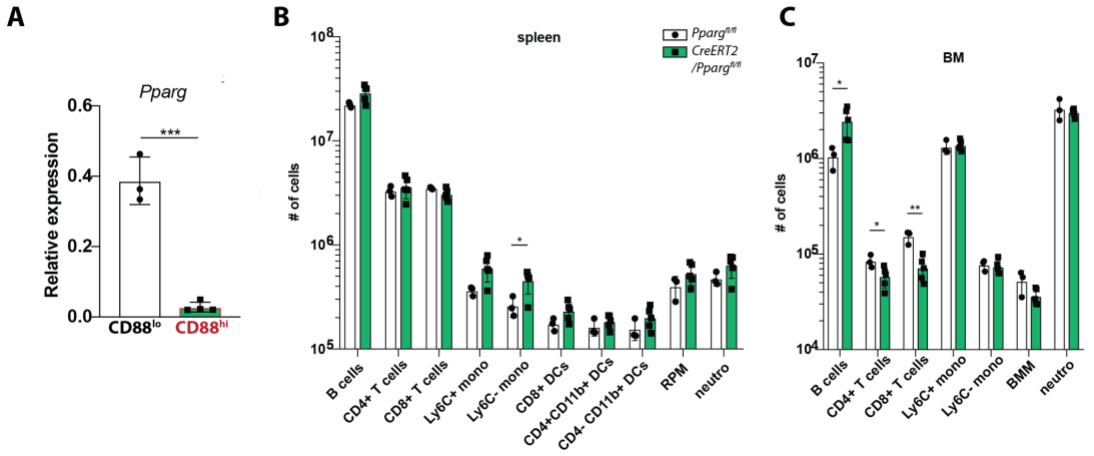

Supplementary figure 8. (A) *Pparg* expression in RPM derived from *Pparg*$_{fl/fl}$ (CD88$_{lo}$) and *CreERT2/Pparg*$_{fl/fl}$ (CD88$_{hi}$) animals treated with tamoxifen; the values are normalized to a house-keeping gene (*G6PDX*). (B, C) Cell counts of indicated populations in *Pparg*$_{fl/fl}$ and *CreERT2/Pparg*$_{fl/fl}$ mice in the spleen (B) and the BM (C). The indicated subsets were gated as live CD45$_+$ cells: CD19$_+$ (B cells), TCRβ$_+$CD4$_+$ (CD4 T cells), TCRβ$_+$CD8$_+$ (CD8 T cells), CD11b$_{hi}$Ly6G$_+$ (neutrophils), F4/80$_+$CD11b$_{lo}$VCAM1$_+$ (RPM/BMEIM), MHCII$_+$CD11c$_+$CD8$_+$ (CD8 DCs), MHCII$_+$CD11c$_+$CD11b$_+$CD4$_+$ or CD4$_-$ (CD11b DCs), MHCII$_-$ CD11c$_-$CD11b$_{hi}$Ly6C$_+$ or Ly6C$_-$ (monocytes). *P<0.05 **P<0.01 ***P<0.001 (unpaired two-tailed Student's t-test). The presented data are representative from three independent experiments (A-E; mean and s.d. from three to five mice per group).

Supplementary figure 9

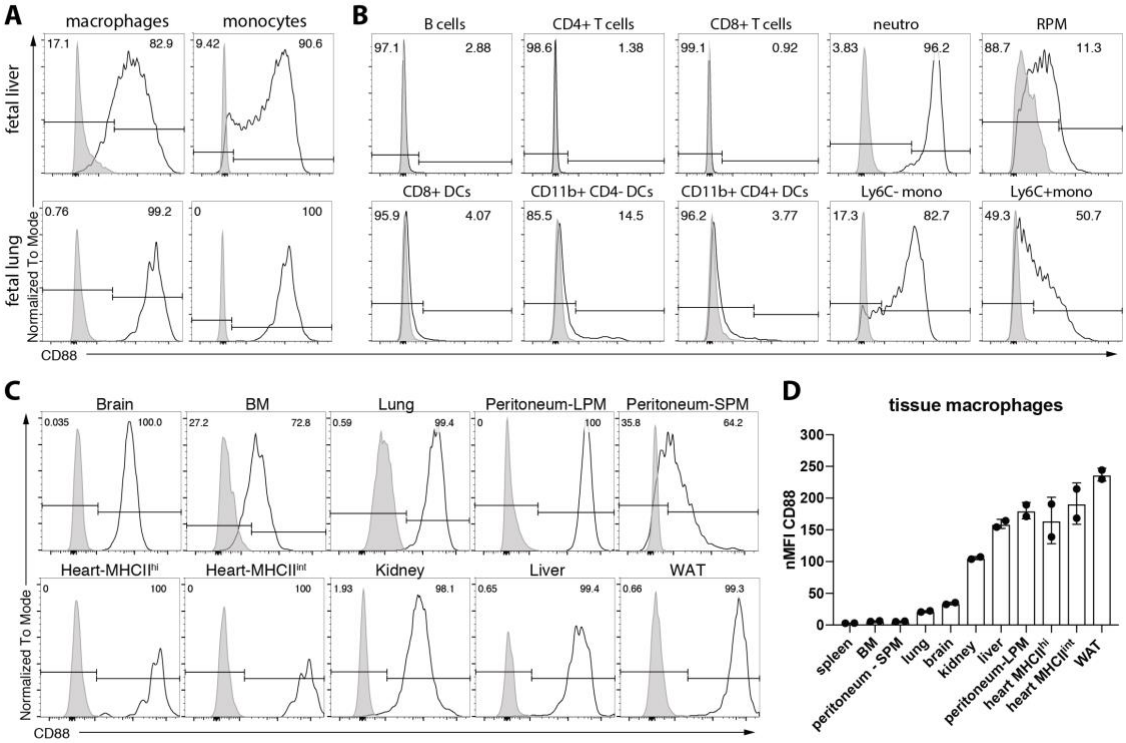

Supplementary figure 9. (A) Representative histograms of CD88 expression on macrophages ($CD45^+CD11b^{int}F4/80^{hi}Ly6C^-$) and monocytes ($CD45^+CD11b^{hi}F4/80^-Ly6C^{hi}$) from fetal liver (upper panel) or fetal lung derived from E14.5 WT embryos. (B) Representative histograms of CD88 expression on indicated populations from spleens of adult WT mice; gated as live $CD45^+$ cells: $CD19^+$ (B cells), $TCR\beta^+CD4^+$ (CD4 T cells), $TCR\beta^+CD8^+$ (CD8 T cells), $CD11b^{hi}Ly6G^+$ (neutrophils), $F4/80^+CD11b^{lo}VCAM1^+$ (RPM), $MHCII^+CD11c^+CD8^+$ (CD8 DCs), $MHCII^+CD11c^+CD11b^+CD4^+$ or $CD4^-$ (CD11b DCs), $MHCII^-CD11c^-CD11b^{hi}Ly6C^+$ or $Ly6C^-$ (monocytes). (C) Representative histograms of CD88 expression on tissue resident macrophages from the indicated organs of adult WT mice; macrophages gated as live $CD45^+$ cells: $CD11b^{hi}F4/80^{lo}CD64^+$ (brain, heart), $CD11b^{int}F4/80^+$ (kidney), $CD11b^{int}F4/80^+CD64^+$ (liver, white adipose tissue (WAT)), $CD11b^{int}F4/80^+CD11c^+SiglecF^+$ (lung), $CD11b^{hi}F4/80^{hi}$ (peritoneum-LPM), $CD11b^{int}F4/80^{lo}$ (peritoneum-SPM), $F4/80^+CD11b^{lo}VCAM1^+$ (BM). (D) MFI of CD88 for macrophages from the indicated organs; MFI normalized to FMO controls. The presented data are from a single experiment with two to five mice per group.

Supplementary figure 10

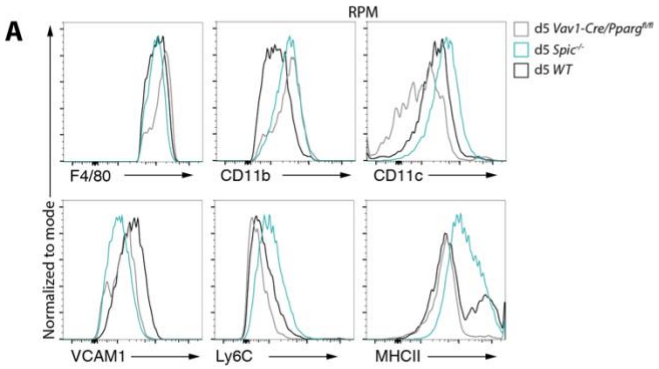

Supplementary figure 10. (A) Representative histograms of the expression of the indicated markers on RPM from 5-day old mice. The presented data are from a single experiment with two to five mice per group.

5.2 CSF2-cultured fetal liver monocytes provide a biologically relevant model system to study alveolar macrophages

Authors:

Fengqi Li[1, *], Katarzyna Okreglicka[1, *], Lea Pohlmeier[1], Christoph Schneider[1], Manfred Kopf[1]

*These authors contributed equally to this work

Affiliations:

[1]Institute of Molecular Health Sciences, Department of Biology, ETH Zürich, Switzerland.

Corresponding author:

Prof. Manfred Kopf, e-mail: manfred.kopf@biol.ethz.ch

Author contributions:

F.L., K.O. and M.K. designed the experiments; F.L. and K.O. performed and analyzed the experiments. L.P. analyzed RNA sequencing data. C.S. and M.K. discussed data and provided conceptualization. F.L., K.O. and M.K. wrote the manuscript.

5.2.1 Abstract

Tissue resident macrophages are phagocytic immune cells which, apart from contributing to host defense, play important roles in tissue development, repair, homeostasis and disease. They are an integral part of the immune system and have been studied extensively for decades. However, new insights into macrophage self-renewal capacity suggesting low input from circulating monocytes and a proven heterogeneity, the use of traditional methods to study tissue resident macrophages based on transformed cell lines or bone marrow-derived macrophages must be reconsidered. We describe here a biologically-relevant platform to study alveolar macrophage (AM) development and function. Our method relies on a two-step differentiation protocol, where fetal monocytes are first expanded *in vitro* with GM-CSF and subsequently transferred to AM-deficient hosts where the cells receive further niche-specific signals necessary for terminal maturation. The resulting AM are fully functional and self-maintaining cells which strongly resemble endogenous AM on the transcriptome level. Moreover, the cells are suitable for genetic modifications. This potent model integrates not only ontogeny but also tissue imprinting to produce AM cells, which could be used for biological studies and in therapeutic approaches.

5.2.2 Introduction

Macrophages are an integral part of the immune system. They are found in virtually every tissue and contribute to host defense, mainly by phagocytosis of pathogens and cellular debris [210]. Despite the fact that macrophages have been studied for over a century, recent technological advances have revolutionized the field by providing novel insights into cell development, phenotype and function. Tissue resident macrophage populations originate from different fetal progenitors, express diverse gene signatures and fulfil tissue-specific functions driven by the local environment [43, 81, 86-89, 92, 99, 102]. Intriguingly, the peritoneum harbors two distinguishable macrophage populations originating from different precursors despite being exposed to common environmental signals [36, 85]. This dissimilarity raised the awareness that cell ontogeny crucially contributes to differences at later developmental stages.

Fate-mapping studies have elucidated the origin of most tissue resident macrophages. The earliest progenitor populations (erythromyeloid progenitor, EMP) derive from the yolk sac (YS) and contribute to the tissue resident populations at birth [49]. Myb independent YS-derived macrophages are also the exclusive source of microglia [19, 48]. In other tissues, YS-derived macrophages are replaced by fetal monocytes, which develop from a second wave of Myb^{+} EMPs, and are claimed to be the true progenitors for most tissue resident populations [50]. Besides EMPs, fetal hematopoietic stem cells (HSCs) are also able to give rise to macrophages [51]. Circulating monocytes, which for decades were believed to replenish resident macrophage populations in adulthood, were shown to contribute minimally to local pools during steady-state [36, 37]. Because fetal-derived tissue resident macrophages and adult bone marrow or monocyte-derived macrophages are fundamentally distinct, due to their different origins, the use of bone marrow precursors for macrophage differentiation research is problematic. Consequently, the study of tissue resident macrophages is not trivial and demands embracing this diversity in order to create biologically valid models. Sorting of primary macrophages from a tissue of interest is often difficult and does not provide a desirable solution because the numbers of isolated cells are low and more importantly, the macrophages modify their enhancer landscapes in culture as a consequence of losing their tissue-imprinted identity [61]. However, as seen for large peritoneal macrophages (LPM), previously characterized, environmental signals, when

supplemented during *in vitro* culture, can partially maintain enhancer marks and therefore the cell identity [61].

Current opinion suggests using a two-step model [242], where ontogenically relevant progenitors are used to generate a macrophage cell line which could be then exposed to niche-specific factors, either by co-culturing the produced macrophages with other tissue cells, or by placing them in the tissue of interest for final imprinting. Successful attempts using iPSC-derived macrophages (iMac) have been made, where the macrophages produced strongly resembled primitive YS macrophages, which provided a good system to study microglial development, function and therapeutic approaches [243]. The cells thus created were also used to reproduce alveolar macrophage (AM) development by pulmonary macrophage transplantation (PMT) into AM-deficient hosts (*Csf2ra*$^{-/-}$). *Csf2ra/b*$^{-/-}$ mice are typically used as a model for hereditary pulmonary alveolar proteinosis (herPAP), a rare lung disease featuring the accumulation of surfactant proteins. This results in long-term respiratory insufficiency and a high susceptibility to infections [244, 245]. iMac-derived AM were functional and cleared proteinosis, as was further confirmed by another group [246, 247]. PMT to the lungs is not difficult and a functional readout is rather simple. Several studies using this approach to test the therapeutic potential of bone marrow monocyte-derived macrophages (BMM) in treating herPAP [248, 249] suggested that BMM produce true AM cells even though AM develop from fetal lung monocytes in GM-CSF-dependent manner and are maintained locally without contribution from circulating monocytes [36, 98, 99].

We provide a biologically relevant model to study AM development and function. We used sorted fetal liver monocytes (FLiMos) and cultured them with GM-CSF, as described previously for whole fetal liver cell cultures [250]. This resulted in a non-transformed, GM-CSF-dependent, homogenous cell line with proliferative capacity and an AM-like phenotype (CSF2-cFLiMo). Moreover, CSF2-cFLiMo did not lose the potential to efficiently reconstitute AM development *in vivo*. We established a robust protocol of transferring cells intranasally (i.n.) into *Csf2ra*$^{-/-}$ newborns and we showed that the best results were obtained if CSF2-cFLiMo were transferred to very young mice. Furthermore, we provide evidence that CSF2-cFLiMo have a *bona fide* AM phenotype while BMM-derived AM do not. CSF2-cFLiMo-derived AM are characterized by a strong self-renewal capacity and are functional not only in clearing surfactant but also during influenza virus

infection. Finally, CSF2RA re-expression in *Csf2ra*$^{-/-}$ FLiMos by retroviral gene transfer restored their potential to develop into *bona fide* AM. Thus, the described model will be a potent tool to study genes involved in AM development and function, as well as for therapeutic approaches.

5.2.3 Materials and methods

Mice

C57BL/6 CD45.2, congenic CD45.1 and, BALB/c mice were originally from the Jackson Laboratory. *Csf2ra*$^{-/-}$ mice were recently established in our laboratory [251]. All mice were housed and bred under specific pathogen-free conditions in individually ventilated cages in a controlled day-night cycle at the ETH Phenomics Facility and were used for experiments on 6-10 weeks (adults) unless otherwise stated. All animal experiments were performed according to the guidelines (Swiss Animal Protection Ordinance (TschV) Zurich) and Swiss animal protection law (TschG) and had been approved by the local animal ethics committee (Kantonales Veterinaersamt Zurich).

Timed pregnancy

Female C57BL/6 CD45.1, CD45.2, or BALB/c mice were housed together with matching male mice overnight. The vaginal plug was checked on the next day and was designated as embryonic day 0.5 (E0.5).

Cell suspension preparation

Mice were euthanized by overdose (400 mg/kg body weight) of sodium pentobarbital by i.p. injection. The lungs were washed three times with 0.4 ml of ice-cold PBS containing 2 mM EDTA through an intratracheal cannula only when mice were older than 4 weeks. BAL fluid was collected and cells were harvested by centrifugation. Lungs were removed after perfusion with ice-cold PBS. Pregnant females were sacrificed by CO2 asphyxiation. Fetal livers were removed at the indicated time points. Organs were minced and then digested at 37 °C in IMDM medium containing 2.0 mg/ml of type IV collagenase (Worthington), 0.125 mg/ml DNase I (Sigma-Aldrich) and 3% FCS for 45 min (lungs) and 15 min (fetal and neonatal livers) respectively, and subsequently passed through a 70-μm-cell strainer (Becton Dickinson). Ammonium-chloride-potassium (ACK) lysing buffer was used for erythrocyte lysis for all samples.

Pulmonary cell transplantation

Neonatal (day 0-3 after birth) *Csf2ra*$^{-/-}$ recipient mice were transferred intranasally (i.n.) with different numbers of cells in 10 µL endotoxin-free PBS. For competitive transfer experiments, 25,000 cells from each origin were mixed and transferred. Adult *Csf2ra*$^{-/-}$ recipient mice were transferred intratracheally (i.t.) with different numbers of cells in 50 µL endotoxin-free PBS.

Flow cytometry and cell sorting

Multiparameter assessment and cell sorting were performed using LSR Fortessa, BD FACS ARIA II and ARIA III (BD Biosciences) and data were analyzed with FlowJo software (TreeStar). After blocking the FcgIII/II receptors by incubation with homemade anti-CD16/32 (2.4G2), single-cell suspensions were incubated with the indicated fluorochrome-conjugated or biotinylated monoclonal antibodies in FACS buffer (PBS containing 2% FCS and 2 mM EDTA) and then washed twice before detection. Monoclonal antibodies specific to mouse CD45 (30-F11), CD11c (N418), F4/80 (BM8), CD11b (M1/70), SiglecF (E50-2440, BD Biosciences), CD45.1 (A20), CD45.2 (104), Ly6C (HK1.4), CD116 (698423, R&D), Gr-1 (RB6-8C5, eBioscience), CD64 (X54-5/7.1) and MHC class II (M5/114.15.2, eBioscience) were purchased from BioLegend unless otherwise stated. Dead cells were excluded using the live/dead marker eFluor780 (eBioscience).

Generation of CSF2-cFLiMo

Fetal livers were harvested from CD45.1$_+$ C57BL/6 embryos. Liver single-cell suspensions were prepared. Monocytes were sorted using flow cytometry. Doublets and debris were excluded using FSC and SSC. pMo-FLi were identified as viable CD45$_+$F4/80$_{lo}$CD11b$_{int}$Ly6C$_+$ cells. Sorted monocytes were cultured in complete RPMI, supplemented with 30 ng/mL recombinant GM-CSF (Peprotech,) *in vitro*. Cells were plated with 1x10$_5$ cells/ml and sub-cultured by splitting them 1:5 every 3 days. CSF2-cFLiMo used for transplantation were cultured for 2 weeks in culture media prior to transfers unless stated otherwise.

Generation of BMM

For the preparation of mouse BM-derived macrophages (BMM), tibias and femurs from the hind legs of adult CD45.1$_+$CD45.2$_+$ donor mice were flushed with PBS. Bone marrow was rinsed through a 70-um cell strainer (Becton Dickinson) followed by red blood cell

depletion with ammonium-chloride-potassium (ACK) lysing buffer. BMM were differentiated *in vitro* in complete RPMI, supplemented with 10 ng/ml recombinant M-CSF (Peptrotech). Medium was replaced on day 3 and day 6. Adherent cells were harvested and used as mature BMM on day 8.

Assessment of total protein

Total protein concentrations in BAL fluid were detected by Pierce BCA Protein Assay Kit according to the manufacturer's instructions (Thermo Scientific).

RNA sequencing

100,000 indicated cell populations were collected into TRIzol (Life Technologies), phase separation was achieved with the addition of chloroform (Sigma-Aldrich), and total RNA was precipitated from the aqueous layer with isopropanol (Sigma-Aldrich) using glycogen (Roche) as a carrier. RNA samples were sent to the Functional Genomics Center Zurich, where the RNA sequencing was performed. The TruSeq RNA Stranded sample kit (Illumina) was used to construct the sequencing libraries. In brief, total RNA samples (100 ng) were poly(A) enriched and reverse-transcribed into double-stranded cDNA, and TruSeq adapters were then ligated to double-stranded cDNA, then fragments containing TruSeq adapters on both ends were selectively enriched with PCR and subsequently sequenced on the Illumina NextSeq 500 in the single-end mode for 150 cycles.

Influenza virus and infection

Influenza virus strain PR8 (A/Puerto Rico/34, H1N1) was originally provided by J. Pavlovic, University Zurich. For infections, the mice were anesthetized and intratracheally (i.t.) inoculated with indicated doses of virus in 50 µl endotoxin-free PBS. Temperature and weight of mice were monitored daily and animals were euthanized if they fulfilled the severity criteria set out by institutional and cantonal guidelines. To determine influenza virus titers in the lungs, samples were collected after infection, homogenized and serially diluted with MDCK cells as described [252]. Infected cells were detected using a monoclonal mouse anti-influenza NP antibody (HB-65, homemade).

RV reconstitution of Csf2ra gene

Two retroviral constructs based on moloney murine leukemia virus, containing Csf2ra cDNA and GFP or GFP only, were used for transfection of retrovirus packaging cell line. Fresh viral supernatants containing non-replicating retroviruses were used for

transduction of pMo-FLi isolated as described above from *Csf2ra*$^{-/-}$ or CD45.1^{+} WT embryos. Cells were cultured in complete RPMI, supplemented with GM-CSF (30 ng/mL) for 7 days. All non-transduced pMo-FLi derived from *Csf2ra*$^{-/-}$ embryos could not proliferate. After a week, a homogenous population of receptor-expressing cells was detected and was used for transfers. For WT cells, all live cells treated with the Csf2ra-overexpressing virus were used (irrespectively of the transduction level).

Statistical analysis

Mean values, SEM and SD were calculated with Prism (GraphPad Software, Inc). Student's t-test (unpaired) was used for comparing two groups, and ANOVA (one way) was used for comparing multiple groups: ns, not significant; *p < 0.05, **p < 0.01, ***p < 0.001.

5.2.4 Results

Fetal liver monocytes cultured in vitro with GM-CSF differentiate into a long-lived, homogeneous, AM-like population

Tissue resident macrophages are extremely heterogenic and recapitulating the ontogenetic, environment-driven differentiation using a common developmental system is therefore not possible. Ideally, a separate, biologically-relevant model for each subset is necessary. While we have reported that AM develop from fetal lung monocytes in a GM-CSF-dependent manner [98, 99], we were interested in optimizing culture conditions for true AM progenitors. Fejer *et al*. described an efficient way to generate a GM-CSF-dependent macrophage population resembling AM from total fetal liver cells *in vitro* [250]. To clarify if GM-CSF-dependent macrophages are derived from fetal monocytes, we purified populations of primary fetal liver monocytes (pMo-FLi, viable CD45^{+}F4/80^{lo} CD11b^{int}Ly6C^{+} cells) and primitive macrophages (viable CD45^{+}F4/80^{hi}CD11b^{lo} cells) from CD45.1 E14.5 wild type (WT) embryos (sFig 1A) and cultured them with GM-CSF *in vitro* (Fig 1A). Fetal liver monocytes grew exponentially, whereas the numbers of fetal liver macrophages slowly decreased over the period of 2 weeks (sFig 1B). At day 3 of the monocyte culture, a new population with macrophage-like (Mac-like) phenotype (F4/80^{+}Ly6C^{-} cells) emerged, which constituted around 40% of all cells (Fig 1B). The remaining cells, with a granulocyte-like phenotype (Gra-like, F4/80^{-}Ly6C^{+} cells), were quickly outnumbered by Mac-like cells and completely disappeared by day 9 (Fig 1B). Cultured fetal liver monocytes became bigger and gradually upregulated F4/80, CD11c,

Figure 1

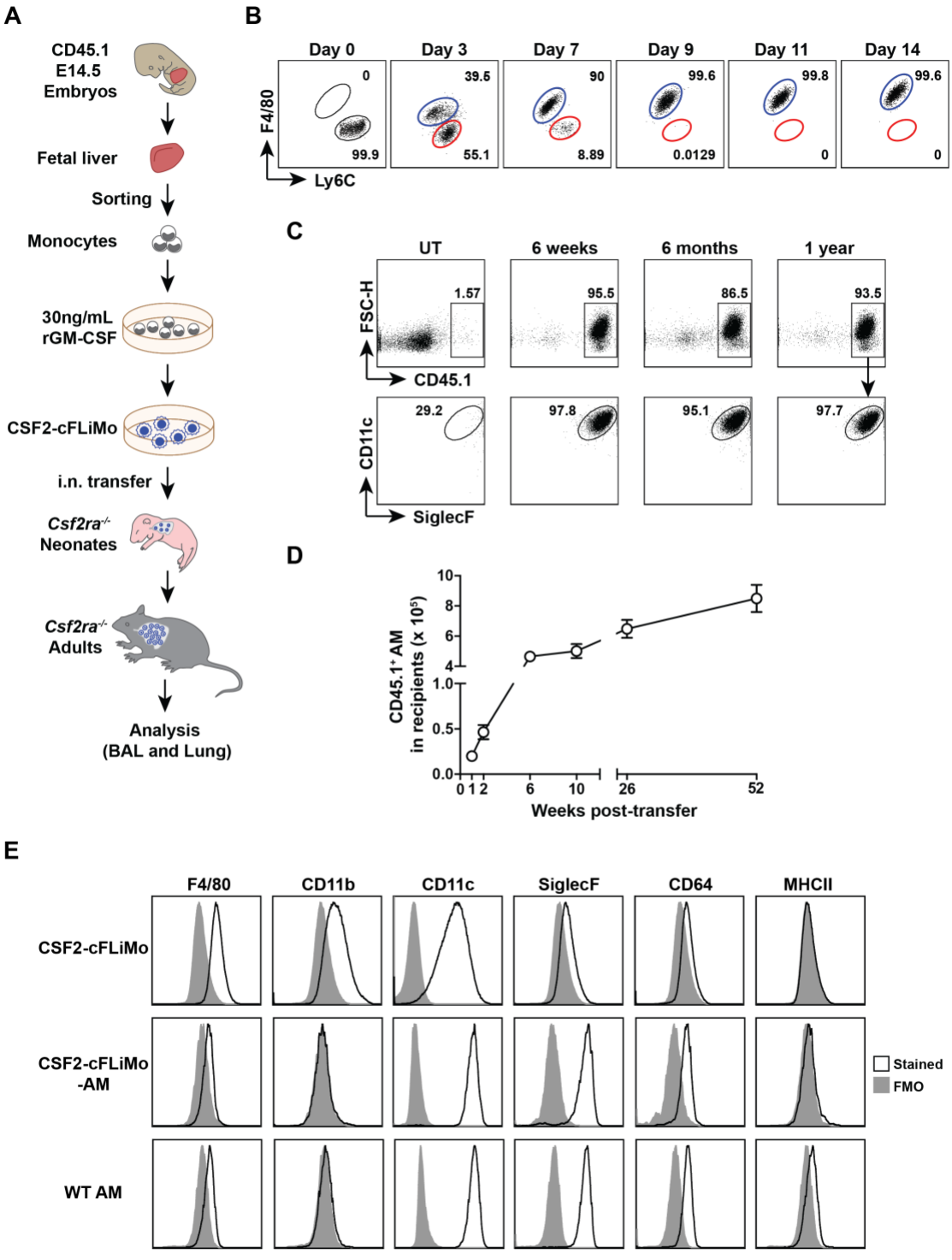

Figure 1. Fetal liver monocytes can proliferate *in vitro* with GM-CSF and further develop into mature AM *in vivo*. (A) Experimental outline. (B) Primary monocytes from fetal liver cultured *in vitro* with GM-CSF. Representative dot plots for F4/80 vs Ly6C are shown for GM-CSF-cultured fetal liver monocytes (CSF2-cFLiMo) at the indicated time points, pregated on viable CD45+ single cells. From day 3, F4/80+Ly6C- cells were gated as macrophage-like (Mac-like, blue) population and F4/80-Ly6C+ cells were gated as

(legend continued on the next page)

granulocyte-like (Gra-like, red) population. (C-E) $5\times10_4$ of CSF2-cFLiMo generated from CD45.1 E14.5 embryos, after 2 weeks of culturing, were intranasally (i.n.) transferred to neonatal (day 0-3 after birth) CD45.2+ *Csf2ra*$^{-/-}$ mice and analyzed at the indicated time points. Flow cytometry was used to characterize and quantitate the cells. (C) Representative dot plots of the CD45.1 donor-derived cells in the BAL of recipients 6 weeks, 6 months and 1 year after transfer, pregated as viable single cells. (D) Total numbers of donor-derived AM from lung (1 and 2 weeks) or from BAL and lung (after 6 weeks) detected in recipients at the indicated time-points. (E) Representative histograms of AM signature marker expression on CSF2-cFLiMo before transfer, CSF2-cFLiMo-derived AM detected in *Csf2ra*$^{-/-}$ recipient mice 6 weeks after transfer, and endogenous AM from age-matched control mice showing FMO control (grey) and specific antibodies against the indicated markers (black line). The data are representative of two to three independent experiments. Values show means ± SEM of three to five mice per group in D.

and SiglecF (sFig 1C), indicating an acquisition of AM-like phenotype and subsequently did not change the expression of these surface markers for more than 18 weeks in culture (sFig 1D). These F4/80+CD11c+CD11b+SiglecF+ differentiated cells are referred to as CSF2-cFliMo. Similar results were obtained when CSF2-cFLiMo were generated from monocytes isolated from E16.5, E18.5, and E20.5 fetal livers (sFig 1E). When established CSF2-cFLiMo cultures were deprived of GM-CSF (sFig 1F), a gradual decrease in CSF2-cFLiMo numbers was observed (sFig 1G) but their surface phenotype did not change (sFig 1H). The long-term maintenance and proliferation of CSF2-cFLiMo were therefore GM-CSF dependent. These results show that fetal liver monocytes cultured with GM-CSF *in vitro* give rise to a non-transformed, long-lived, homogeneous cell line with an AM-like phenotype.

CSF2-cFLiMo retain the potential to develop into mature AM and can be maintained long term in vivo

In order to assess whether CSF2-cFLiMo could truly substitute AM *in vivo*, we transferred congenically marked CSF2-cFLiMo intranasally (i.n.) into *Csf2ra*$^{-/-}$ neonatal (d0-3) mice (Fig 1A), which are devoid of endogenous AM [251]. Analysis of the BAL and lung of *Csf2ra*$^{-/-}$ recipients showed that considerable numbers of donor-derived mature AM, characterized as CD11chiSiglecFhi cells, could be detected even 1 year after transfer (Fig 1C, sFig 2). The numbers of donor-derived AM rapidly increased in *Csf2ra*$^{-/-}$ recipients within the first 6 weeks before expanding at a slower rate at later times (Fig 1D). CSF2-cFLiMo before transfer exhibited a F4/80+CD11b+CD11c+SiglecFloCD64lo MHCII- phenotype (Fig 1E). Six weeks after transfer, CSF2-cFLiMo-derived cells down-

regulated F4/80 and CD11b, up-regulated CD11c, SiglecF, and CD64, resembling the AM phenotype from age-matched WT mice (Fig 1E).

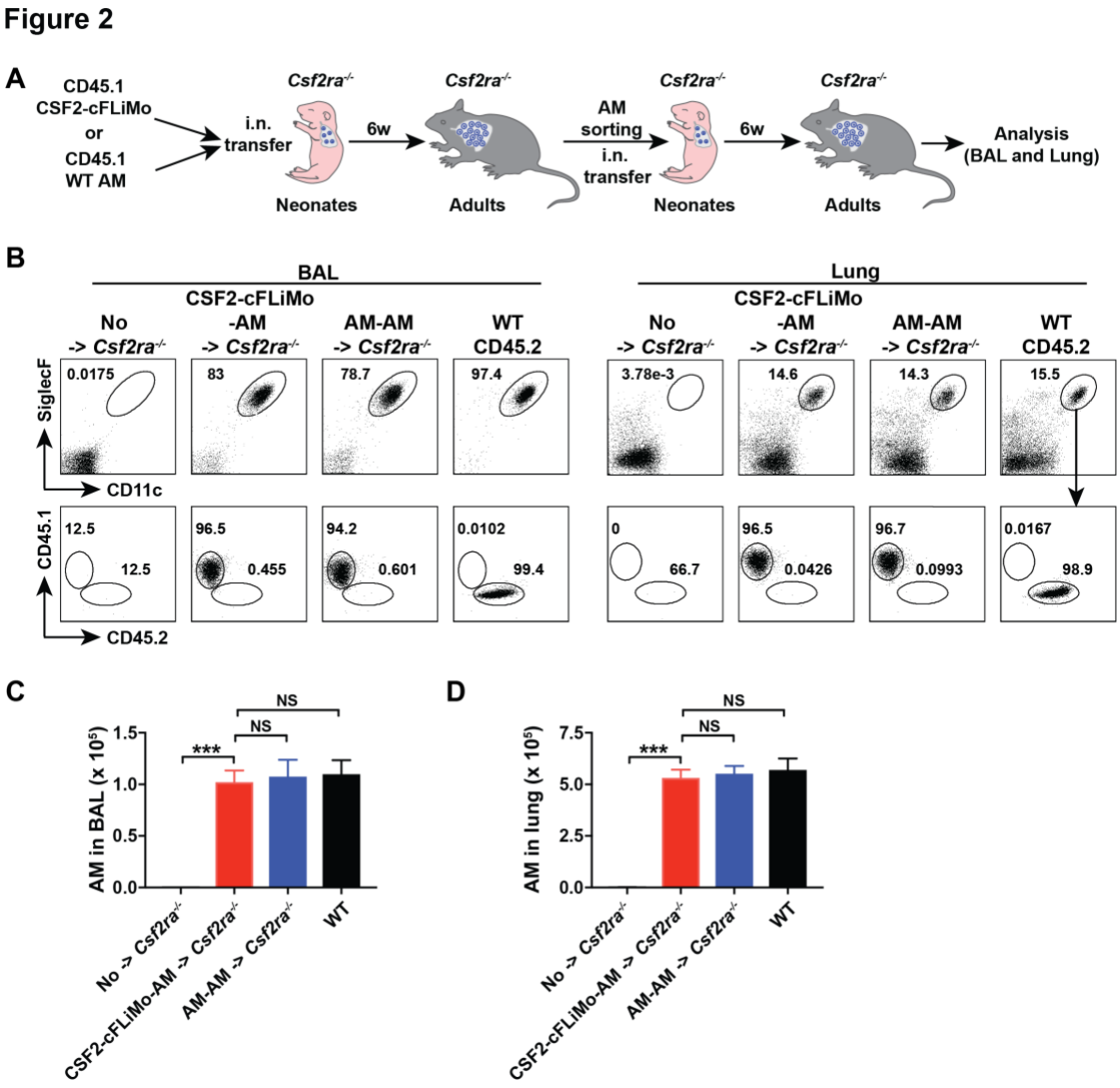

Figure 2. CSF2-cFLiMo-derived AM have ability to self-renew *in vivo*. (A) Experimental outline. $5\times10_4$ of CD45.1 CSF2-cFLiMo generated from E14.5 embryos after 2-week culture or CD45.1 AM sorted from WT adult mice were intranasally transferred to neonatal CD45.2 *Csf2ra*$^{-/-}$ mice. After 6 weeks, donor-derived AM were sorted and $5\times10_4$ of cells were intranasally transferred to new neonatal CD45.2 *Csf2ra*$^{-/-}$ mice. BAL and lung were analyzed 6 weeks after second-round transfer. (B-D) Flow cytometry was used to characterize and quantitate reconstituted cells. (B) Representative dot plots showing the phenotype of CD45.1 donor-derived AM in the BAL and lung, pregated as viable $CD45_+$ single cells. (C-D) Numbers of donor-derived AM and endogenous AM in the BAL (C) and lung (D). Age-matched *Csf2ra*$^{-/-}$ and CD45.2 WT mice were included as negative and positive controls, respectively. The data are representative of two experiments. Values show means ± SEM of three to four mice per group. Student's t test (unpaired) was used in C-D: ns, not significant; *p < 0.05, **p < 0.01, ***p < 0.001.

Bone marrow derived macrophages (BMM) are widely used in studies of macrophage biology and high-throughput screens. To directly compare the capacity of BMM and CSF2-cFLiMo to give rise to AM, we mixed them in a 1:1 ratio and transferred them into neonatal *Csf2ra*$^{-/-}$ recipient mice (sFig 3A). Under these competitive conditions, more than 70% of AM were CSF2-cFLiMo-derived (sFig 3B-C). Compared to BMM-derived AM, CSF2-cFLiMo-derived AM and endogenous AM exhibited a lower expression of CD11b and a higher expression of CD64 and SiglecF (sFig 3D-E). Thus, CSF2-cFLiMo possess a higher potential to develop into mature AM in recipient's lungs compared to BMM.

In summary, when transferred into the lung of AM-deficient neonatal *Csf2ra*$^{-/-}$ mice, CSF2-cFLiMo further differentiate into mature AM and can be maintained long term.

CSF2-cFLiMo-derived AM can self-renew in vivo

AM are maintained locally through self-renewal and are largely independent of adult hematopoiesis at steady-state [98, 99]. Serial transplantation remains the gold standard for experimental assessment of long-term repopulating and self-renewal capacity of hematopoietic stem cells [253], but similar experiments have not been done for tissue macrophages. To determine the long-term self-renewing capacity of CSF2-cFLiMo-derived AM, we serially transferred CSF2-cFLiMo or mature AM isolated from WT adult mice into neonatal *Csf2ra*$^{-/-}$ mice, and after 6 weeks, donor-derived AM were sorted again and transferred into new *Csf2ra*$^{-/-}$ recipient neonates (Fig 2A). CSF2-cFLiMo-derived AM (CSF2-cFLiMo-AM) and AM-derived AM (AM-AM) expanded in the BAL and lung (Fig 2B-D) of *Csf2ra*$^{-/-}$ recipients. Their surface staining (CD11c^{hi}SiglecF^{hi}) (Fig 2B), and their numbers in the BAL (Fig 2C) and lung (Fig 2D), were comparable to AM in untreated WT controls. These results demonstrate that CSF2-cFLiMo-derived AM have self-renewal capacity *in vivo*, comparable to WT AM.

CSF2-cFLiMo cannot survive in MHC-mismatched recipient lungs

Our data strongly suggests that CSF2-cFLiMo could be used as an *in vitro* and *in vivo* system to study the function and development of AM. The survival of CSF2-cFLiMo in MHC- or gender-mismatched recipient lungs is an important technical aspect that needs to be checked. We first evaluated the MHC compatibility in an allogeneic CSF2-cFLiMo transfer. For this purpose, we generated CSF2-cFLiMo from BALB/c E14.5 embryos. We transferred them in a 1:1 ratio with B6 CSF2-cFLiMo or separately into neonatal *Csf2ra*$^{-/-}$

Figure 3

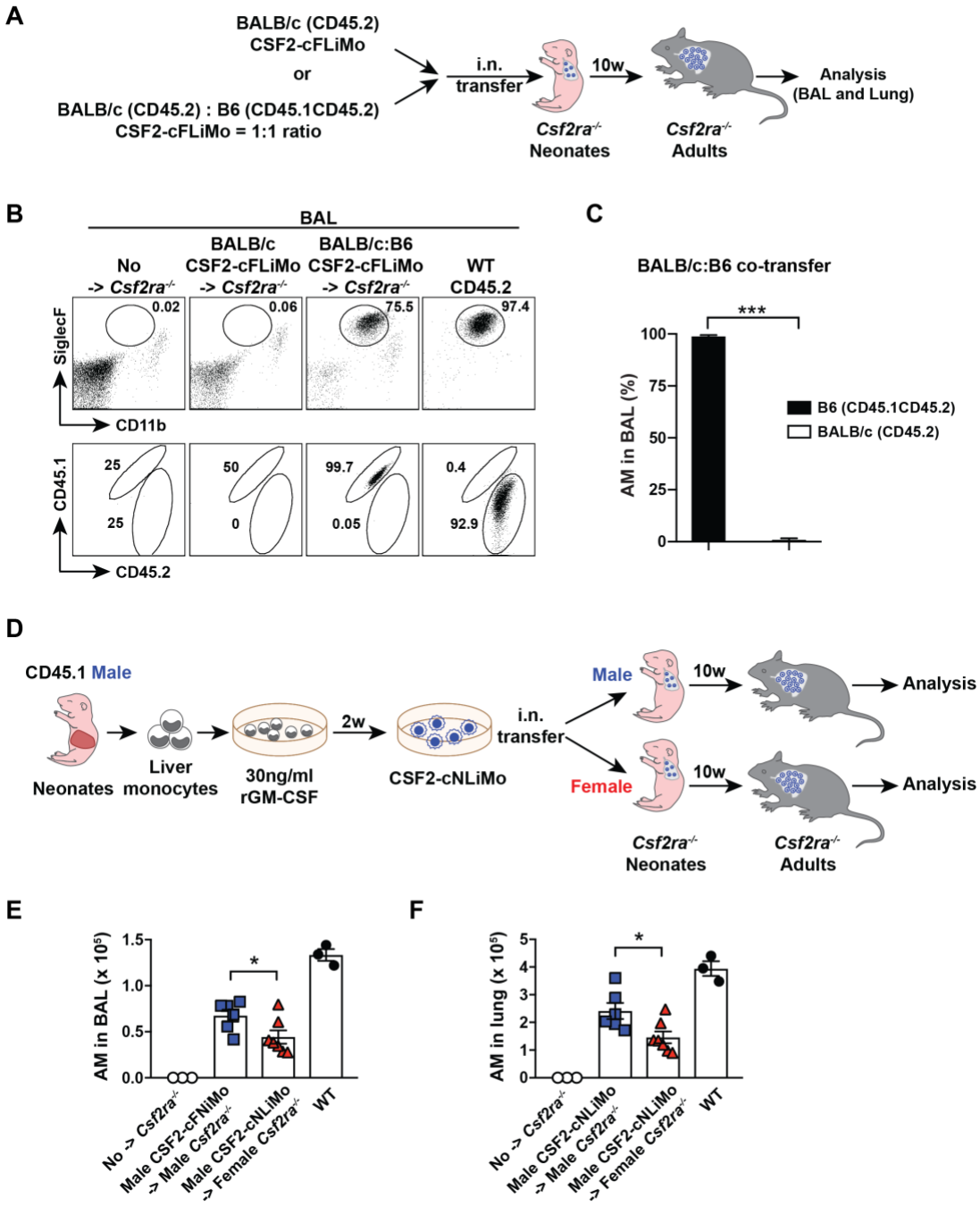

Figure 3. The MHC and gender compatibility in allogenic CSF2-cFLiMo transfers. (A-C) CD45.2 BALB/c and CD45.1 B6 CSF2-cFLiMo were generated from E14.5 embryos and cultured 2 weeks *in vitro*. BALB/c CSF2-cFLiMo were transferred to neonatal CD45.2 *Csf2ra*$^{-/-}$ mice (B6 background) either separately or in 1:1 ratio with B6 CSF2-cFLiMo and analyzed 10 weeks later. (B) Representative dot plots showing the phenotype of donor-derived AM in the BAL, pregated on viable CD45^{+} single cells. (C) Percentage of donor-derived AM in BAL of co-transferred recipients. (D-F) CSF2-cNLiMo generated from CD45.1 WT male neonates after 2-week culture were transferred i.n. to neonatal CD45.2 *Csf2ra*$^{-/-}$ mice and analyzed after 10

(legend continued on the next page)

weeks. Mice were grouped according to gender. Numbers of donor-derived AM and endogenous AM (WT) in the BAL (E) and lung (F) are shown. Age-matched *Csf2ra*$^{-/-}$ and CD45.2 WT mice were included as negative and positive controls in B, E and F. The data are representative of two experiments. Values show means ± SEM in C, E and F and Student's t test (unpaired) was used: ns, not significant; *p < 0.05, **p < 0.01, ***p < 0.001.

mice (B6 background) and analyzed BAL and lung 10 weeks later (Fig 3A). There were almost no BALB/c CSF2-cFLiMo-derived AM either in competitively transferred or BALB/c CSF2-cFLiMo-only transferred mice (Fig 3B-C, sFig 4), indicating that there was a massive rejection of BALB/c-derived cells in B6 recipients.

As we usually generated CSF2-cFLiMo from pooled embryonic livers (both male and female origin), we then investigated the Y chromosome compatibility in allogeneic CSF2-cFLiMo transfer. We generated CSF2 cultured-monocytes from male neonatal livers (CSF2-cNLiMo) and transferred them i.n. to neonatal *Csf2ra*$^{-/-}$ males or females (Fig 3D). Analysis of BAL and lung of *Csf2ra*$^{-/-}$ recipients 10 weeks after transfer showed that donor-derived AM could be detected in all transferred animals independently of sex (Fig 3E-F). Interestingly, female recipients had slightly lower AM counts than male recipients in the BAL (Fig 3E) and lung (Fig 3F). This indicates either a minor Y chromosome-dependent selection or corresponds to the generally lower AM numbers in naïve WT females when compared to age-matched males.

Together, these data indicate that MHC compatibility require consideration in allogeneic transfer of CSF2-cFLiMo.

CSF2-cFLiMo acquire AM-specific transcriptional signature in vivo

To further support that CSF2-cFLiMo acquire AM identity *in vivo*, we compared the transcriptomes of CSF2-cFLiMo, CSF2-cFLiMo-derived AM to endogenous AM and E14.5 fetal liver monocytes (Fig 4A). Principal-component analysis (PCA) and matrix clustering, based on all detected genes, revealed that fetal liver monocytes, CSF2-cFLiMo and CSF2-cFLiMo-derived AM differed in their gene expression profiles, while CSF2-cFLiMo-derived AM and endogenous AM were most related and clustered together (Fig 4B-C). Both CSF2-cFLiMo-derived AM and endogenous AM expressed low levels of several well-known monocyte markers, including *Ly6c1* (Ly6C), *Fcgr1* (CD64), *Itgam* (CD11b) (Fig 4D). Moreover, the relative mRNA expression of several established AM markers, including *Marco*, *Pparg*, *Itgax* (CD11c), *MerTk*, *Cd14*, *Fcgr2b* (CD32), *Siglec5* (SiglecF) and

Figure 4

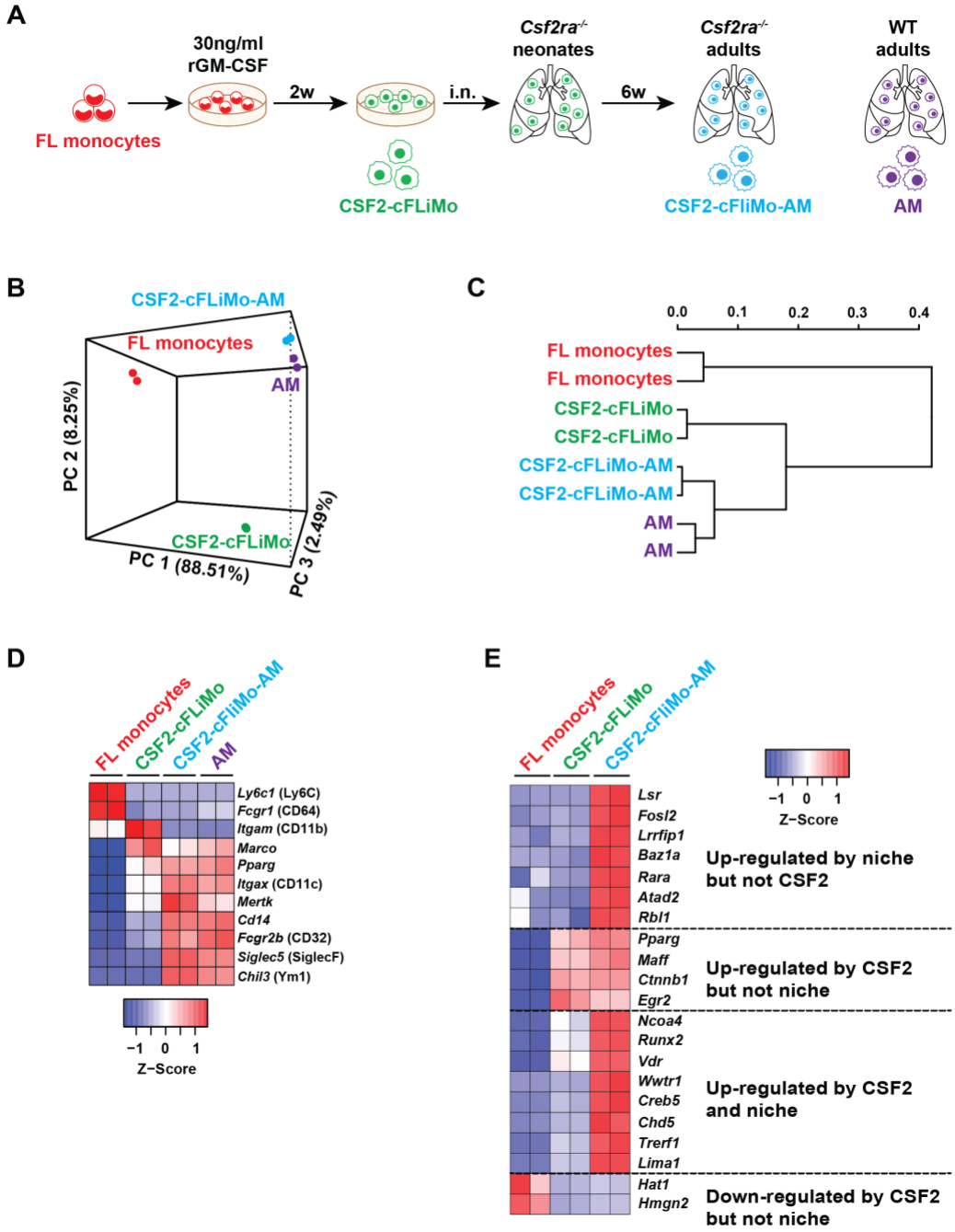

Figure 4. Gene expression profiles of transferred CSF2-cFLiMo in *Csf2ra*$^{-/-}$ mice. (A) Experimental outline. Primary monocytes from E14.5 fetal liver were sorted using flow cytometry. GM-CSF (CSF2)-cultured fetal liver monocytes (CSF2-cFLiMo) were collected after 2 weeks. CSF2-cFLiMo were intranasally transferred to neonatal *Csf2ra*$^{-/-}$ mice. Mice were analyzed 6 weeks after transfer and CSF2-cFLiMo-derived mature AM (CSF2-cFLiMo-AM) were sorted from the BAL as viable CD45^{+}CD11c^{hi}F4/80^{+}SiglecF^{hi}CD11b^{lo} cells. AM from 6-week old WT mice were sorted as control. All sorted samples are biological replicates. RNA sequencing was performed. (B) Principal component analysis (PCA) and (C) matrix clustering of the

(legend continued on the next page)

transcriptomes of all samples are shown. (D-E) Heat maps showing expression of monocyte and AM markers (D) and AM signature transcription factors (E).

Chil3 (Ym1) was similar between CSF2-cFLiMo-derived AM and endogenous AM (Fig 4D). A study, which compared gene expression profiles of lung, spleen, brain, and peritoneal cavity macrophages, described an AM-specific signature gene list [58]. We extracted these genes from our transcriptome data and grouped them into heat maps presenting down- and up-regulated signature genes (sFig 5). Almost all AM signature-down (sFig 5A) and AM signature-up (sFig 5B) genes were similarly expressed in CSF2-cFLiMo-derived AM and endogenous AM. Most of the AM signature-up genes showed low expression in primary fetal liver monocytes (sFig 5B). Some of these genes were upregulated upon culturing with GM-CSF *in vitro,* suggesting that they are directly or indirectly regulated by GM-CSF, which these cells normally encounter in the fetal lung. However, the other signature genes were only upregulated to the level of mature AM after transfer and maturation *in vivo* (sFig 5B).

The *in vitro* culture of precursors followed by *in vivo* transfer described here creates a model to study GM-CSF and other niche factors during AM development. Comparison of the CSF2-cFLiMo and fetal liver monocyte transcriptomes revealed 3301 upregulated and 2657 downregulated genes, which were dependent on CSF2 (sFig 6A). Similarly, comparing the transcriptomes of CSF2-cFLiMo-AM to CSF2-cFLiMo, we found 2032 niche factors-upregulated and 1813 of niche factors-downregulated genes (sFig 6A). Only minor fraction of CSF2-upregulated genes was further upregulated (11.9%) and downregulated (20.3%) by niche factors (sFig 6B). Similarly, 8.8% and 7.8% of CSF2-downregulated genes were further upregulated or downregulated by niche factors, respectively (sFig 6B). These results showed that the majority of genes were separately regulated by CSF2 and by additional niche factors. Additionally, more than half of the gene expression changes were exclusive to CSF2 (sFig 6B), indicating its major contribution to AM development. In order to further understand the transcriptional regulation during the differentiation process, we extracted transcription factors and transcription co-factors (TF) and analyzed them separately. We found 395 CSF2-upregulated and 317 CSF2-downregulated TF, and 417 niche factor-upregulated and 128 niche factor-downregulated TF (sFig 6A). Again, only a minor fraction of the TF was co-regulated by CSF2 and additional niche factors (sFig 6C-D). Next, we focused our analysis on 21 AM-specific TF (signature TF) [58]. We found that 11 AM-specific TF were separately

regulated by CSF2 and niche factors (Fig 4E). 4 of them, including *Pparg*, *Maff*, *Ctnnb1* and *Egr2*, were upregulated by CSF2 but not niche factors, and 7 of them, including *Lsr*, *Fosl2*, *Lrrfip1*, *Baz1a*, *Rara*, *Atad2* and *Rbl2*, were upregulated by niche factors but not CSF2. 8 of the AM-specific TF, including *Ncoa4*, *Runx2*, *Vdr*, *Wwtr1*, *Creb5*, *Chd5*, *Trerf1* and *Lima1* were slightly upregulated by GM-CSF stimulation and further upregulated by additional niche factors (Fig 4E).

Taken together, our results show that CSF2-cFLiMo acquire a partial AM-specific phenotype and gene expression profile in culture with CSF2, while additional niche factors contribute to full AM maturation *in situ* after transfer into the recipient lungs.

CSF2-cFLiMo give rise to functional AM that prevent PAP

While we showed that CSF2-cFLiMo-derived AM acquired AM signature *in vivo,* we wanted to test their functional potential. Naïve *Csf2ra*$^{-/-}$ mice are devoid of endogenous AM and, as a consequence, develop pulmonary alveolar proteinosis (PAP), which manifests with pronounced protein accumulation in the BAL [251]. CSF2-cFLiMo-derived AM could maintain low protein levels in the BAL for at least 1year post-transfer, protecting mice from PAP (Fig 5A-B). These data show that CSF2-cFLiMo-derived AM were functionally equivalent and could efficiently and durably prevent PAP.

To determine the number of donor cells required to fully reconstitute the AM compartment, we titrated the number of transferred CSF2-cFLiMo (Fig 5C). When neonatal *Csf2ra*$^{-/-}$ mice received less than 5×10^4 CSF2-cFLiMo, AM numbers did not reach endogenous levels within 6 weeks and consequently mice developed PAP (Fig 5D-E). Use of higher numbers resulted in good reconstitution and similar AM counts. All mice transferred with more than 5×10^4 CSF2-cFLiMo were protected from PAP (Fig 5D-E). Moreover, extended 4 month-long *in vitro* culture did not affect the proliferative and functional potential of CSF2-cFLiMo-derived AM *in vivo* (Fig 5D-E).

Next, we assessed whether CSF2-cFLiMo could substitute functional AM upon transfer into adult *Csf2ra*$^{-/-}$ mice, which had already developed PAP. Adult *Csf2ra*$^{-/-}$ mice received 0.5, 1 or 2 Mio congenically marked CSF2-cFLiMo i.t. (Fig 5F). Ten weeks after transfer, donor-derived AM were detectable in the BAL and lung of *Csf2ra*$^{-/-}$ only in recipients transferred with 2 Mio cells (Fig 5G). The protein levels in the BAL from mice

Figure 5

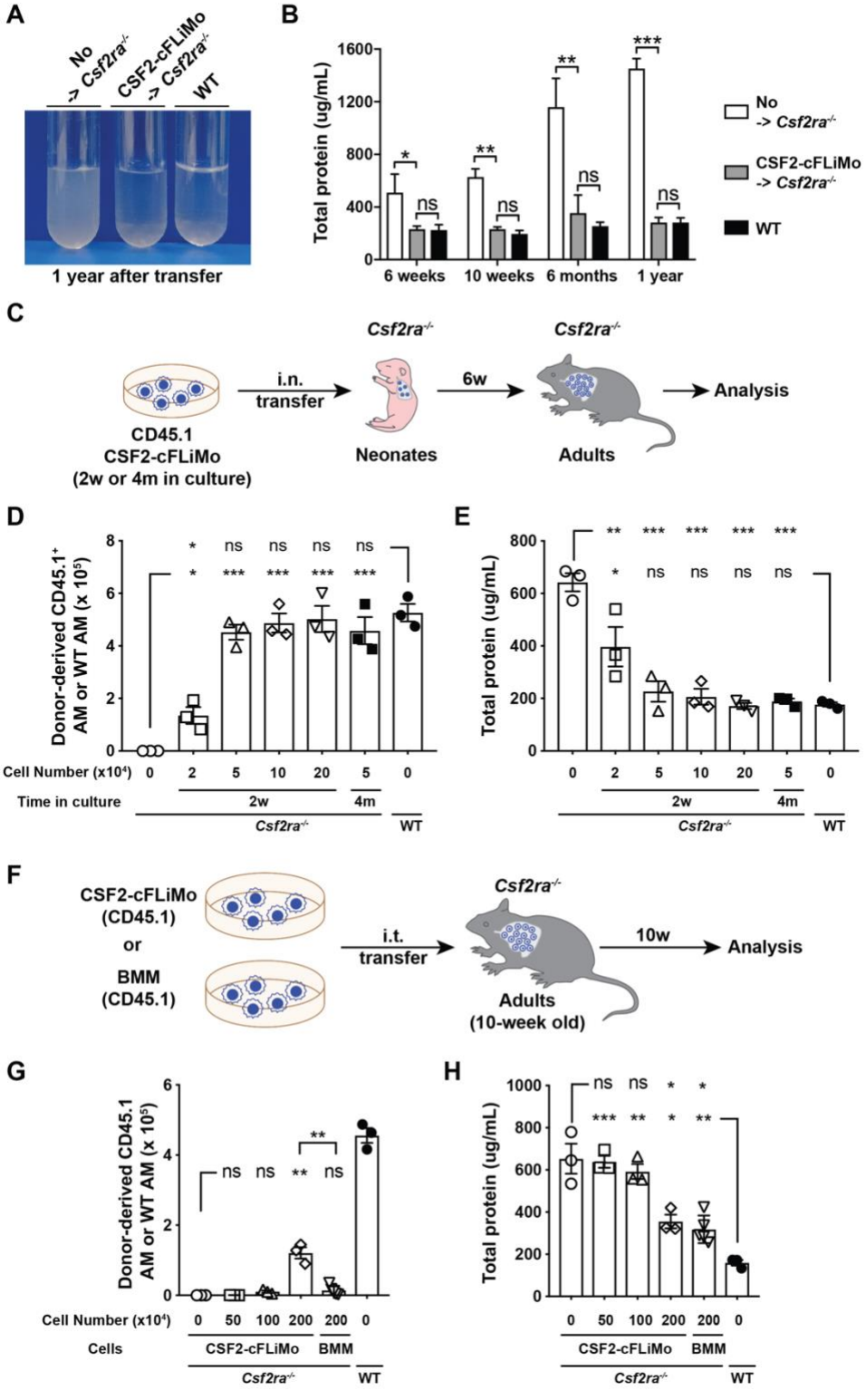

Figure 5. CSF2-cFLiMo give rise to functional AM that prevent PAP. (A-B) $5\times10_4$ of CSF2-cFLiMo generated from CD45.1 E14.5 embryos, after 2 weeks of culturing, were i.n. transferred to neonatal CD45.2 *Csf2ra*$^{-/-}$ mice and analyzed at indicated time points. (A) Appearance of BAL fluid 1 year after transfer. (legend continued on the next page)

(B) Total protein in the BAL at indicated time points. (C) Experimental outline. Different numbers of CD45.1 CSF2-cFLiMo after 2-week (2w) or 4-month (4m) of culturing were intranasally transferred to neonatal CD45.2 *Csf2ra*$^{-/-}$ mice and analyzed 6 weeks later. (D) Total numbers of donor-derived AM in the BAL and lung of recipient *Csf2ra*$^{-/-}$ mice or AM in the BAL and lung of WT mice. (E) Total protein levels in the BAL are shown. (F) Experimental outline. CD45.1 B6 CSF2-cFLiMo were generated from E14.5 embryos and cultured 2 weeks *in vitro*. CD45.1 bone marrow-derived macrophages (BMM) were generated from adults and cultured 7 days *in vitro*. Different numbers of CSF2-cFLiMo or BMM were transferred to 10-week-old adult *Csf2ra*$^{-/-}$ mice intratracheally (i.t.) and analyzed 10 weeks later. (G) Total numbers of donor-derived AM in the BAL and lung of recipient *Csf2ra*$^{-/-}$ mice or AM in the BAL and lung of WT mice. (H) Total protein levels in the BAL are shown. Age-matched *Csf2ra*$^{-/-}$ and WT C57BL/6 mice were included as negative and positive controls, respectively. Values show means ± SEM and the results are representative of two to three experiments. Student's t test (unpaired) was used in B and ANOVA (one way) was used in D and E: ns, not significant; *p < 0.05, **p < 0.01, ***p < 0.001.

transferred with $2\times10_6$ cells were significantly lower when compared to naïve *Csf2ra*$^{-/-}$ mice, suggesting that transferred cells were able to reduce proteinosis, although they did so less efficiently than endogenous AM in WT mice (Fig 5H). Recent studies have shown that transplantation of BMM could decrease proteinosis in adult *Csf2rb*$^{-/-}$ mice [248, 254]. To compare the functional potential of BMM- and CSF2-cFLiMo-derived AM, we transferred 2 Mio congenically marked BMM into adult *Csf2ra*$^{-/-}$ mice (Fig 5F). In agreement with previous reports, we detected reduced protein levels in BMM-transplanted mice (Fig 5H). The effect was similar to the one observed for mice transplanted with the same amount of CSF2-cFLiMo. However, the numbers of BMM-derived AM were much lower than CSF2-cFLiMo-derived AM at the analyzed timepoint (Fig 5G), suggesting that despite their ability to reduce proteinosis, transferred BMM did not engraft as efficiently in adult *Csf2ra*$^{-/-}$ lungs. Compared to endogenous AM, both CSF2-cFLiMo- and BMM-derived AM exhibited higher expression of F4/80 and CD11b, and lower expression of SiglecF and CD64 (sFig 7A-B), indicating that transferred cells could not fully reproduce AM phenotype in the adult lung.

Transplantation of CSF2-cFLiMo in neonatal *Csf2ra*$^{-/-}$ mice results in robust AM reconstitution and low protein levels comparable to that detected in WT animals (Fig 5A-E). However, transplantation of CSF2-cFLiMo in adult *Csf2ra*$^{-/-}$ mice only partially reduced excess of protein, and cells could not effectively engraft in the lung (Fig 5F-H). One possible reason is the occurrence of proteinosis in adults, which might obstruct the contact between transplanted cells and lung epithelial cells, which might be crucial for

proper engraftment. To check this hypothesis, we i.t. transferred different numbers of congenically marked CSF2-cFLiMo into 2-week old *Csf2ra*$^{-/-}$ mice, before the onset of PAP (sFig 8A). Ten weeks after transfer, donor-derived AM were detectable in the BAL and lung of *Csf2ra*$^{-/-}$ recipients (sFig 8B). Expectedly, the protein levels in the BAL from mice transferred with more than $2\times10_5$ CSF2-cFLiMo were comparable to the level detected in naïve WT mice (sFig 8C). Therefore, transplantation before onset of PAP

Figure 6

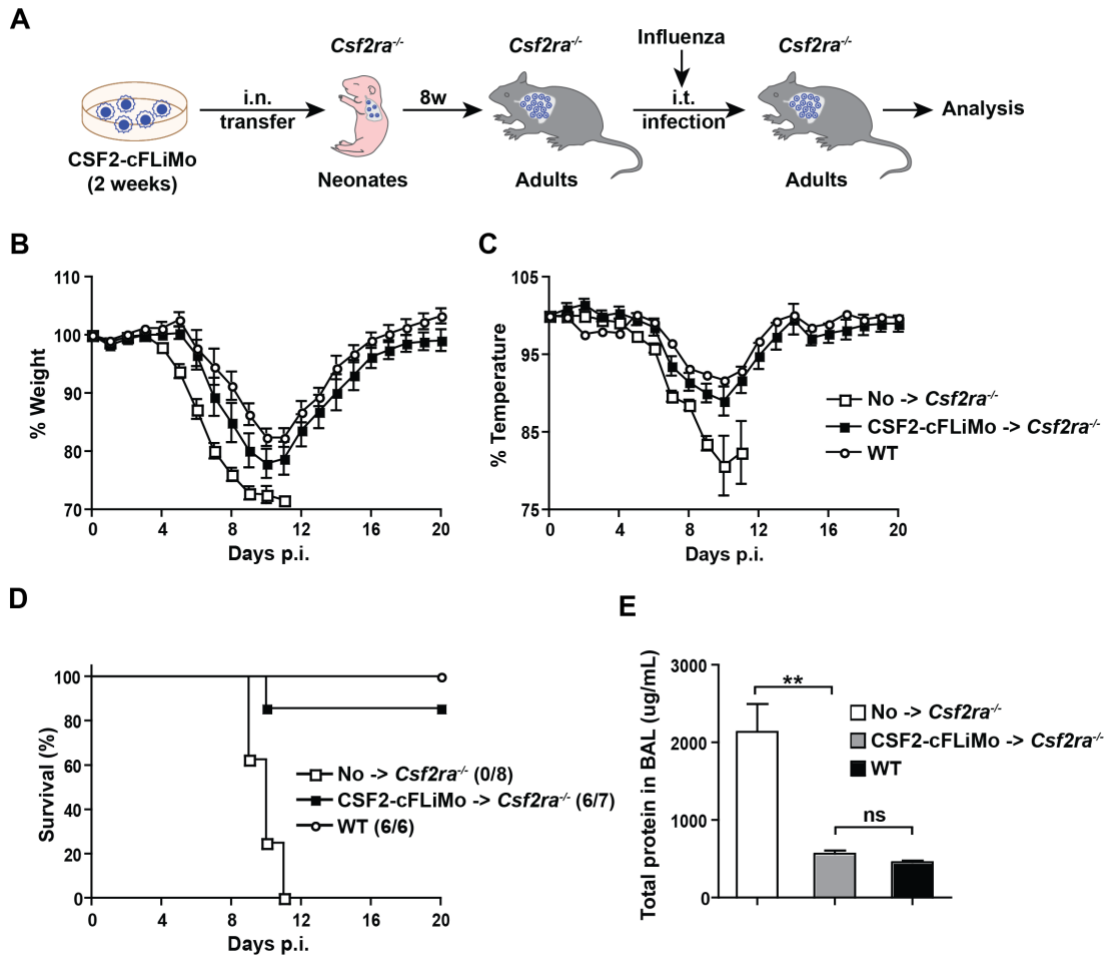

Figure 6. CSF2-cFLiMo transplantation protects *Csf2ra*$^{-/-}$ mice from respiratory failure following influenza infection. (A) Experimental outline. CSF2-cFLiMo generated from E14.5 embryos after 2-week culture were transferred i.n. to neonatal CD45.2 *Csf2ra*$^{-/-}$ mice. Recipient mice were i.t. infected with 10 pfu PR8 influenza virus eight weeks after transfer. Shown are loss of body weight (B) and temperature (C), relative to the day of infection. (D) Survival curve showing the fraction of surviving animals for each day after infection. (E) Total protein in the BAL at 5 days post infection. Age-matched *Csf2ra*$^{-/-}$ and WT mice were included as negative and positive controls, respectively. Values show means ± SEM and the results are representative of three experiments. Student's t test (unpaired) was used in E: ns, not significant; *p < 0.05, **p < 0.01, ***p < 0.001.

improved the functional outcome. However, CSF2-cFLiMo-derived AM exhibited higher expression of F4/80 and CD11b, and lower expression of SiglecF and CD64 when compared to endogenous AM (sFig 8D-E), indicating that the AM phenotype was not fully recapitulated but intermediate between AM-derived from CSF2-cFLiMo transferred to neonates and AM-derived from CSF2-cFLiMo transplanted to adult mice. These results show that CSF2-cFLiMo can reproduce AM phenotype and function most adequately only when transferred to neonatal *Csf2ra*$^{-/-}$ mice.

CSF2-cFLiMo-derived AM are able to robustly protect Csf2ra$^{-/-}$ *mice from mortality and respiratory failure during influenza infection*

In addition to the homeostatic function, AM play an essential role in protecting influenza virus-infected mice from morbidity by maintaining lung integrity through the removal of dead cells and excess surfactant [111]. To assess the function of CSF2-cFLiMo-derived AM during pulmonary virus infection, we infected mice with influenza virus PR8 eight weeks after CSF2-cFLiMo transfer (Fig 6A). CSF2-cFLiMo-derived AM protected *Csf2ra*$^{-/-}$ mice from severe morbidity and mortality following influenza infection (Fig 6B-D). Moreover, the protein concentration in the BAL in *Csf2ra*$^{-/-}$ mice with CSF2-cFLiMo-derived AM was reduced to the level detected in WT controls (Fig 6E). Thus, these results demonstrate that CSF2-cFLiMo-derived AM support protection of reconstituted *Csf2ra*$^{-/-}$ mice from mortality and respiratory failure during influenza infection.

Csf2ra-reconstitution of Csf2ra$^{-/-}$ *CSF2-cFLiMo reveals the potential for genetic manipulation*

AM specific reconstitution with cultivatable precursors should open the possibility for genetic manipulation. To test this hypothesis, pMo-FLi were purified from E14.5 *Csf2ra*$^{-/-}$ or WT embryos and transduced with a GM-CSFRa-GFP-encoding or GFP control retrovirus (RV) (Fig 7A). CSF2-Csf2ra$_{reconst}$-cFLiMo expanded in the presence of GM-CSF *in vitro* (Fig 7B) and outgrew all non-transduced cells, as indicated by the presence of almost 100% GFP^{+} cells by day 7 of culture (Fig 7B-C). As expected, *Csf2ra*$^{-/-}$ pMo-FLi, that were transduced with a control RV, could not expand in culture (Fig 7B-C). Notably, WT cFLiMo, which overexpressed the GM-CSFRa (Fig. 7C), had a selective advantage over non-transduced cells (Fig. 7B), indicated by the increasing abundance of GFP^{+} cells, suggesting that GM-CSF signaling is a limiting factor for the expansion of CSF2-cFLiMo cells *in vitro.* To address whether transduced CSF2-cFLiMo cells are able to reconstitute

Figure 7

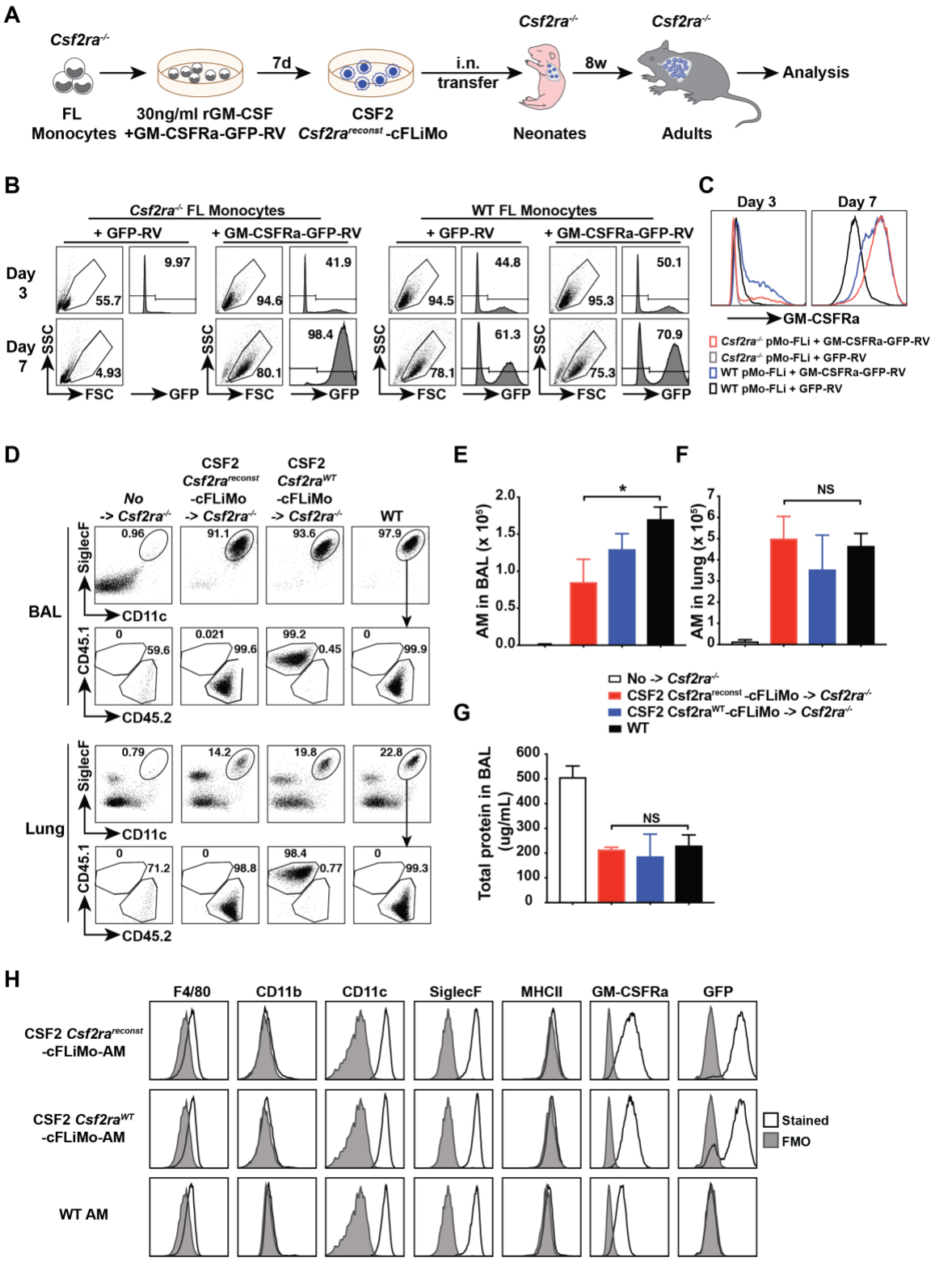

Figure 7. Csf2ra-reconstituted *Csf2ra*$^{-/-}$ CSF2-cFLiMo can differentiate into functional AM *in vivo*. (A) Experimental outline. Fetal liver monocytes were purified from E14.5 CD45.2 *Csf2ra*$^{-/-}$ or CD45.1 WT embryos and spin infected with GM-CSFRa-GFP or GFP (control) retrovirus. Cells were cultured with CSF2 (legend continued on the next page)

for 7 days. *Csf2ra*-reconstituted *Csf2ra*$^{-/-}$ CSF2-cFLiMo (CSF2-Csf2ra$_{reconst}$-cFLiMo) or identically treated CD45.1 WT CSF2-cFLiMo (CSF2-Csf2ra$_{WT}$-cFLiMo) were i.n. transferred to neonatal CD45.2^{+} *Csf2ra*$^{-/-}$ mice and evaluated after 8 weeks. (B) Efficiency of spin infection (GFP^{+}) and survival of cultured cells at day 3 and 7 post-infection. (C) Expression levels of GM-CSFRa on reconstituted *Csf2ra*$^{-/-}$ or CD45.1 WT cFLiMo at day 3 and 7 post-infection. (D) Representative dot plots showing the phenotype of donor-derived cells in the BAL and lung, pregated on viable CD45^{+} single cells. (E-F) Numbers of donor-derived F4/80^{hi}CD11c^{hi}CD11b^{lo}SiglecF^{hi} AM and endogenous AM in the BAL (E) and lung (F). (G) Total protein levels in the BAL are shown. Age-matched *Csf2ra*$^{-/-}$ and CD45.2 WT mice were included as negative and positive controls in D-G, respectively. (H) Representative histograms of AM signature marker expression, GM-CSFRa and GFP on CSF2-Csf2ra$_{reconst}$-cFLiMo-derived AM, CSF2-Csf2ra$_{WT}$-cFLiMo-derived AM and endogenous AM showing FMO control (grey) and specific antibodies against indicated markers (black line). The data are representative of three experiments. Values show means ± SD of three to four mice per group. Student's t test (unpaired) was used in E-G: ns, not significant; *p < 0.05, **p < 0.01, ***p < 0.001.

AM, Csf2ra-reconstituted *Csf2ra*$^{-/-}$ CSF2-cFLiMo (CSF2-Csf2ra$_{reconst}$-cFLiMo) or identically treated WT CSF2-cFLiMo (CSF2-Csf2ra$_{WT}$-cFLiMo) were harvested on day 7 of culture and transferred into neonatal *Csf2ra*$^{-/-}$ mice. 8 weeks later, CSF2-Csf2ra$_{reconst}$-cFLiMo and CSF2-Csf2ra$_{WT}$-cFLiMo equally expanded *in vivo* and restored a functional AM compartment, that prevented development of PAP (Fig 7F-G). Transfer of Csf2ra-overexpressing WT cFLiMo did not result in higher AM numbers suggesting that *in vivo*, GM-CSF bioavailability rather than receptor expression is the limiting factor. RV transduced cFLiMo-derived AM were phenotypically indistinguishable from non-transduced native AM for multiple surface markers, including F4/80, CD11b, CD11c, SiglecF, and MHCII (Fig 7H). These results provide a proof-of-concept that gene-modified CSF2-cFLiMo differentiate into functional *bona fide* AM, therefore allowing genetic manipulation of this important tissue macrophage compartment.

5.2.5 Discussion

This study describes a two-step AM differentiation model, in which a homogenous, non-transformed immature AM-like population (CSF2-cFLiMo) generated from murine fetal liver monocytes *in vitro* could efficiently engraft a recipient lung and further differentiate into *bona fide* AM *in vivo*. These derived AM resemble endogenous AM phenotypically, genetically, and functionally, and are amenable to genetic modifications. We propose that this AM model, which integrates not only ontogeny but also tissue imprinting in the production of an AM equivalent, will be a potent tool to study AM development and function, as well as opening possibilities for therapeutic approaches.

In our *in vitro* culture system, CSF2-cFLiMo were generated from WT fetal liver monocytes with GM-CSF, while monocytes from *Csf2ra*$^{-/-}$ fetal livers did not expand in presence of GM-CSF, demonstrating that the generation of CSF2-cFLiMo is GM-CSF dependent *in vitro*. Maintenance of an established CSF2-cFliMo culture is also GM-CSF dependent because the numbers of established CSF2-cFLiMo decreased over time after deprivation of GM-CSF. These results agree with the previous *in vivo* studies that GM-CSF is critical for differentiation of fetal monocytes into AM [98, 99] and show that created cell line is a non-transformed population.

CSF2-cFLiMo retain the potential to develop into mature AM *in vivo*. Upon transfer, cells gained a *bona fide* AM phenotype and transcriptional signature. Importantly, transferred cells could completely fill the empty lung niche in 6 weeks and their self-renewing potential was maintained long-term *in vivo*. Furthermore, transferred CSF2-cFLiMo developed into functionally competent AM upon transfer to neonatal lungs. They could prevent PAP and protect from the lethal effects of influenza infection. Collectively, our modeled AM recapitulated features of AM both in homeostasis and during infection.

GM-CSF has been considered as a critical lung-specific signal for promoting a transcriptional program that mediates AM development [98, 99]. In our study, even though cultured cells differentiated into macrophages and upregulated a series of AM signature genes in the presence of GM-CSF, they did not recapitulate all AM features. However, when transferred into the lung environment, these cultured cells could further differentiate into *bona fide* AM. Here, our two-step model allows us to separate the transcriptional regulation induced by GM-CSF from other niche factors provided by lung environment during AM development. We show that the majority of transcription factors are regulated independently, either by GM-CSF or by other niche factors. Further studies using this model would help to understand transcriptional regulation during AM development.

Tissue macrophages constitute a multifunctional and heterogeneous population [100, 255]. Bone marrow-derived macrophages (BMM), generated from bone marrow precursors upon culturing with M-CSF, are widely used in studies concerning macrophage biology. However, these cells have a limited lifespan and represent only a subset of the macrophage population. They cannot recapitulate features of most tissue resident populations. Notably, M-CSF is dispensable for AM development [123]. Another

primary macrophage population used as an *in vitro* macrophage model are induced-pluripotent-stem-cell (iPSC)-derived macrophages (iMac), which are genetically and functionally similar to yolk sac (YS)-derived primitive macrophages [243, 256]. AM are long-lived, self-renewing tissue resident macrophages in the lungs. They develop from fetal monocytes and are independent of either YS primitive macrophages or bone marrow precursors during homeostasis. CSF2-cFLiMo derive from true AM progenitors, characterized by longevity, proliferation. Extensive time in culture does not alter their phenotype and reconstitution capacity. Compared to BMM, CSF2-cFLiMo show a better potential to expand and acquire a *bona fide* AM phenotype *in vivo*. Despite being able to reduce proteinosis when transferred in adult *Csf2ra*$^{-/-}$ lung, BMM did not engraft efficiently in adult lungs as our derived AM. In addition, our unpublished data show that YS-derived primitive macrophages could not efficiently upregulate SiglecF and downregulate CD11b after transfer into neonatal *Csf2ra*$^{-/-}$ lung, indicating that YS-derived macrophage is not a proper source for the production of AM equivalents. Thus, we propose that CSF2-cFLiMo represent the most suitable cellular source of AM better than BMM and YS-like macrophages.

We show that transplantation of large numbers of CSF2-cFLiMo ($2x10_6$ cells) into the lungs of adult *Csf2ra*$^{-/-}$ mice can reduce proteinosis, while transfer of as few as $5x10_4$ CSF2-cFLiMo to neonatal lung protected from developing PAP during adulthood in *Csf2ra*$^{-/-}$ mice. Furthermore, CSF2-cFLiMo transferred into neonatal lung expanded and gave rise to *bona fide* AM, while when transplanted into adult lung, they could not efficiently expand and upregulate SiglecF, CD64 and downregulate CD11b. These results demonstrate that macrophage transplantation is more efficient in neonates than in adults. There could be two possible reasons. Firstly, the occurrence of proteinosis in adults might obstruct the contact between transplanted cells and lung epithelial cells, which is important for the survival and engraftment of transplanted cells. Secondly, the neonatal lung niche could more efficiently promote AM maturation compared to the adult lung niche, because AM represent a distinct lineage of tissue resident macrophages that mature during neonatal development [93, 98, 99].

Our two-step AM differentiation model is suitable to study the relationship between AM and lung tissue. Genetically modified CSF2-cFLiMo could be used as a high-throughput screening system for genes involved in AM development and function.

Furthermore, CSF2-cFLiMo could help to overcome the number limitation of primary macrophages and be used as a therapeutic approach for PAP disease or in other macrophage-based cell therapies for lung fibrosis, lung infectious disease and lung cancer [257, 258].

Acknowledgements

We thank Malgorzata Kisielow and Anette Schütz (ETH Flow Cytometry Core Facility) for cell sorting. We thank the Swiss National Science Foundation for funding of this project (310030-124922/1).

5.2.6 Supplementary material

sFigure 1

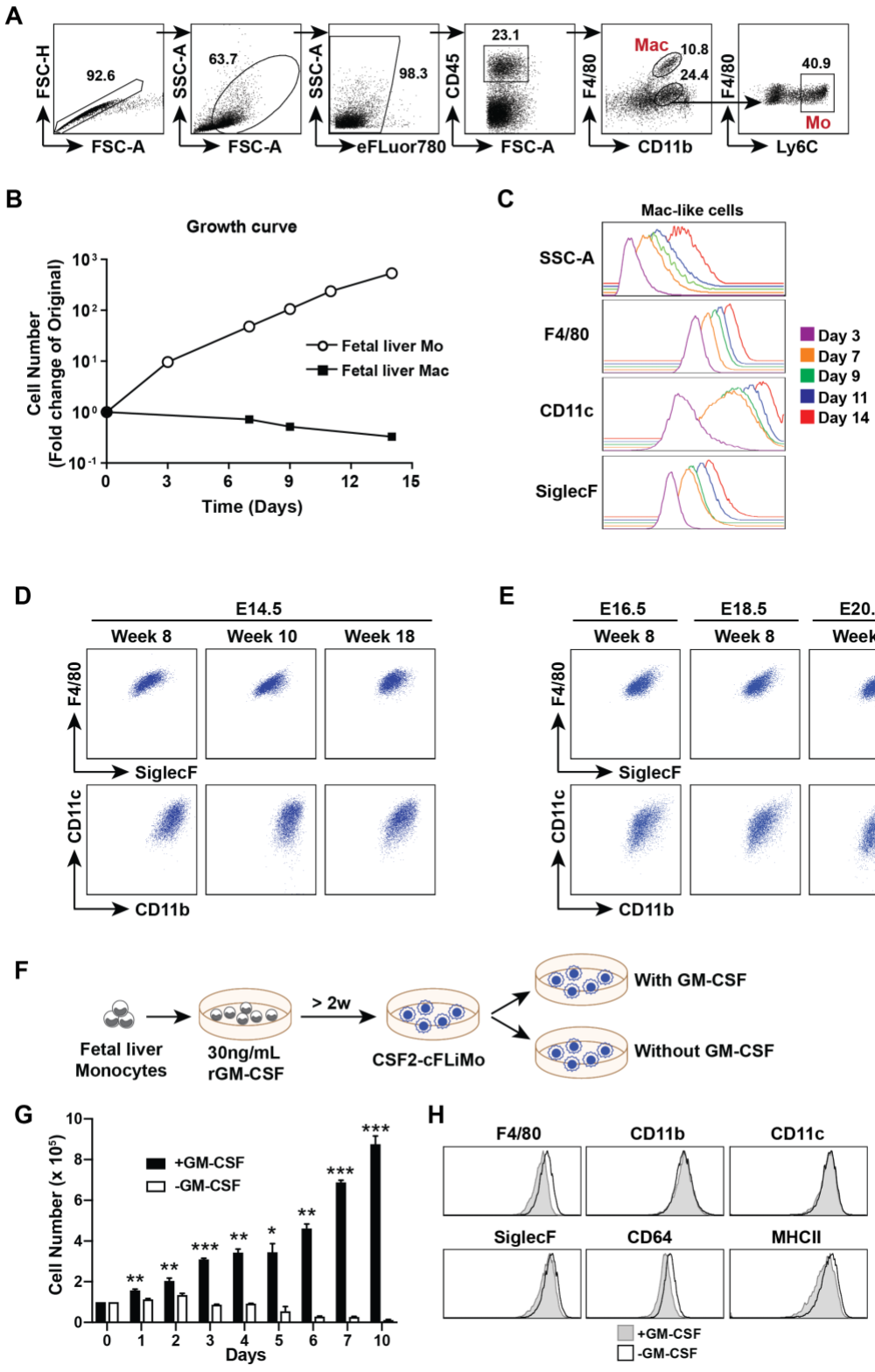

sFigure 1. Fetal liver monocytes differentiate into long-lived, homogeneous, AM-like cells *in vitro* in the presence of GM-CSF, related to Figure 1. (A) Sorting strategy for primary monocytes (Mo) and macrophages (Mac) from fetal liver. Fetal livers were harvested from CD45.1 C57BL/6 embryos. Mo and Mac were sorted using flow cytometry. Doublets and debris were excluded using FSC and SSC. Mo were identified as viable $CD45^{+}F4/80^{lo}CD11b^{int}Ly6C^{+}$ cells and Mac were identified as viable $CD45^{+}F4/80^{hi}CD11b^{lo}$ cells. (B) Growth curves of fetal liver Mo and Mac cultured *in vitro* with GM-CSF (30 ng/mL). (C-E) Flow cytometry was used to characterize cultured cells. Histograms for SSC-A, F4/80, CD11c and SiglecF expression on Mac-like cells ($F4/80^{+}Ly6C^{-}$) at the indicated time points (C). Representative dot plots of CSF2-cFLiMo from E14.5 embryos after 8, 10 and 18 weeks (D) or from E16.5, E18.5 and E20.5 embryos after 8 weeks *in vitro* (E), pregated on viable $CD45^{+}$ single cells. (F-H) CSF2-cFLiMo cultured for more than 2 weeks were either deprived of GM-CSF or kept in culture with GM-CSF. (G) Numbers of CSF2-cFLiMo after removing GM-CSF. (H) Phenotype of CSF2-cFLiMo 6 days after removing GM-CSF. The data are representative of two or three experiments. Values show means ± SEM of two to three wells per group in G. Student's t test (unpaired) was used: ns, not significant; *p < 0.05, **p < 0.01, ***p < 0.001.

sFigure 2

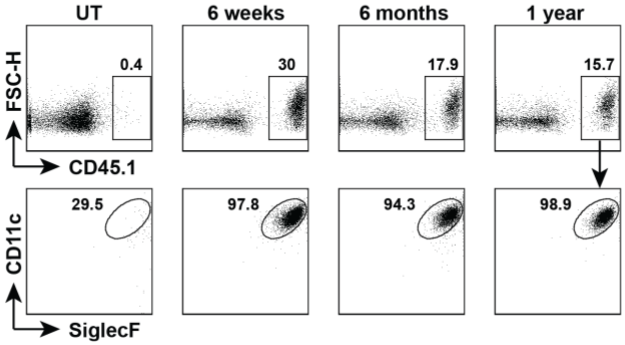

sFigure 2. CSF2-cFLiMo have the potential to further differentiate into mature AM, related to Figure 1. 5×10^{4} of CSF2-cFLiMo generated from CD45.1 E14.5 embryos, after 2 weeks of culturing, were transferred i.n. to neonatal (day 0-3 after birth) CD45.2 *Csf2ra*$^{-/-}$ mice and analyzed at the indicated time points. Representative dot plots of the CD45.1 donor-derived cells in the lung of recipients 6 weeks, 6 months and 1 year after transfer, pregated as viable single cells.

sFigure 3

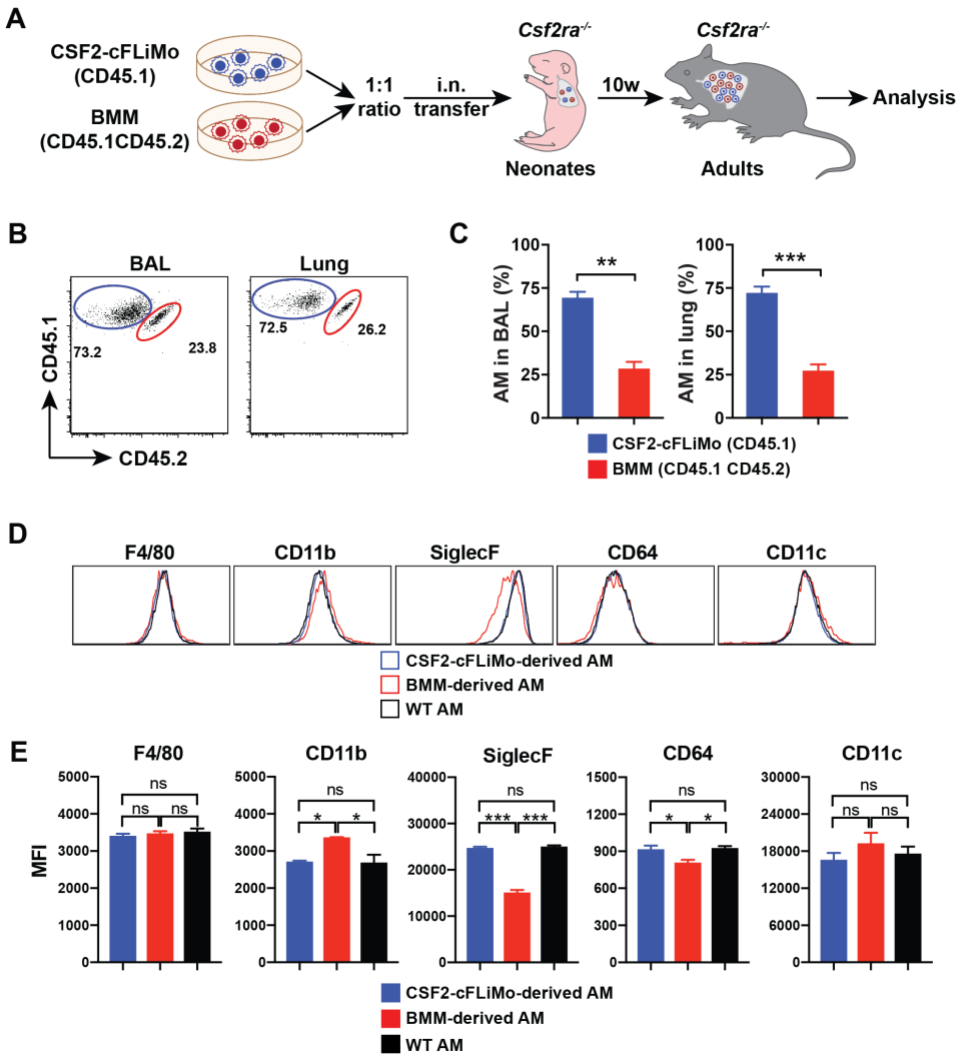

sFigure 3. CSF2-cFLiMo have higher proliferation capacity than BMM in *Csf2ra*$^{-/-}$ neonatal lung, related to Figure 1. (A) Experimental outline. CD45.1 CSF2-cFLiMo were generated from E14.5 embryos and cultured 2 weeks *in vitro*. CD45.1CD45.2 bone marrow-derived macrophages (BMM) were generated from adults and cultured 7 days *in vitro*. CSF2-cFLiMo and BMM were pooled in 1:1 ratio and transferred i.n. to neonatal CD45.2 *Csf2ra*$^{-/-}$ mice and analyzed 10 weeks later. Shown are representative dot plots (B) and percentage (C) of donor-derived AM in BAL and lung of the recipients. (D-E) Representative histograms (D) and mean fluorescence intensity (MFI) (E) of AM signature markers on CSF2-cFLiMo- and BMM-derived AM and endogenous AM. The data are representative of two or three experiments. Values show means ± SEM of three mice per group in C and E. Student's t-test (unpaired) was used in C and ANOVA (one way) was used in E: ns, not significant; *p < 0.05, **p < 0.01, ***p < 0.001.

sFigure 4

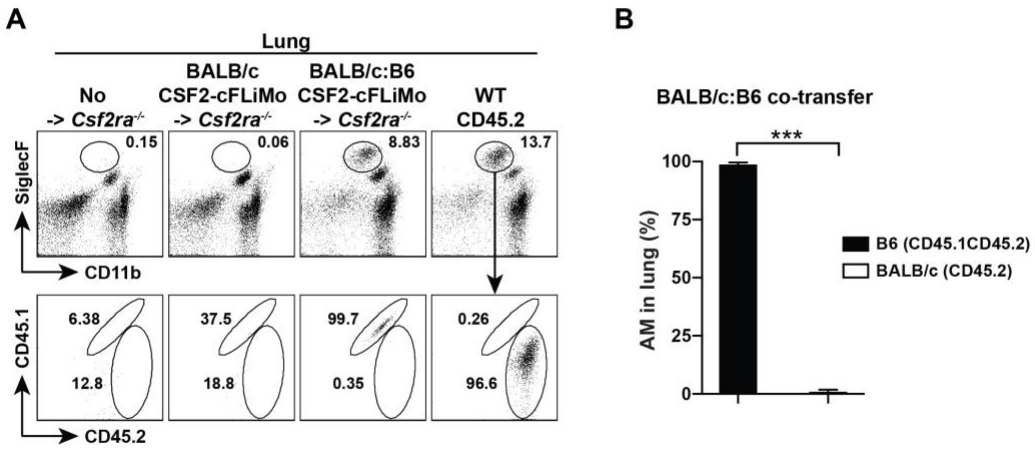

sFigure 4. The MHC compatibility of allogenic CSF2-cFLiMo transfer, related to Figure 3. CD45.2 BALB/c and CD45.1 B6 CSF2-cFLiMo were generated from E14.5 embryos and cultured 2 weeks *in vitro*. BALB/c CSF2-cFLiMo were transferred to neonatal CD45.2 *Csf2ra*$^{-/-}$ mice (B6 background) either separately or in 1:1 ratio with B6 CSF2-cFLiMo and analyzed 10 weeks later. (A) Representative dot plots showing the phenotype of donor-derived AM in the lung, pregated on viable CD45^{+} single cells. (C) Percentage of donor-derived AM in lungs of co-transferred recipients. Age-matched *Csf2ra*$^{-/-}$ and CD45.2 WT mice were included as negative and positive controls in A. The data are representative of two experiments. Values show means ± SEM in B and Student's t test (unpaired) was used: ns, not significant; *$p < 0.05$, **$p < 0.01$, ***$p < 0.001$.

sFigure 5

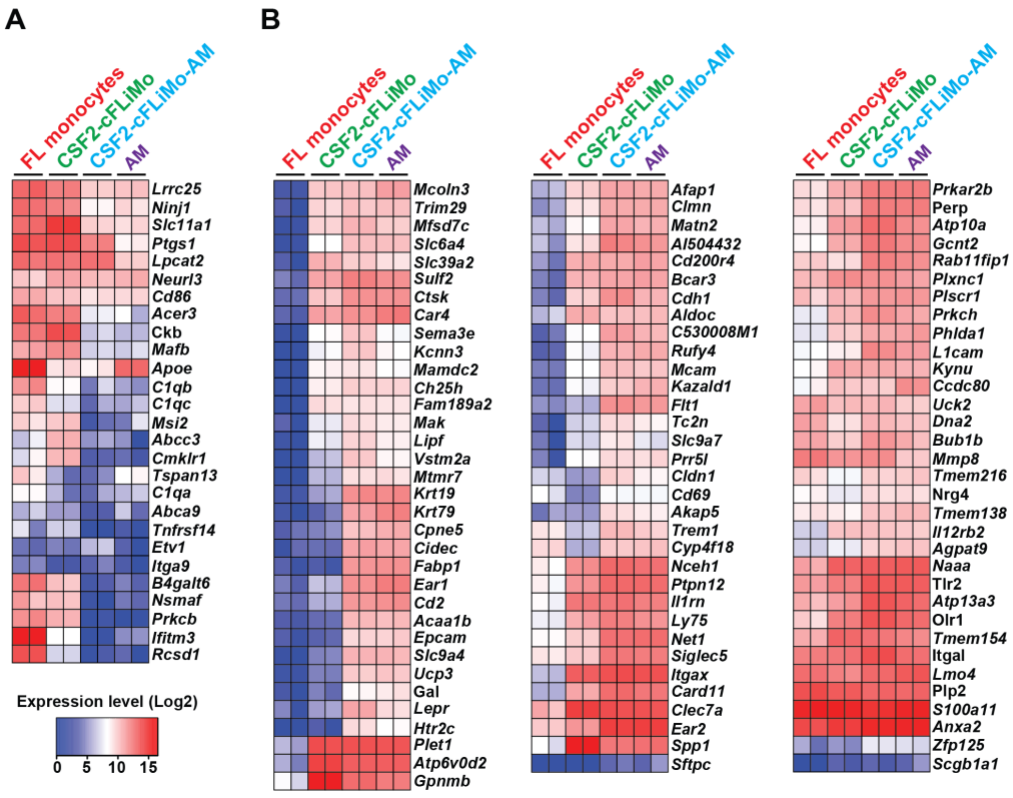

sFigure 5. Gene expression profiles of transferred CSF2-cFLiMo in *Csf2ra*$^{-/-}$ mice, related to Figure 4.

RNA sequencing data were obtained as described for Figure 4. Heat maps showing expression of AM signature-down genes (A) and signature-up genes (B).

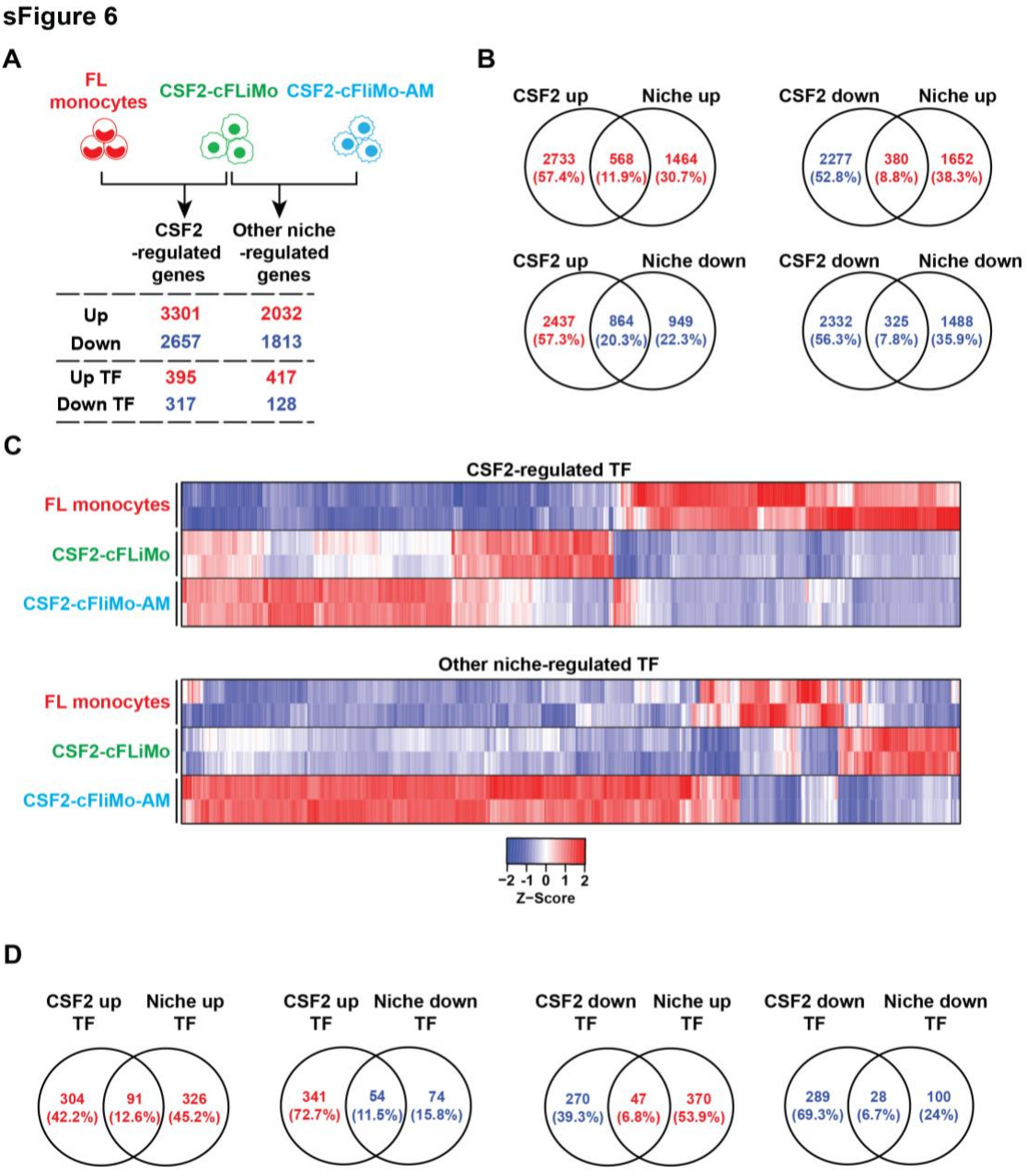

sFigure 6. CSF2- and niche factor-regulated genes, related to Figure 4. RNA sequencing data were obtained as described for Figure 4. (A) CSF2-regulated genes were defined as differentially expressed genes between CSF2-cFLiMo and primary fetal liver monocytes. Other niche-regulated genes were defined as differentially expressed genes between CSF2-cFLiMo-AM and CSF2-cFLiMo. Differentially expressed genes were identified as at least 2-fold differentially expressed ($P < 0.01$, FDR < 0.05) in each comparison. The numbers of upregulated and downregulated genes and transcription factors and transcription co-factors (TF) are shown. (B) Venn diagram of differentially expressed genes. Intersections of CSF2-upregulated or CSF2-downregulated vs niche-upregulated or niche-downregulated genes. The absolute gene numbers and percentages in the intersections are shown. (C) Heat maps showing expression of CSF2-regulated TF and niche-regulated TF. (D) Venn diagram of differentially expressed TF. Intersections of CSF2-upregulated or

CSF2-downregulated vs niche-upregulated or niche-downregulated TF. The absolute TF numbers and percentages in the intersections are shown.

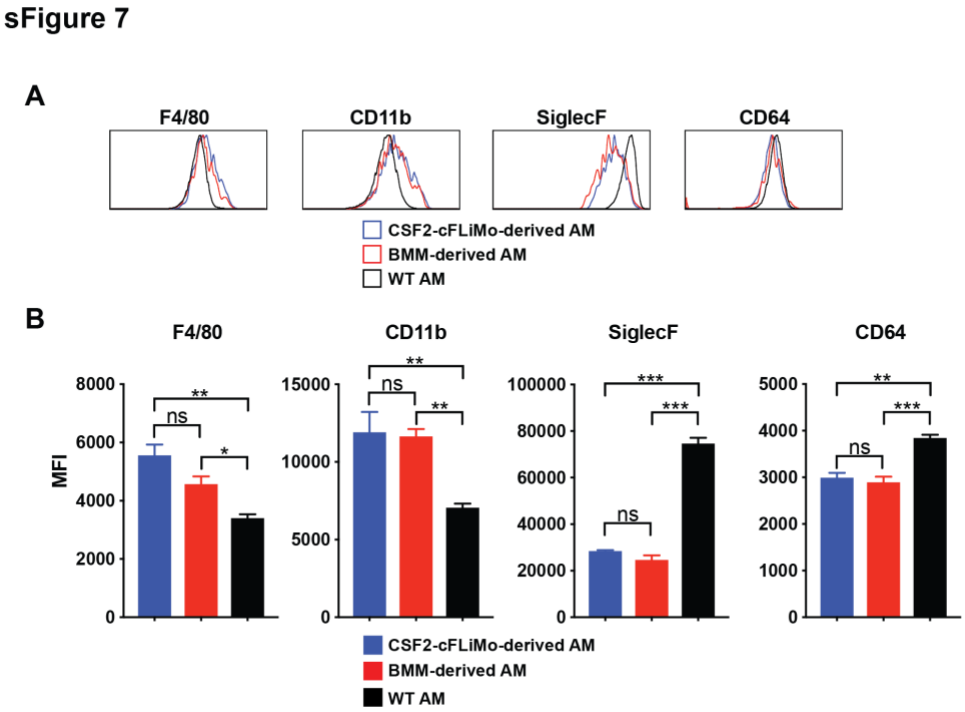

sFigure 7. Transplantation of CSF2-cFLiMo in adult *Csf2ra*$^{-/-}$ mice decrease PAP, related to Figure 5. (A-B) Representative histograms (A) and MFI (B) of AM signature markers on CSF2-cFLiMo- and BMM-derived AM and endogenous AM. The data are representative of two experiments. Values show means ± SEM in B, C and E. ANOVA (one way) was used: ns, not significant; *p < 0.05, **p < 0.01, ***p < 0.001.

sFigure 8

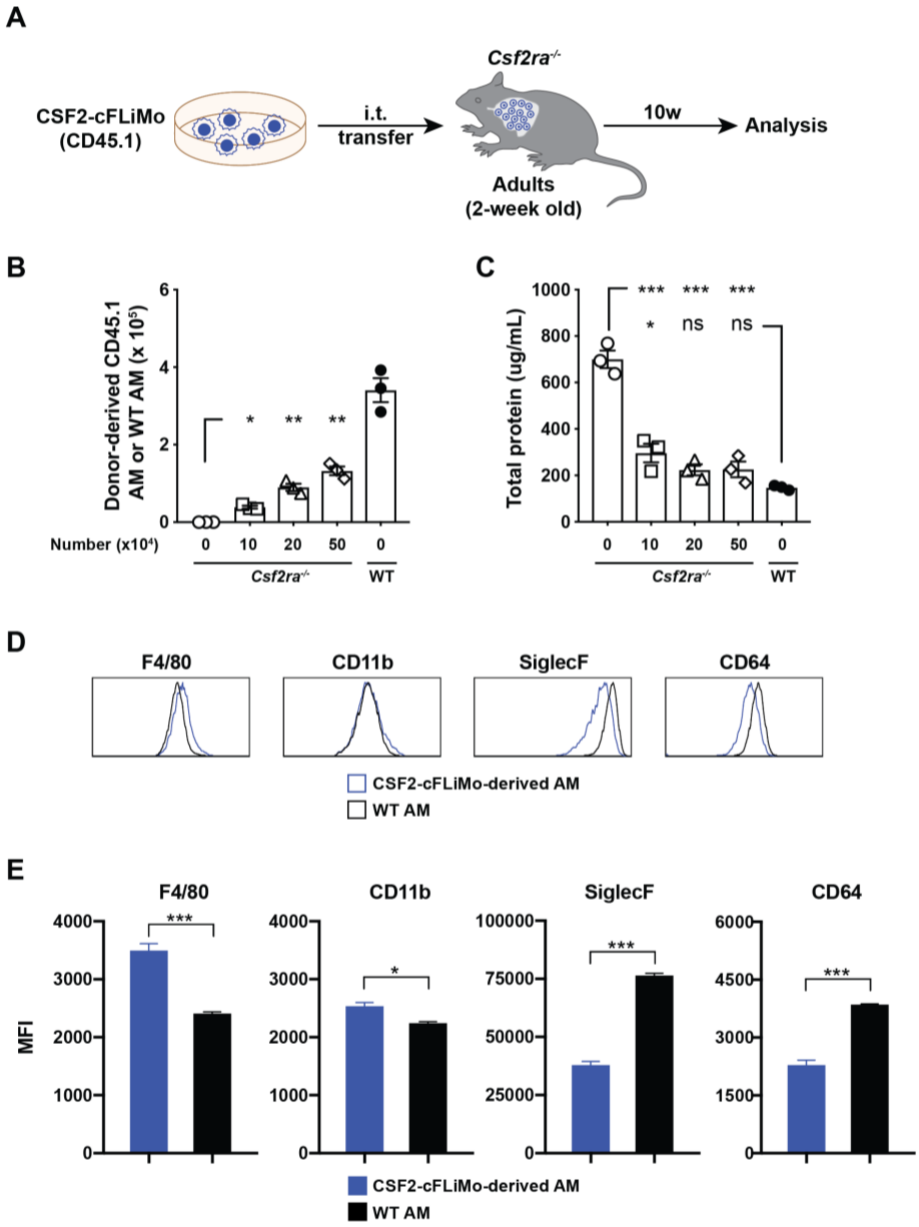

sFigure 8. Transplantation of CSF2-cFLiMo in young *Csf2ra*$^{-/-}$ mice prevent PAP, related to Figure 5. (A) Experimental outline. CD45.1 B6 CSF2-cFLiMo were generated from E14.5 embryos and cultured 2 weeks *in vitro*. Different numbers of CSF2-cFLiMo were transferred to 2-week-old young *Csf2ra*$^{-/-}$ mice i.t. and analyzed 10 weeks later. (B) Total numbers of donor-derived AM in the BAL and lung of recipient *Csf2ra*$^{-/-}$ mice or AM in the BAL and lung of WT mice. (C) Total protein levels in the BAL are shown. Age-matched *Csf2ra*$^{-/-}$ and WT C57BL/6 mice in B-C were included as negative and positive controls, respectively. (D-E) Representative histograms (D) and MFI (E) of AM signature markers on CSF2-cFLiMo-derived AM and endogenous AM. The data are from one experiment. Values show means ± SEM in B, C and E. ANOVA (one way) was used in B-C and Student's t test (unpaired) was used in E: ns, not significant; *$p < 0.05$, **$p < 0.01$, ***$p < 0.001$.

5.3 HoxB4-overexpressing bone marrow cells as a platform to study genes related to alveolar macrophage development

5.3.1 Materials and methods

Production of HoxB4 retroviral vector

Human HoxB4 was amplified from pLXSP-hHoxB4 (vector from Jan Kisielow) and cloned into retroviral construct based on moloney murine leukemia virus (pMY) which contained internal ribosome entry site (IRES) and mutated mCherry (mut_mCherry, also called fluorescent timer, FT) [259, 260]. Created vector was subsequently transfected into retrovirus packaging cell line (Phoenix). Produced virus was collected at day 3 and 4 post-transfection from cell supernatant, concentrated and used to infect BM cells (BMCs).

Production of bone marrow cells overexpressing HoxB4

Six weeks old WT mice were i.p. injected with 5-fluorouracil (5-FU, 150mg/kg). Bone marrow (BM) was isolated four days later from femurs and tibiae of the injected mice. BMCs were then counted and plated on 10cm Petri dishes in IMDM + GlutaMAX supplemented with 20% FBS, 100 U/mL penicillin, 100 µg/mL streptomycin, 50 µM β-mercaptoethanol (all Gibco), 20ng/ml rIL-6, 10ng/ml rIL-3, 50ng/ml rmSCF (all Peprotech). After initial cell expansion, BMCs were spin infected with freshly produced retrovirus (containing HoxB4 and FT). FT^+ cells were sorted 4 days later and expanded. Produced cell line was used at day 14 post isolation, frozen in 90% FBS and 10% DMSO or kept in culture for further experiments.

Electroporation of $HoxB4^+$ BMCs with CRISPR vectors

$1x10^6$ $HoxB4^+$ BMCs were resuspended in Opti-MEM together with 5 µg of p458 vector containing sgRNA1/2, Cas9 and GFP. NEPA21 electroporator was used and best electroporation conditions were optimized (Table 1). GFP^+ cells were sorted to 96-well plate containing 50% filtered medium from confluent BMC culture and 50% fresh medium (IMDM supplemented with 20% FBS, 100 U/mL penicillin, 100 µg/mL streptomycin, 50 µM β-mercaptoethanol, 20ng/ml rIL-6, 10ng/ml rIL-3, 50ng/ml rmSCF). After 7 days, expanding clones were transferred to 24-well plates and when cells reached confluency, half was used for DNA isolation and assessment of successful

deletion. Sequenced clones which had deletion in *Csf2ra* locus were either used for further experiments or frozen in 90% FBS and 10% DMSO.

Poring Pulse						Transfer Pulse					
V	Length (ms)	Interval (ms)	No.	D. Rate (%)	Polarity	V	Length (ms)	Interval (ms)	No.	D. Rate (%)	Polarity
135	5	50	5	10	+	20	50	50	5	40	+/-

Table 1. Successful set up on NEPA21 for HoxB4$_+$ BMC electroporation.

Differentiation of HoxB4$_+$ BMCs to BMDMs and BMDCs

HoxB4$_+$ BMCs were resuspended in RPMI 1640 + GlutaMAX, 10 % FCS, 100 U/mL penicillin, 100 µg/mL streptomycin, 50 µM β-mercaptoethanol (all Gibco) and 10ng/ml rM-CSF or 30 ng/ml rGM-CSF (both PeproTech). After seven days in culture, cells were detached from Petri dishes with PBS containing 2mM EDTA and analyzed by flow cytometry.

Reconstitution of AM-deficient mice with HoxB4$_+$ BMCs

50 000 CD45.1$_+$ HoxB4$_+$ BMCs were mixed 1:1 with CD45.2$_+$ HoxB4$_+$ BMCs and resuspended in 10 µL endotoxin-free PBS. Cells were subsequently transferred intranasally (i.n.) to neonatal (day 0-3 after birth) *Csf2ra*$_{-/-}$ recipient. Animals were analyzed 8 weeks post-transfer.

BM chimeras

C57BL/6 (CD45.1$_+$xCD45.2$_+$) recipient mice were irradiated with 9.5 Gy in a RS 2000 (Rad Source Technologies Inc., Alpharetta, USA). One day post-irradiation mice were i.v. injected with a mix of freshly isolated BM cells (25%) and HoxB4$_+$ BMCs (75%). Each mouse received 1.4x10$_6$ cells. Animals were analyzed 7 weeks later.

Cell suspensions preparation

Recipient mice were euthanized 8 weeks (for AM reconstitution) or 7 weeks (for BM chimeras) post-transfers by overdose (400 mg/kg body weight) of sodium pentobarbital. The lungs were then washed three times with 0.4 ml of ice-cold PBS containing 2 mM EDTA through an intratracheal cannula in order to collect BAL fluid. Lungs, spleens, LNs, thymuses, bones and livers were removed after perfusion with ice-cold PBS. Organs were minced and then digested at 37 °C in IMDM medium containing 2 mg/ml of type IV collagenase (Worthington), 50U/ml DNase I (Sigma-Aldrich) and 3% FCS for 45 min

(lungs, liver) and 30 min (spleen). Spleens and lungs were directly passed through a 70-μm-cell strainer (Becton Dickinson) while livers were first centrifuged at 20*g* for 5 min and the supernatants with reduced number of hepatocytes were resuspended in 30% Percoll (GE Healthcare) prior to density centrifugation at 2000 r.p.m. for 20 min at 25 °C, with low acceleration and no brake. Bone marrow was flushed from femur and tibia from mouse hindlimb and passed through a 70-μm cell strainer. Thymus and LN were passed through a 70-μm cell strainer with no prior digestion. Ammonium-chloride-potassium (ACK) lysing buffer was used for erythrocyte lysis for all samples.

Flow cytometry

The analysis was performed with LSR Fortessa (BD), and followed by data analysis with FlowJo software (TreeStar). Dead cells were gated out with use of the live-dead marker eFluor780 (eBioscience). FcγIII/II receptors were blocked by incubation with anti-CD16/32 (2.4G2) purified from hybridoma supernatant (home-made) before staining. Single-cell suspensions were incubated with fluorochrome-conjugated or biotinylated monoclonal antibodies in PBS containing 2% FCS. Monoclonal antibodies specific to mouse CD45 (30-F11), CD11c (N418), F4/80 (BM8), CD11b (M1/70), SiglecF (E50-2440, BD Biosciences or ES22-10D8, Miltenyi Biotec), CD45.1 (A20), CD45.2 (104), Ly6C (HK1.4), CD64 (X54-5/7.1), MHC class II (M5/114.15.2, eBioscience), mCsf2ra-APC (698423, R&D Systems), VCAM1 (429, eBioscience), Ly6G (1A8), CD8 (53-6.7), CD4 (RM4-5), CD19 (6D5 or 1D3, eBioscience), and TCRβ (H57-597) were purchased from BioLegend unless otherwise stated.

5.3.2 Results

HoxB4+ BMCs have potential to differentiate into AM

Overexpression of homeobox B4 (HoxB4) in adult bone marrow cells (BMCs) leads to profound expansion of hematopoietic stem and progenitor cells *in vitro* and *in vivo* without affecting cell numbers of mature cells generated *in vivo* or inducing leukemia [261]. We prompted to test the potential of HoxB4-overexpressing BMCs in differentiation to macrophages *in vitro* and AM reconstitution *in vivo* (Figure 1A). We have isolated BMCs from six weeks old WT animal and cultured them in full medium supplemented with 20ng/ml rIL-6, 10ng/ml rIL-3, 50ng/ml rmSCF. After initial expansion, cells were transduced with retroviral vector (RV) carrying human HoxB4 and

Figure 1

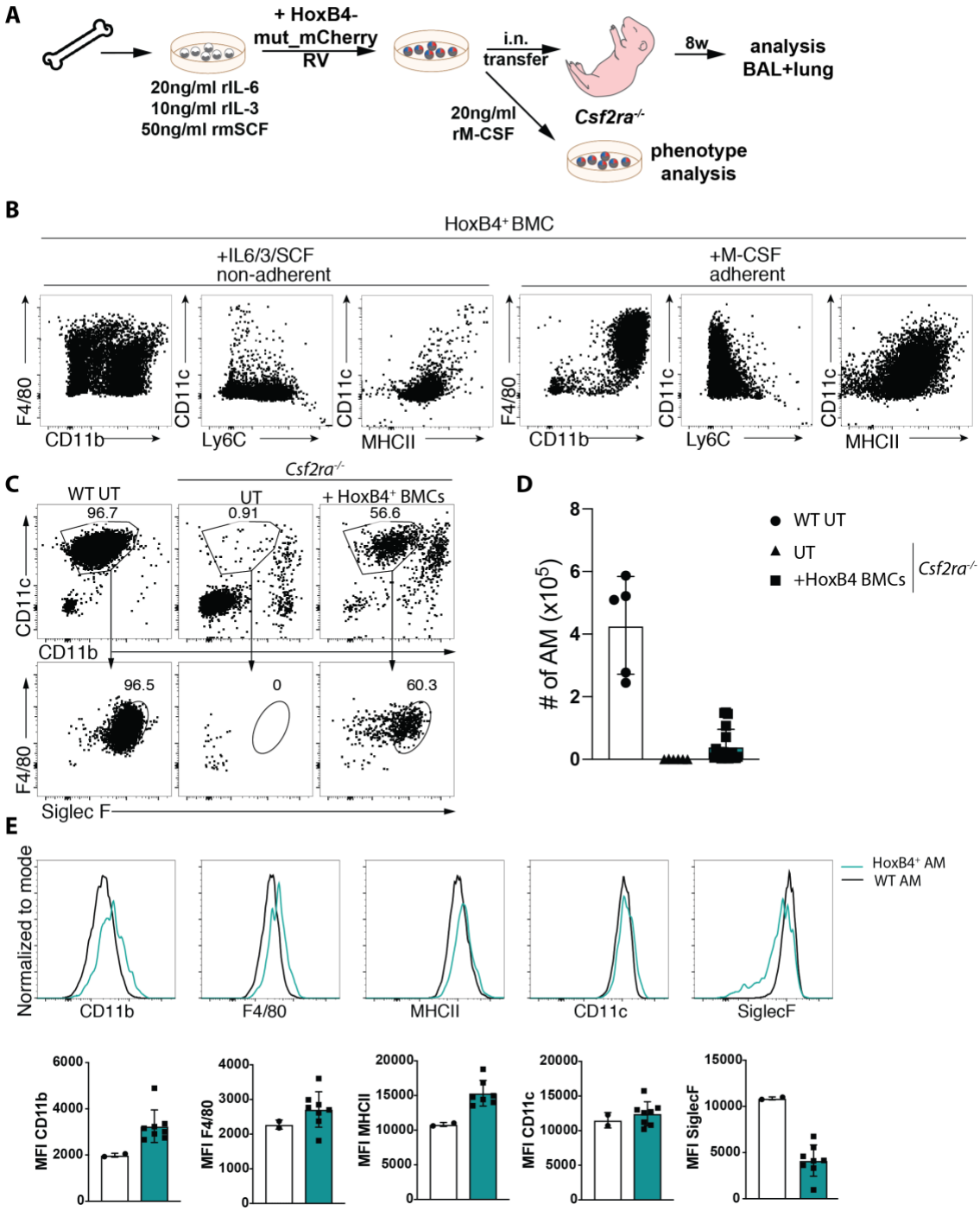

Figure 1. HoxB4-overexpressing BMCs differentiate to alveolar macrophages in vivo. (A) Graphical presentation of experimental design. (B) Flow cytometry of HoxB4+ BMCs after seven days in culture with M-CSF. (C, D) Flow cytometry of BAL eight weeks after intranasal transfer of HoxB4+ BMCs to *Csf2ra*-/- newborns (B) supplemented with total AM counts (BAL + lung) (C). (E) Representative histograms of indicated markers expressed by AM supplemented with mean fluorescent intensity (MFI) bar graphs (below the histogram plots). Data pooled from three independent experiments.

mutant mCherry (later called fluorescent timer, FT). HoxB4+ (FT+) BMCs were sorted and either cultured with rM-CSF for seven days or transferred intranasally (i.n.) to *Csf2ra*$^{-/-}$ newborns which lack AM. Reconstitution of AM was assessed eight weeks later. Cultured HoxB4+ BMCs with rM-CSF became adherent, upregulated expression of F4/80, CD11b, CD11c, MHCII and decreased Ly6C (Figure 1B) indicating differentiation to macrophages. Moreover, all transferred animals had detectable levels of HoxB4+ BMC-derived AM (Figure 1C) and despite the fact that cell numbers varied from mouse to mouse (Figure 1D), all cells acquired AM-like phenotype (Figure 1E). Thus, HoxB4+ BMC have a strong potential to differentiate into AM, while cell numbers are lower than in WT controls.

HoxB4+ BMCs can be genetically modified

We have failed in establishing CRISPR/Cas9-based genetic modifications in fetal monocyte cultures. Therefore, we have approached that issue in our new cell line. The work flow is depicted in Figure 2A. We have optimized a suitable electroporation condition, single cell expansion protocols, and we decided to target *Csf2ra*, a gene known to be crucial for AM development for proof of concept. In order to efficiently delete *Csf2ra*, we have designed guide RNA (gRNA) to target a site in a conserved domain in exon 9, just upstream of the transmembrane domain (Figure 2B). The best survival (around 80% live cells) together with a good frequency (above 1%) of targeted cells was achieved with Nepa21 electroporator with 5 poring pulses at 135V and 5 transfer pulses at 20V (Figure 2C). Targeted cells (GFP+) were sorted as single cells to 96-well plate and cultured in fresh medium supplemented with filtered medium from expanding HoxB4+ BMCs. This conditioned medium supported fast expansion of clones, allowing further DNA isolation and PCR of targeted region. Electrophoresis of gene fragments allowed selection of shorter fragments, most probably targeted by both gRNA what led to deletion (Figure 2D). We have purified shorter fragments and sequenced them. As expected, most of isolated clones characterized with 40bp deletion in targeted region (Figure 2E). WT HoxB4+ BMCs do not express Csf2ra on their surface, therefore we have differentiated selected clones and WT cells to macrophages as described previously and assessed their upregulation of Csf2ra (Figure 2F). As expected, rM-CSF/rGM-CSF supplementation induced expression of Csf2ra in WT HoxB4+ BMCs, while no positive cells were detected in targeted cultures (Figure 2G, shown for clone 11). Importantly, these results prove

effective and optimized gene targeting in HoxB4+ BMCs. Moreover, HoxB4+ BMCs did not depend on Csf2ra expression, therefore could be easily expanded in culture.

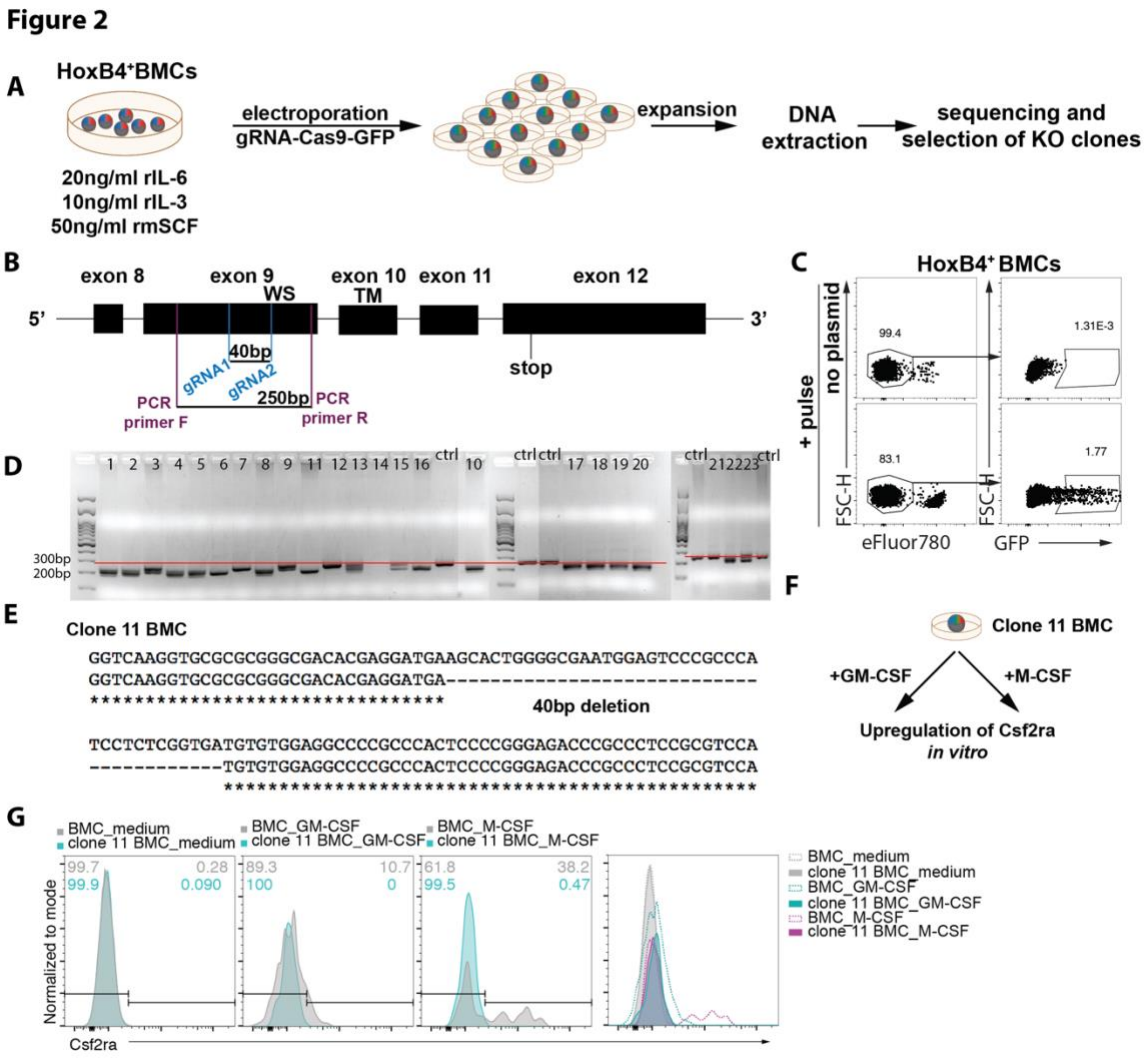

Figure 2. HoxB4+ BMCs can be genetically modified. (A) Graphical presentation of experimental design. (B) The last five exons of the *Csf2ra* locus together with marked size of targeted region (by gRNA1 and gRNA2) and PCR product for selection of mutants; WS, WSXWS motif; TM, transmembrane domain. (C) Flow cytometry of HoxB4+ BMCs 24h post-electroporation with plasmid containing gRNA1/gRNA2, Cas9 and GFP. (D) PCR using flanking primers on expanded HoxB4+GFP+ BMC clones; red line indicates size of 250 bp (WT band). (E) Sanger sequencing result for one of the clones (clone 11) aligned to WT *Csf2ra* locus. (F) Graphical presentation of experiment designed to check deletion of Csf2ra at protein level. (G) Histograms showing expression of Csf2ra on WT HoxB4+ BMC (BMC) and Csf2ra mutant (clone 11 BMC) at 7 days of stimulation with GM/M-CSF *in vitro*.

HoxB4+ BMC with mutated Csf2ra are not able to give rise to AM in vivo

For final proof of concept, we have transferred a 1:1 mix of a selected clone with a defective *Csf2ra* gene (CD45.2) or WT HoxB4+ BMCs (CD45.2) together with WT HoxB4+ BMCs (CD45.1) to *Csf2ra-/-* newborns (Figure 3A). BAL and lungs were analyzed eight weeks post-transfer (Figure 2B, shown for BAL). It appeared that CD45.2+ WT HoxB4+ cell line had much better potential to reconstitute AM, while in WT:WT mixes only CD45.2+ cells could be detected. This could be due to the fact that CD45.1-derived HoxB4+

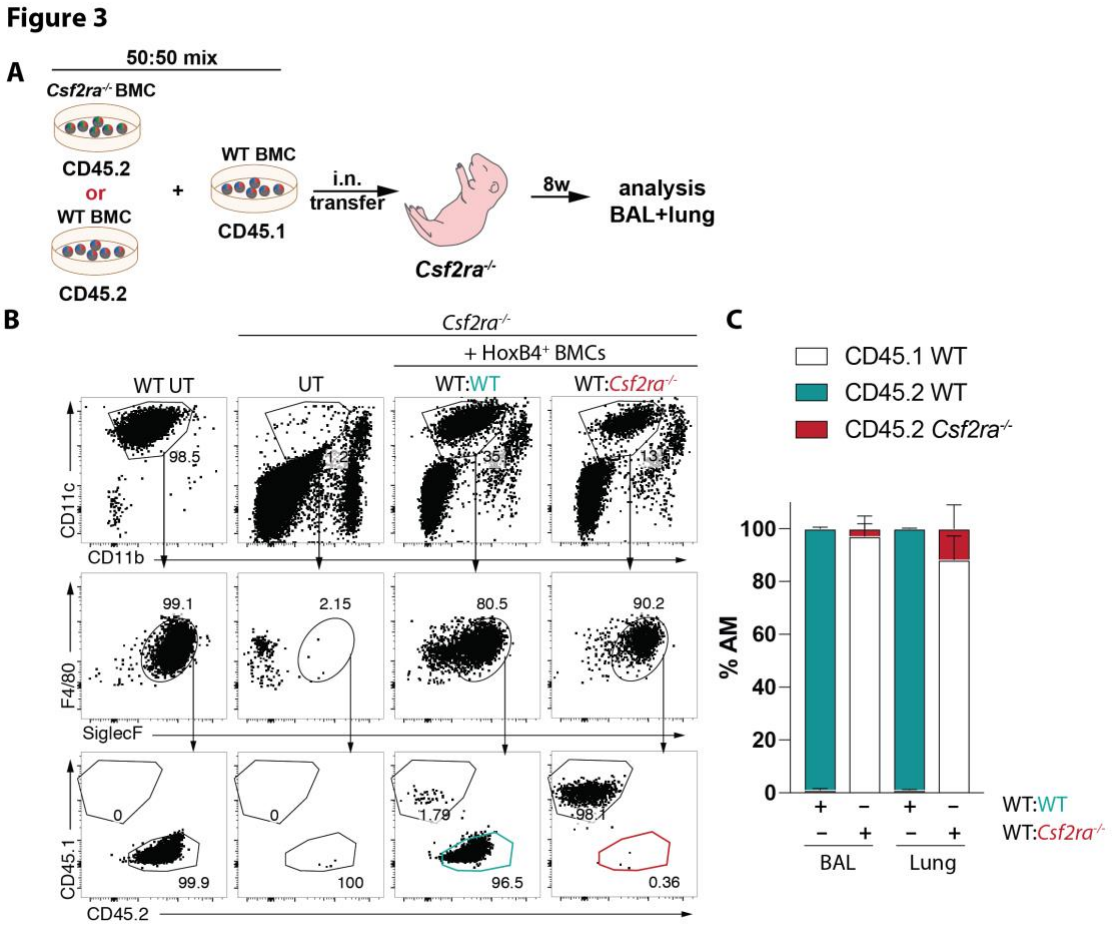

Figure 3. HoxB4+ BMC with mutated *Csf2ra* are not able to give rise to AM. (A) Graphical presentation of experimental design. (B, C) Flow cytometry of BAL eight weeks after intranasal transfer of HoxB4+ BMCs to *Csf2ra-/-* newborns (B) supplemented with frequencies of AM in BAL and lung reconstituted by WT HoxB4+ or *Csf2ra-/-* HoxB4+ BMCs (C).

BMCs were cultured for longer time *in vitro*, therefore performing worse in the competitive conditions *in vivo*. Importantly, when CD45.2+ cells had modified *Csf2ra* gene, they lost ability to give rise to AM and majority of detected AM were of CD45.1 origin.

HoxB4+ BMCs were shown to give rise to lymphoid and myeloid lineages if transferred into lethally irradiated mice [262]. In our hands, lethally irradiated recipients injected only with HoxB4+ BMC, died shortly after transfer since the transferred cells failed to reconstitute the immune system. To circumvent death of recipient, we decided to transfer a mixture of HoxB4+ BMCs together with a small number of freshly isolated

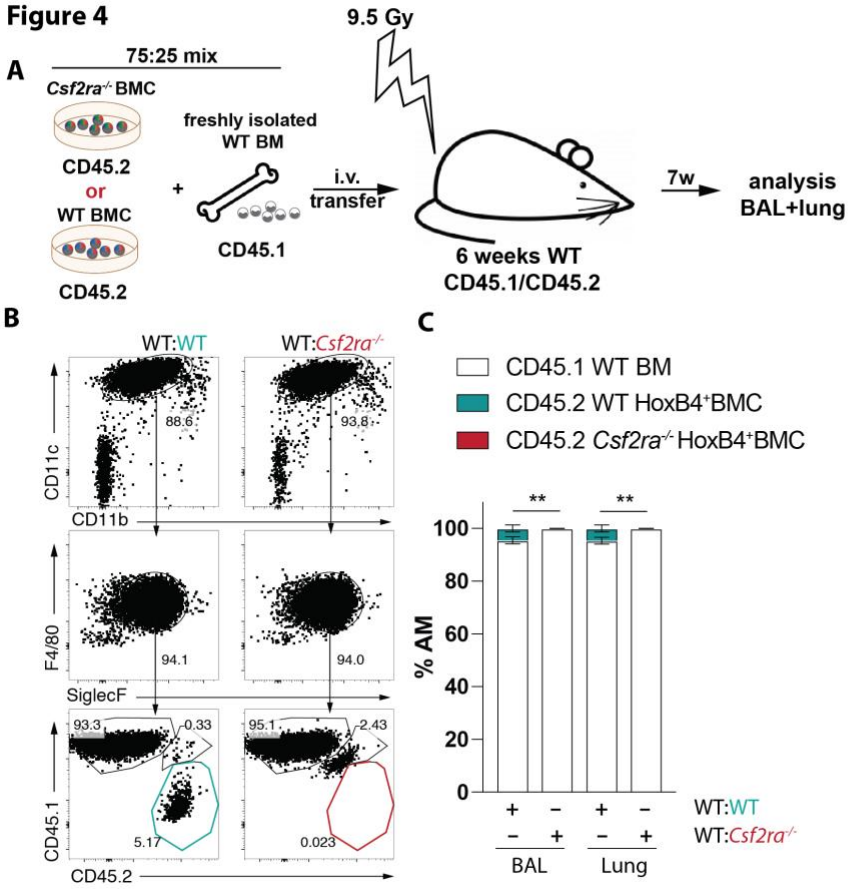

Figure 4. HoxB4+ BMC with mutated *Csf2ra* are not able to give rise to AM in BM chimeras. (A) Graphical presentation of experimental design. (B, C) Flow cytometry of BAL seven weeks after i.v. injection of HoxB4+ BMCs mixed with freshly isolated BM to lethally irradiated mice (B) supplemented with frequencies of AM in BAL and lung reconstituted with 25:75 mixtures of WT BM (CD45.1) together with either WT HoxB4+ BMCs (CD45.2) or *Csf2ra*-/- HoxB4+ BMC (CD45.2) (C).

bone marrow cells. We have transferred to lethally irradiated mice (CD45.1xCD45.2) a 75:25 mixture of clonal *Csf2ra*-deficient HoxB4+ BMC (CD45.2) or WT HoxB4+ BMCs (CD45.2) together with freshly isolated bone marrow cells from WT mice (CD45.1) (Figure 4A). Recipients reconstituted with the mixture survived. Analysis 7 weeks post transfer showed that AM (CD45.1) derived from fresh BMC prevailed (Figure 4B, shown for BAL). However, a small fraction (around 5%) of AM were derived from WT HoxB4+

BMCs (CD45.2). In contrast, no AM of *Csf2ra*-deficient HoxB4+ BMC (CD45.2) origin were detected in recipients transferred with WT:KO mixture (Figure 4C).

Designed experiments confirmed the crucial role of Csf2ra in AM development and proved establishment of a robust protocol for genetic modification in HoxB4+ BMCs, which upon transfer either i.n. to AM-deficient newborns or i.v. to lethally irradiated mice give rise to AM as long as genes necessary for their development are present in created cell line.

6 General discussion

The main aim of this thesis was to understand tissue-specific programs induced during macrophage development, in particular alveolar macrophages (AM) and red pulp macrophages (RPM), and the role of the transcription factor PPARγ in this process.

Recent years have considerably changed our understanding of tissue resident macrophage biology. First of all, tissue resident macrophages have been shown to develop from fetal progenitors and self-renew in adulthood. A long held scientific dogma, according to which circulating monocytes continuously enter tissues and differentiate into macrophages, was disproved and new insights connected this known phenomenon mainly to non-homeostatic situations, like inflammation or infection. Moreover, new methodologies, enabling analysis of the whole cell transcriptome and epigenome, revealed fascinating heterogeneity among tissue macrophages and identified gene signatures related to specific subsets. Environmental cues were proved to be fundamental to macrophage imprinting [62]. Collectively, cell ontogeny and the tissue itself dictate the programming, phenotype and function of resident macrophage populations. It is crucial to advance from novel discoveries and further dissect macrophage complexity by identifying subset-specific signaling pathways and correlating them with the functional outcome.

Our lab has reported previously requirement of the transcription factor PPARγ for AM development. We have established that fetal monocytes upon seeding the developing lung are exposed to GM-CSF, secreted by lung epithelial cells, what results in induction of PPARγ expression. PPARγ regulates many downstream genes involved in lipid metabolism, necessary for catabolism of surfactant. Surfactant is a complex of phospholipids and surfactant proteins required for proper function of the lung and its excess needs to be cleared. Lack of PPARγ expression leads to the surfactant lipid accumulation, which eventually results in the disease pulmonary alveolar proteinosis (PAP). Therefore, this study described the first transcription factor known to drive the program necessary for functional adaptation to the lung environment. PPARγ was indispensable for development and proper function of the alveolar macrophage and no other cell type could efficiently catabolize surfactant in its absence.

In this thesis, we provide evidence that PPARγ is also required for development of RPM and a subset of VCAM1$_+$ macrophages in the bone marrow, which have been described as bone marrow erythroid island macrophages (BMEIM). PPARγ deficiency led to dramatic reduction of both RPM and BMEIM numbers early after birth. Notably, both RPM and BMEIM have been shown previously to depend critically on the transcription factor Spi-C and are known to be required for efficient iron-recycling and clearance of malformed and/or senescent RBCs. Thus, both *Pparg*- and *Spic*-deficient animals eventually exhibit the iron accumulation in the spleen. However, our study revealed an interesting difference in the timing of requirement between PPARγ and Spi-C. We showed that PPARγ was absolutely essential already within the first week after birth for expansion of RPM, at a time when Spi-C appeared to be dispensable. However, although *Spic*-deficient pups had normal levels of RPM and BMEIM, in contrast to *Pparg*-deficient pups, the transcriptome of RPM was already considerably changed when Spi-C was absent. Moreover, RNA sequencing of a tiny population of VCAM1$_+$F4/80$_+$ cells that were found in the absence of PPARγ, showed striking differences but also some similarities to the *Spic*$_{-/-}$ RPM. In the absence of Spi-C, many genes related to iron metabolism were significantly reduced, while *Pparg* deficiency barely affected genes involved in iron-recycling. When we focused on genes that are dysregulated in both *Pparg*- and *Spic*-deficient RPM, we identified *C5ar1* (encoding for CD88 protein), *Cx3cr1* and *Itgal* (encoding for CD11a protein), among others, as commonly upregulated. Notably, cell surface expression of both CD88 and CD11a on WT RPM was down-regulated within the first days of life. In contrast, the *Pparg*- and *Spic*-deficient RPM failed to downregulate these proteins. On the other hand, *Itgad* showed the strongest decrease in the absence of either PPARγ and Spi-C. *Itgad* encodes for integrin α_D which, according to ImmGen.org, is expressed fairly selectively by RPM, but with unknown functions. High expression of the integrin α_D has been implicated in increased cell adhesiveness and retention of foamy macrophages in atherosclerotic plaques. Taken together, our data indicate that Spi-C and PPARγ collaborate in RPM and BMEIM development by promoting migration and proper localization of the progenitor by differential regulation of CD11a and integrin α_D. Surprisingly, in the absence of PPARγ, we found only little changes in expression of well-established PPARγ target genes involved in lipid metabolism, indicating that these are not necessarily required for RPM and BMEIM development and iron metabolism and are therefore not upregulated in RPM. Whether *C5ar1, Itgad*, and *Itgal*, whose expression is

altered in the absence of PPARγ, are true downstream PPARγ targets remains to be studied.

Studying tissue resident macrophage development *in vitro* is a difficult task due to their heterogeneity imposed by the unique environment of the individual tissue. Most of the environmental cues influencing gene expression are not identified. Also, slow turnover as well as loss of specific signature *ex vivo* limits use of sorted macrophages. We have established an efficient system of transferring fetal AM precursors into *Csf2ra*$^{-/-}$ newborns, which lack endogenous AM. Transferred cells differentiated into fully functional AM and were able to support lung homeostasis [99]. We reasoned that gene manipulation in cultured AM progenitors prior transfer to *Csf2ra*$^{-/-}$ recipients would enable rapid identification of genes involved in AM development and maintenance. Therefore, we focused on optimizing culture conditions for fetal monocytes, the true AM progenitor and most powerful among other potential macrophage progenitors (yolk sac macrophages, adult blood monocytes) when transferred in competitive manner [109]. A previous publication provided an example of *in vitro* culture of total fetal liver cells [250]. We prompted to test the established culture conditions on sorted fetal liver monocytes (pMo-FLi). Cells could expand efficiently within first weeks of culture and became a homogenous population by day nine. Cultured fetal liver monocytes (cFLiMos) acquired expression of CD11c and SiglecF, characteristic AM surface markers, and could efficiently reconstitute AM if transferred into newborn *Csf2ra*$^{-/-}$ mice. cFLiMo-derived AM showed great self-renewal capacity *in vivo*. When sorted from reconstituted adult mice, they could repopulate secondary hosts to comparable levels as *bona fide* AM. Moreover, cFLiMo-derived AM expressed the typical AM signature gene pattern. Furthermore, we have observed that time of *in vitro* culture did not influence the efficiency of reconstitution. cFLiMo-derived AM protected mice from proteinosis and influenza virus infection proving their functionality and full maturation into *bona fide* AM. Low cell numbers required for transfers, great AM reconstitution potential and the high-quality performance of the created cell line allow not only modeling of AM but could also serve useful for therapeutic purposes. Finally, our results showing that retroviral overexpression of *Csf2ra* in *Csf2ra*-deficient cFLiMos restored their capacity to develop into AM, demonstrate that genetic manipulation of cFLiMos prior transfer is feasible and can be exploited.

Next, we focused on improving the described AM model system with CRISPR/Cas9-based gene editing instead of retroviral gene transfers. We tested many commercially available reagents as well as three different electroporators but none of the methods gave promising results. Retroviral vectors were the only effective way to introduce extrinsic DNA to cFLiMos. Unfortunately, we failed to optimize efficient gene deletions with home-made retroviral CRISPR vectors. Therefore, we searched for another potential AM progenitor. Induced pluripotent stem cell (iPSC)-derived macrophages (iMac) as well as bone marrow-derived macrophages (BMM) were shown to differentiate to functional AM upon transfer to adult AM-deficient mice [243, 248]. While BMM are short-lived *in vitro* and therefore tricky for gene editing, we tried to produce iMacs but unfortunately never managed to receive sufficient amounts. We then considered usage of bone marrow cells (BMCs) transduced with homeobox B4 (*HoxB4*) gene. Indeed, overexpression of HoxB4 in BMCs was reported to selectively expand hematopoietic stem and progenitor cells [261]. HoxB4$_{+}$ BMCs were easy to culture, highly proliferative and upon transfer to AM-deficient mice could differentiate to AM. Although cells did not expand in the lungs as efficiently as cFLiMos, HoxB4$_{+}$ BMC-derived AM showed surface expression of typical AM markers. We have optimized electroporation, freezing and culturing conditions for the HoxB4$_{+}$ BMCs. We successfully deleted fragment of *Csf2ra* gene disabling AM development from modified cells *in vivo*. *Csf2ra*-mutated cells characterized with strong proliferation *in vitro,* while *Csf2ra* is not expressed by WT HoxB4$_{+}$ BMCs unless differentiated towards macrophages with M-CSF. Overall, this data provided a promising method for high-throughput screens of genes involved in AM development.

Collectively, this thesis describes the identification of the transcription factor PPARγ as a critical driver of RPM development. Moreover, it provides novel approaches allowing generation and long-term culture of AM-precursors with the potential to differentiate into *bona fide* AM upon transfer to AM-deficient recipients. By virtue of possible gene manipulation, proposed AM model could serve as basis to high-throughput screens leading to identification of genes required for AM development and function.

7 References

1. Bikard, D. and L.A. Marraffini, *Innate and adaptive immunity in bacteria: mechanisms of programmed genetic variation to fight bacteriophages.* Curr Opin Immunol, 2012. **24**(1): p. 15-20.

2. Price, A.A., A. Grakoui, and D.S. Weiss, *Harnessing the Prokaryotic Adaptive Immune System as a Eukaryotic Antiviral Defense.* Trends Microbiol, 2016. **24**(4): p. 294-306.

3. Delves, P.J. and I.M. Roitt, *The immune system. Second of two parts.* N Engl J Med, 2000. **343**(2): p. 108-17.

4. Parkin, J. and B. Cohen, *An overview of the immune system.* Lancet, 2001. **357**(9270): p. 1777-89.

5. Delves, P.J. and I.M. Roitt, *The immune system. First of two parts.* N Engl J Med, 2000. **343**(1): p. 37-49.

6. Bonilla, F.A. and H.C. Oettgen, *Adaptive immunity.* J Allergy Clin Immunol, 2010. **125**(2 Suppl 2): p. S33-40.

7. Turvey, S.E. and D.H. Broide, *Innate immunity.* J Allergy Clin Immunol, 2010. **125**(2 Suppl 2): p. S24-32.

8. Akira, S., S. Uematsu, and O. Takeuchi, *Pathogen recognition and innate immunity.* Cell, 2006. **124**(4): p. 783-801.

9. Medzhitov, R. and C. Janeway, Jr., *Innate immunity.* N Engl J Med, 2000. **343**(5): p. 338-44.

10. Bianchi, M.E., *DAMPs, PAMPs and alarmins: all we need to know about danger.* J Leukoc Biol, 2007. **81**(1): p. 1-5.

11. Joncker, N.T. and D.H. Raulet, *Regulation of NK cell responsiveness to achieve self-tolerance and maximal responses to diseased target cells.* Immunol Rev, 2008. **224**(1): p. 85-97.

12. Metchnikoff, E., *Leçons sur la pathologie comparée de l'inflammation Faites à l'Institut Pasteur en Avril et Mai 1891.* G. Masson, 1892.

13. Aschoff, L., *Das reticuloendotheliale system.* Ergebnisse der Inneren Medizin und Kinderheilkunde, 1924. **26**: p. 1–117

14. Volterra, M., *Ricerche sul sistema reticulo-istiociterio.* Lo Sperimentale. Archivio di Biologia normale e patologica, 1927. **81**(319).

15. van Furth, R. and Z.A. Cohn, *The origin and kinetics of mononuclear phagocytes.* J Exp Med, 1968. **128**(3): p. 415-35.

16. Parwaresch, M.R. and H.H. Wacker, *Origin and kinetics of resident tissue macrophages. Parabiosis studies with radiolabelled leucocytes.* Cell Tissue Kinet, 1984. **17**(1): p. 25-39.

17. Naito, M., et al., *Development, differentiation, and phenotypic heterogeneity of murine tissue macrophages.* J Leukoc Biol, 1996. **59**(2): p. 133-8.

18. Sawyer, R.T., P.H. Strausbauch, and A. Volkman, *Resident macrophage proliferation in mice depleted of blood monocytes by strontium-89*. Vol. 46. Lab Invest., 1982, 165-70.

19. Ginhoux, F., et al., *Fate mapping analysis reveals that adult microglia derive from primitive macrophages.* Science, 2010. **330**(6005): p. 841-5.

20. Hoeffel, G., et al., *Adult Langerhans cells derive predominantly from embryonic fetal liver monocytes with a minor contribution of yolk sac-derived macrophages.* J Exp Med, 2012. **209**(6): p. 1167-81.

21. Keefer, L.K., et al., *Targeting nitric oxide to macrophages with prodrugs of the O-2-glycosylated diazenitandiolate family.* Nitric Oxide-Biology and Chemistry, 2006. **14**(4): p. A50-A50.

22. Kono, H. and K.L. Rock, *How dying cells alert the immune system to danger.* Nat Rev Immunol, 2008. **8**(4): p. 279-89.

23. Erwig, L.P. and P.M. Henson, *Immunological consequences of apoptotic cell phagocytosis.* Am J Pathol, 2007. **171**(1): p. 2-8.

24. Zhang, X. and D.M. Mosser, *Macrophage activation by endogenous danger signals.* J Pathol, 2008. **214**(2): p. 161-78.

25. Cai, X., Y.H. Chiu, and Z.J. Chen, *The cGAS-cGAMP-STING pathway of cytosolic DNA sensing and signaling.* Mol Cell, 2014. **54**(2): p. 289-96.

26. Kawasaki, T. and T. Kawai, *Toll-like receptor signaling pathways.* Front Immunol, 2014. **5**: p. 461.

27. Takeuchi, O. and S. Akira, *Pattern recognition receptors and inflammation.* Cell, 2010. **140**(6): p. 805-20.

28. Gordon, S. and A. Pluddemann, *Tissue macrophages: heterogeneity and functions.* BMC Biol, 2017. **15**(1): p. 53.

29. Palis, J. and M.C. Yoder, *Yolk-sac hematopoiesis: the first blood cells of mouse and man.* Exp Hematol, 2001. **29**(8): p. 927-36.

30. Orkin, S.H. and L.I. Zon, *Hematopoiesis: an evolving paradigm for stem cell biology.* Cell, 2008. **132**(4): p. 631-44.

31. Jagannathan-Bogdan, M. and L.I. Zon, *Hematopoiesis.* Development, 2013. **140**(12): p. 2463-7.

32. Ginhoux, F. and M. Guilliams, *Tissue-Resident Macrophage Ontogeny and Homeostasis.* Immunity, 2016. **44**(3): p. 439-449.

33. Geissmann, F., et al., *Development of monocytes, macrophages, and dendritic cells.* Science, 2010. **327**(5966): p. 656-61.

34. Hettinger, J., et al., *Origin of monocytes and macrophages in a committed progenitor.* Nat Immunol, 2013. **14**(8): p. 821-30.

35. Cheong, C., et al., *Microbial stimulation fully differentiates monocytes to DC-SIGN/CD209(+) dendritic cells for immune T cell areas.* Cell, 2010. **143**(3): p. 416-29.

36. Yona, S., et al., *Fate mapping reveals origins and dynamics of monocytes and tissue macrophages under homeostasis.* Immunity, 2013. **38**(1): p. 79-91.

37. Hashimoto, D., et al., *Tissue-resident macrophages self-maintain locally throughout adult life with minimal contribution from circulating monocytes.* Immunity, 2013. **38**(4): p. 792-804.

38. Varol, C., et al., *Monocytes give rise to mucosal, but not splenic, conventional dendritic cells.* J Exp Med, 2007. **204**(1): p. 171-80.

39. Bogunovic, M., et al., *Origin of the lamina propria dendritic cell network.* Immunity, 2009. **31**(3): p. 513-25.

40. Bain, C.C., et al., *Constant replenishment from circulating monocytes maintains the macrophage pool in the intestine of adult mice.* Nat Immunol, 2014. **15**(10): p. 929-937.

41. Tamoutounour, S., et al., *Origins and functional specialization of macrophages and of conventional and monocyte-derived dendritic cells in mouse skin.* Immunity, 2013. **39**(5): p. 925-38.

42. Epelman, S., et al., *Embryonic and adult-derived resident cardiac macrophages are maintained through distinct mechanisms at steady state and during inflammation.* Immunity, 2014. **40**(1): p. 91-104.

43. A-Gonzalez, N., et al., *The nuclear receptor LXRalpha controls the functional specialization of splenic macrophages.* Nat Immunol, 2013. **14**(8): p. 831-9.

44. Ginhoux, F. and S. Jung, *Monocytes and macrophages: developmental pathways and tissue homeostasis.* Nat Rev Immunol, 2014. **14**(6): p. 392-404.

45. Guilliams, M. and C.L. Scott, *Does niche competition determine the origin of tissue-resident macrophages?* Nat Rev Immunol, 2017. **17**(7): p. 451-460.

46. Theurl, I., et al., *On-demand erythrocyte disposal and iron recycling requires transient macrophages in the liver.* Nat Med, 2016. **22**(8): p. 945-51.

47. Samokhvalov, I.M., N.I. Samokhvalova, and S. Nishikawa, *Cell tracing shows the contribution of the yolk sac to adult haematopoiesis.* Nature, 2007. **446**(7139): p. 1056-1061.

48. Schulz, C., et al., *A lineage of myeloid cells independent of Myb and hematopoietic stem cells.* Science, 2012. **336**(6077): p. 86-90.

49. Gomez Perdiguero, E., et al., *Tissue-resident macrophages originate from yolk-sac-derived erythro-myeloid progenitors.* Nature, 2015. **518**(7540): p. 547-51.

50. Hoeffel, G., et al., *C-Myb(+) erythro-myeloid progenitor-derived fetal monocytes give rise to adult tissue-resident macrophages.* Immunity, 2015. **42**(4): p. 665-78.

51. Sheng, J., C. Ruedl, and K. Karjalainen, *Most Tissue-Resident Macrophages Except Microglia Are Derived from Fetal Hematopoietic Stem Cells.* Immunity, 2015. **43**(2): p. 382-93.

52. Platt, A.M., et al., *An independent subset of TLR expressing CCR2-dependent macrophages promotes colonic inflammation.* J Immunol, 2010. **184**(12): p. 6843-54.

53. Zigmond, E., et al., *Ly6C hi monocytes in the inflamed colon give rise to proinflammatory effector cells and migratory antigen-presenting cells.* Immunity, 2012. **37**(6): p. 1076-90.

54. Molawi, K., et al., *Progressive replacement of embryo-derived cardiac macrophages with age.* J Exp Med, 2014. **211**(11): p. 2151-8.

55. Ensan, S., et al., *Self-renewing resident arterial macrophages arise from embryonic CX3CR1(+) precursors and circulating monocytes immediately after birth.* Nat Immunol, 2016. **17**(2): p. 159-68.

56. Scott, C.L., et al., *Bone marrow-derived monocytes give rise to self-renewing and fully differentiated Kupffer cells.* Nat Commun, 2016. **7**: p. 10321.

57. Mowat, A.M., C.L. Scott, and C.C. Bain, *Barrier-tissue macrophages: functional adaptation to environmental challenges.* Nat Med, 2017. **23**(11): p. 1258-1270.

58. Gautier, E.L., et al., *Gene-expression profiles and transcriptional regulatory pathways that underlie the identity and diversity of mouse tissue macrophages.* Nat Immunol, 2012. **13**(11): p. 1118-28.

59. Jojic, V., et al., *Identification of transcriptional regulators in the mouse immune system.* Nat Immunol, 2013. **14**(6): p. 633-43.

60. Miller, J.C., et al., *Deciphering the transcriptional network of the dendritic cell lineage.* Nat Immunol, 2012. **13**(9): p. 888-99.

61. Gosselin, D., et al., *Environment drives selection and function of enhancers controlling tissue-specific macrophage identities.* Cell, 2014. **159**(6): p. 1327-40.

62. Lavin, Y., et al., *Tissue-resident macrophage enhancer landscapes are shaped by the local microenvironment.* Cell, 2014. **159**(6): p. 1312-26.

63. Winter, D.R. and I. Amit, *The role of chromatin dynamics in immune cell development.* Immunol Rev, 2014. **261**(1): p. 9-22.

64. Ostuni, R. and G. Natoli, *Lineages, cell types and functional states: a genomic view.* Curr Opin Cell Biol, 2013. **25**(6): p. 759-64.

65. Heinz, S., et al., *Simple combinations of lineage-determining transcription factors prime cis-regulatory elements required for macrophage and B cell identities.* Mol Cell, 2010. **38**(4): p. 576-89.

66. Garber, M., et al., *A high-throughput chromatin immunoprecipitation approach reveals principles of dynamic gene regulation in mammals.* Mol Cell, 2012. **47**(5): p. 810-22.

67. Felsenfeld, G. and M. Groudine, *Controlling the double helix.* Nature, 2003. **421**(6921): p. 448-53.

68. Kouzarides, T., *Chromatin modifications and their function.* Cell, 2007. **128**(4): p. 693-705.

69. Bernstein, B.E., et al., *A bivalent chromatin structure marks key developmental genes in embryonic stem cells.* Cell, 2006. **125**(2): p. 315-26.

70. Davies, L.C., et al., *Distinct bone marrow-derived and tissue-resident macrophage lineages proliferate at key stages during inflammation.* Nat Commun, 2013. **4**: p. 1886.

71. Wang, Y., et al., *IL-34 is a tissue-restricted ligand of CSF1R required for the development of Langerhans cells and microglia.* Nat Immunol, 2012. **13**(8): p. 753-60.

72. Cirillo, L.A., et al., *Opening of compacted chromatin by early developmental transcription factors HNF3 (FoxA) and GATA-4.* Mol Cell, 2002. **9**(2): p. 279-89.

73. Amit, I., D.R. Winter, and S. Jung, *The role of the local environment and epigenetics in shaping macrophage identity and their effect on tissue homeostasis.* Nat Immunol, 2016. **17**(1): p. 18-25.

74. Zhang, D.E., et al., *The macrophage transcription factor PU.1 directs tissue-specific expression of the macrophage colony-stimulating factor receptor.* Mol Cell Biol, 1994. **14**(1): p. 373-81.

75. Feng, R., et al., *PU.1 and C/EBPalpha/beta convert fibroblasts into macrophage-like cells.* Proc Natl Acad Sci U S A, 2008. **105**(16): p. 6057-62.

76. Aziz, A., et al., *MafB/c-Maf deficiency enables self-renewal of differentiated functional macrophages.* Science, 2009. **326**(5954): p. 867-71.

77. Kelly, L.M., et al., *MafB is an inducer of monocytic differentiation.* EMBO J, 2000. **19**(9): p. 1987-97.

78. Okabe, Y., *Molecular control of the identity of tissue-resident macrophages.* Int Immunol, 2018. **30**(11): p. 485-491.

79. Sevenich, L., *Brain-Resident Microglia and Blood-Borne Macrophages Orchestrate Central Nervous System Inflammation in Neurodegenerative Disorders and Brain Cancer.* Front Immunol, 2018. **9**: p. 697.

80. Nayak, D., T.L. Roth, and D.B. McGavern, *Microglia development and function.* Annu Rev Immunol, 2014. **32**(1): p. 367-402.

81. Ginhoux, F., et al., *Origin and differentiation of microglia.* Front Cell Neurosci, 2013. **7**: p. 45.

82. Abutbul, S., et al., *TGF-beta signaling through SMAD2/3 induces the quiescent microglial phenotype within the CNS environment.* Glia, 2012. **60**(7): p. 1160-71.

83. Buttgereit, A., et al., *Sall1 is a transcriptional regulator defining microglia identity and function.* Nat Immunol, 2016. **17**(12): p. 1397-1406.

84. Ghosn, E.E., et al., *Two physically, functionally, and developmentally distinct peritoneal macrophage subsets.* Proc Natl Acad Sci U S A, 2010. **107**(6): p. 2568-73.

85. Kim, K.W., et al., *MHC II+ resident peritoneal and pleural macrophages rely on IRF4 for development from circulating monocytes.* J Exp Med, 2016. **213**(10): p. 1951-9.

86. Okabe, Y. and R. Medzhitov, *Tissue-specific signals control reversible program of localization and functional polarization of macrophages.* Cell, 2014. **157**(4): p. 832-44.

87. Gautier, E.L., et al., *Gata6 regulates aspartoacylase expression in resident peritoneal macrophages and controls their survival.* J Exp Med, 2014. **211**(8): p. 1525-31.

88. Rosas, M., et al., *The transcription factor Gata6 links tissue macrophage phenotype and proliferative renewal.* Science, 2014. **344**(6184): p. 645-648.

89. Charles, J.F. and A.O. Aliprantis, *Osteoclasts: more than 'bone eaters'.* Trends Mol Med, 2014. **20**(8): p. 449-59.

90. Wada, T., et al., *RANKL-RANK signaling in osteoclastogenesis and bone disease.* Trends Mol Med, 2006. **12**(1): p. 17-25.

91. Aliprantis, A.O., et al., *NFATc1 in mice represses osteoprotegerin during osteoclastogenesis and dissociates systemic osteopenia from inflammation in cherubism.* J Clin Invest, 2008. **118**(11): p. 3775-89.

92. Krenkel, O. and F. Tacke, *Liver macrophages in tissue homeostasis and disease.* Nat Rev Immunol, 2017. **17**(5): p. 306-321.

93. Mass, E., et al., *Specification of tissue-resident macrophages during organogenesis.* Science, 2016. **353**(6304): p. aaf4238.

94. Strong, N., et al., *Inhibitor of differentiation 1 (Id1) and Id3 proteins play different roles in TGFbeta effects on cell proliferation and migration in prostate cancer cells.* Prostate, 2013. **73**(6): p. 624-33.

95. Fainaru, O., et al., *Runx3 regulates mouse TGF-beta-mediated dendritic cell function and its absence results in airway inflammation.* EMBO J, 2004. **23**(4): p. 969-79.

96. Hacker, C., et al., *Transcriptional profiling identifies Id2 function in dendritic cell development.* Nat Immunol, 2003. **4**(4): p. 380-6.

97. Schridde, A., et al., *Tissue-specific differentiation of colonic macrophages requires TGFbeta receptor-mediated signaling.* Mucosal Immunol, 2017. **10**(6): p. 1387-1399.

98. Guilliams, M., et al., *Alveolar macrophages develop from fetal monocytes that differentiate into long-lived cells in the first week of life via GM-CSF.* J Exp Med, 2013. **210**(10): p. 1977-92.

99. Schneider, C., et al., *Induction of the nuclear receptor PPAR-gamma by the cytokine GM-CSF is critical for the differentiation of fetal monocytes into alveolar macrophages.* Nat Immunol, 2014. **15**(11): p. 1026-37.

100. Davies, L.C., et al., *Tissue-resident macrophages.* Nat Immunol, 2013. **14**(10): p. 986-95.

101. Haldar, M., et al., *Heme-mediated SPI-C induction promotes monocyte differentiation into iron-recycling macrophages.* Cell, 2014. **156**(6): p. 1223-1234.

102. Kohyama, M., et al., *Role for Spi-C in the development of red pulp macrophages and splenic iron homeostasis.* Nature, 2009. **457**(7227): p. 318-21.

103. Ball, M. and D. Padalia. *Anatomy, Airway.* In: StatPearls [Internet]. Treasure Island (FL): StatPearls Publishing; 2018 Jan-. Available from: https://www.ncbi.nlm.nih.gov/books/NBK459258/ [Updated: 2019 Jan 11] Accessed: 2019 Mar 4].

104. Kopf, M., C. Schneider, and S.P. Nobs, *The development and function of lung-resident macrophages and dendritic cells.* Nat Immunol, 2015. **16**(1): p. 36-44.

105. Westphalen, K., et al., *Sessile alveolar macrophages communicate with alveolar epithelium to modulate immunity.* Nature, 2014. **506**(7489): p. 503-6.

106. Peão, M.N.D., et al., *Morphological Evidence for Migration of Particle-Laden Macrophages through the Interalveolar Pores of Kohn in the Murine Lung*. Vol. 147. Acta Anat., 1993, 227-32.

107. Joshi, N., J.M. Walter, and A.V. Misharin, *Alveolar Macrophages.* Cell Immunol, 2018. **330**: p. 86-90.

108. Epelman, S., K.J. Lavine, and G.J. Randolph, *Origin and functions of tissue macrophages.* Immunity, 2014. **41**(1): p. 21-35.

109. van de Laar, L., et al., *Yolk Sac Macrophages, Fetal Liver, and Adult Monocytes Can Colonize an Empty Niche and Develop into Functional Tissue-Resident Macrophages.* Immunity, 2016. **44**(4): p. 755-68.

110. Murphy, J., et al., *The prolonged life-span of alveolar macrophages.* Am J Respir Cell Mol Biol, 2008. **38**(4): p. 380-5.

111. Schneider, C., et al., *Alveolar macrophages are essential for protection from respiratory failure and associated morbidity following influenza virus infection.* PLoS Pathog, 2014. **10**(4): p. e1004053.

112. Aberdein, J.D., et al., *Alveolar macrophages in pulmonary host defence the unrecognized role of apoptosis as a mechanism of intracellular bacterial killing.* Clin Exp Immunol, 2013. **174**(2): p. 193-202.

113. Goss, V., A.N. Hunt, and A.D. Postle, *Regulation of lung surfactant phospholipid synthesis and metabolism.* Biochim Biophys Acta, 2013. **1831**(2): p. 448-58.

114. Glasser, J.R. and R.K. Mallampalli, *Surfactant and its role in the pathobiology of pulmonary infection.* Microbes Infect, 2012. **14**(1): p. 17-25.

115. Borie, R., et al., *Pulmonary alveolar proteinosis.* Eur Respir Rev, 2011. **20**(120): p. 98-107.

116. Shibata, Y., et al., *GM-CSF regulates alveolar macrophage differentiation and innate immunity in the lung through PU.1.* Immunity, 2001. **15**(4): p. 557-567.

117. Garbi, N. and B.N. Lambrecht, *Location, function, and ontogeny of pulmonary macrophages during the steady state.* Pflugers Arch, 2017. **469**(3-4): p. 561-572.

118. Janssen, W.J., et al., *Surfactant proteins A and D suppress alveolar macrophage phagocytosis via interaction with SIRP alpha.* Am J Respir Crit Care Med, 2008. **178**(2): p. 158-67.

119. Bourdonnay, E., et al., *Transcellular delivery of vesicular SOCS proteins from macrophages to epithelial cells blunts inflammatory signaling.* J Exp Med, 2015. **212**(5): p. 729-42.

120. Soroosh, P., et al., *Lung-resident tissue macrophages generate Foxp3+ regulatory T cells and promote airway tolerance.* J Exp Med, 2013. **210**(4): p. 775-88.

121. Dranoff, G., et al., *Involvement of granulocyte-macrophage colony-stimulating factor in pulmonary homeostasis.* Science, 1994. **264**(5159): p. 713-6.

122. Robb, L., et al., *Hematopoietic and lung abnormalities in mice with a null mutation of the common beta subunit of the receptors for granulocyte-macrophage colony-stimulating factor and interleukins 3 and 5.* Proc Natl Acad Sci U S A, 1995. **92**(21): p. 9565-9.

123. Sauter, K.A., et al., *Pleiotropic effects of extended blockade of CSF1R signaling in adult mice.* J Leukoc Biol, 2014. **96**(2): p. 265-74.

124. Nakamura, A., et al., *Transcription repressor Bach2 is required for pulmonary surfactant homeostasis and alveolar macrophage function.* J Exp Med, 2013. **210**(11): p. 2191-204.

125. Baldan, A., et al., *Deletion of the transmembrane transporter ABCG1 results in progressive pulmonary lipidosis.* J Biol Chem, 2006. **281**(39): p. 29401-10.

126. Bates, S.R., et al., *Pulmonary abnormalities due to ABCA1 deficiency in mice.* Am J Physiol Lung Cell Mol Physiol, 2005. **289**(6): p. L980-9.

127. McNeish, J., et al., *High density lipoprotein deficiency and foam cell accumulation in mice with targeted disruption of ATP-binding cassette transporter-1.* Proc Natl Acad Sci U S A, 2000. **97**(8): p. 4245-50.

128. Akiyama, T.E., et al., *Conditional disruption of the peroxisome proliferator-activated receptor gamma gene in mice results in lowered expression of ABCA1, ABCG1, and apoE in macrophages and reduced cholesterol efflux.* Mol Cell Biol, 2002. **22**(8): p. 2607-19.

129. Yu, X., et al., *The Cytokine TGF-beta Promotes the Development and Homeostasis of Alveolar Macrophages.* Immunity, 2017. **47**(5): p. 903-912 e4.

130. Todd, E.M., et al., *Alveolar macrophage development in mice requires L-plastin for cellular localization in alveoli.* Blood, 2016. **128**(24): p. 2785-2796.

131. Cain, D.W., et al., *Identification of a tissue-specific, C/EBPbeta-dependent pathway of differentiation for murine peritoneal macrophages.* J Immunol, 2013. **191**(9): p. 4665-75.

132. Cesta, M.F., *Normal structure, function, and histology of the spleen.* Toxicol Pathol, 2006. **34**(5): p. 455-65.

133. Saito, H., et al., *Reticular meshwork of the spleen in rats studied by electron microscopy.* Am J Anat, 1988. **181**(3): p. 235-52.

134. Jinushi, M., et al., *MFG-E8-mediated uptake of apoptotic cells by APCs links the pro- and antiinflammatory activities of GM-CSF.* J Clin Invest, 2007. **117**(7): p. 1902-13.

135. Mebius, R.E. and G. Kraal, *Structure and function of the spleen.* Nat Rev Immunol, 2005. **5**(8): p. 606-16.

136. Kurotaki, D., et al., *CSF-1-dependent red pulp macrophages regulate CD4 T cell responses.* J Immunol, 2011. **186**(4): p. 2229-37.

137. Korolnek, T. and I. Hamza, *Macrophages and iron trafficking at the birth and death of red cells.* Blood, 2015. **125**(19): p. 2893-7.

138. Chasis, J.A. and N. Mohandas, *Erythroblastic islands: niches for erythropoiesis.* Blood, 2008. **112**(3): p. 470-8.

139. Yoshida, H., et al., *Phosphatidylserine-dependent engulfment by macrophages of nuclei from erythroid precursor cells.* Nature, 2005. **437**(7059): p. 754-8.

140. Murata, Y., et al., *The CD47-SIRPalpha signalling system: its physiological roles and therapeutic application.* J Biochem, 2014. **155**(6): p. 335-44.

141. Burger, P., et al., *CD47 functions as a molecular switch for erythrocyte phagocytosis.* Blood, 2012. **119**(23): p. 5512-21.

142. White, C., et al., *HRG1 is essential for heme transport from the phagolysosome of macrophages during erythrophagocytosis.* Cell Metab, 2013. **17**(2): p. 261-70.

143. Gottlieb, Y., et al., *Endoplasmic reticulum anchored heme-oxygenase 1 faces the cytosol.* Haematologica, 2012. **97**(10): p. 1489-93.

144. Kristiansen, M., et al., *Identification of the haemoglobin scavenger receptor.* Nature, 2001. **409**(6817): p. 198-201.

145. Hvidberg, V., et al., *Identification of the receptor scavenging hemopexin-heme complexes.* Blood, 2005. **106**(7): p. 2572-9.

146. Knutson, M.D., et al., *Iron release from macrophages after erythrophagocytosis is up-regulated by ferroportin 1 overexpression and down-regulated by hepcidin.* Proc Natl Acad Sci U S A, 2005. **102**(5): p. 1324-8.

147. Harrison, P.M. and P. Arosio, *The ferritins: molecular properties, iron storage function and cellular regulation.* Biochim Biophys Acta, 1996. **1275**(3): p. 161-203.

148. Soares, M.P. and I. Hamza, *Macrophages and Iron Metabolism.* Immunity, 2016. **44**(3): p. 492-504.

149. Taille, C., et al., *Induction of heme oxygenase-1 inhibits NAD(P)H oxidase activity by down-regulating cytochrome b558 expression via the reduction of heme availability.* J Biol Chem, 2004. **279**(27): p. 28681-8.

150. Haider, A., et al., *Regulation of cyclooxygenase by the heme-heme oxygenase system in microvessel endothelial cells.* J Pharmacol Exp Ther, 2002. **300**(1): p. 188-94.

151. Soares, M.P. and G. Weiss, *The Iron age of host-microbe interactions.* EMBO Rep, 2015. **16**(11): p. 1482-500.

152. Cecchini, M.G., et al., *Role of colony stimulating factor-1 in the establishment and regulation of tissue macrophages during postnatal development of the mouse.* Development, 1994. **120**(6): p. 1357-72.

153. Dutta, P., et al., *Macrophages retain hematopoietic stem cells in the spleen via VCAM-1.* J Exp Med, 2015. **212**(4): p. 497-512.

154. Poss, K.D. and S. Tonegawa, *Heme oxygenase 1 is required for mammalian iron reutilization.* Proc Natl Acad Sci U S A, 1997. **94**(20): p. 10919-24.

155. Kovtunovych, G., et al., *Dysfunction of the heme recycling system in heme oxygenase 1-deficient mice: effects on macrophage viability and tissue iron distribution.* Blood, 2010. **116**(26): p. 6054-62.

156. Sadahira, Y., T. Yoshino, and Y. Monobe, *Very late activation antigen 4-vascular cell adhesion molecule 1 interaction is involved in the formation of erythroblastic islands.* J Exp Med, 1995. **181**(1): p. 411-5.

157. Kurotaki, D., et al., *IRF8 inhibits C/EBPalpha activity to restrain mononuclear phagocyte progenitors from differentiating into neutrophils.* Nat Commun, 2014. **5**: p. 4978.

158. Yamamoto, M., et al., *Shared and distinct functions of the transcription factors IRF4 and IRF8 in myeloid cell development.* PLoS One, 2011. **6**(10): p. e25812.

159. Satoh, T., et al., *Critical role of Trib1 in differentiation of tissue-resident M2-like macrophages.* Nature, 2013. **495**(7442): p. 524-8.

160. Mangelsdorf, D.J. and R.M. Evans, *The RXR heterodimers and orphan receptors.* Cell, 1995. **83**(6): p. 841-50.

161. Evans, R.M., G.D. Barish, and Y.X. Wang, *PPARs and the complex journey to obesity.* Nat Med, 2004. **10**(4): p. 355-61.

162. Issemann, I. and S. Green, *Activation of a member of the steroid hormone receptor superfamily by peroxisome proliferators.* Nature, 1990. **347**(6294): p. 645-50.

163. Poulsen, L., M. Siersbaek, and S. Mandrup, *PPARs: fatty acid sensors controlling metabolism.* Semin Cell Dev Biol, 2012. **23**(6): p. 631-9.

164. Luquet, S., et al., *Roles of PPAR delta in lipid absorption and metabolism: a new target for the treatment of type 2 diabetes.* Biochim Biophys Acta, 2005. **1740**(2): p. 313-7.

165. Ahmadian, M., et al., *PPARgamma signaling and metabolism: the good, the bad and the future.* Nat Med, 2013. **19**(5): p. 557-66.

166. Nagy, L., et al., *Oxidized LDL Regulates Macrophage Gene Expression through Ligand Activation of PPARγ.* Cell, 1998. **93**(2): p. 229-240.

167. Kliewer, S.A., et al., *A prostaglandin J2 metabolite binds peroxisome proliferator-activated receptor gamma and promotes adipocyte differentiation.* Cell, 1995. **83**(5): p. 813-9.

168. Forman, B.M., et al., *15-Deoxy-Δ12,14-Prostaglandin J2 is a ligand for the adipocyte determination factor PPARγ.* Cell, 1995. **83**(5): p. 803-812.

169. Harris, P.K. and R.F. Kletzien, *Localization of a pioglitazone response element in the adipocyte fatty acid-binding protein gene.* Mol Pharmacol, 1994. **45**(3): p. 439-45.

170. Kletzien, R.F., et al., *Adipocyte fatty acid-binding protein: regulation of gene expression in vivo and in vitro by an insulin-sensitizing agent.* Mol Pharmacol, 1992. **42**(4): p. 558-62.

171. Lehmann, J.M., et al., *An antidiabetic thiazolidinedione is a high affinity ligand for peroxisome proliferator-activated receptor gamma (PPAR gamma).* J Biol Chem, 1995. **270**(22): p. 12953-6.

172. Nagy, L., et al., *Nuclear receptor repression mediated by a complex containing SMRT, mSin3A, and histone deacetylase.* Cell, 1997. **89**(3): p. 373-80.

173. Karagianni, P. and J. Wong, *HDAC3: taking the SMRT-N-CoRrect road to repression.* Oncogene, 2007. **26**(37): p. 5439-49.

174. Viswakarma, N., et al., *Coactivators in PPAR-Regulated Gene Expression.* PPAR Res, 2010. **2010**: p. 1-21.

175. Puigserver, P., et al., *A cold-inducible coactivator of nuclear receptors linked to adaptive thermogenesis.* Cell, 1998. **92**(6): p. 829-39.

176. van Beekum, O., V. Fleskens, and E. Kalkhoven, *Posttranslational modifications of PPAR-gamma: fine-tuning the metabolic master regulator.* Obesity (Silver Spring), 2009. **17**(2): p. 213-9.

177. Hu, E., et al., *Inhibition of Adipogenesis Through MAP Kinase-Mediated Phosphorylation of PPAR* Science, 1996. **274**(5295): p. 2100-2103.

178. Camp, H.S. and S.R. Tafuri, *Regulation of peroxisome proliferator-activated receptor gamma activity by mitogen-activated protein kinase.* J Biol Chem, 1997. **272**(16): p. 10811-6.

179. Compe, E., et al., *Dysregulation of the peroxisome proliferator-activated receptor target genes by XPD mutations.* Mol Cell Biol, 2005. **25**(14): p. 6065-76.

180. Choi, J.H., et al., *Anti-diabetic drugs inhibit obesity-linked phosphorylation of PPARgamma by Cdk5.* Nature, 2010. **466**(7305): p. 451-6.

181. Qiang, L., et al., *Brown remodeling of white adipose tissue by SirT1-dependent deacetylation of Ppargamma.* Cell, 2012. **150**(3): p. 620-32.

182. Shimizu, M., et al., *Aspects of the regulatory mechanisms of PPAR functions: analysis of a bidirectional response element and regulation by sumoylation.* Mol Cell Biochem, 2006. **286**(1-2): p. 33-42.

183. Pascual, G., et al., *A SUMOylation-dependent pathway mediates transrepression of inflammatory response genes by PPAR-gamma.* Nature, 2005. **437**(7059): p. 759-63.

184. Hauser, S., et al., *Degradation of the peroxisome proliferator-activated receptor gamma is linked to ligand-dependent activation.* J Biol Chem, 2000. **275**(24): p. 18527-33.

185. Tontonoz, P., et al., *Adipocyte-specific transcription factor ARF6 is a heterodimeric complex of two nuclear hormone receptors, PPAR gamma and RXR alpha.* Nucleic Acids Res, 1994. **22**(25): p. 5628-34.

186. Tontonoz, P., E. Hu, and B.M. Spiegelman, *Stimulation of adipogenesis in fibroblasts by PPARγ2, a lipid-activated transcription factor.* Cell, 1994. **79**(7): p. 1147-1156.

187. Rosen, E.D., et al., *PPARγ Is Required for the Differentiation of Adipose Tissue In Vivo and In Vitro.* Molecular Cell, 1999. **4**(4): p. 611-617.

188. Wu, Z., N.L. Bucher, and S.R. Farmer, *Induction of peroxisome proliferator-activated receptor gamma during the conversion of 3T3 fibroblasts into adipocytes is mediated by C/EBPbeta, C/EBPdelta, and glucocorticoids.* Mol Cell Biol, 1996. **16**(8): p. 4128-36.

189. Wu, Z., et al., *Conditional ectopic expression of C/EBP beta in NIH-3T3 cells induces PPAR gamma and stimulates adipogenesis.* Genes Dev, 1995. **9**(19): p. 2350-63.

190. Tontonoz, P. and B.M. Spiegelman, *Fat and beyond: the diverse biology of PPARgamma.* Annu Rev Biochem, 2008. **77**(1): p. 289-312.

191. He, W., et al., *Adipose-specific peroxisome proliferator-activated receptor gamma knockout causes insulin resistance in fat and liver but not in muscle.* Proc Natl Acad Sci U S A, 2003. **100**(26): p. 15712-7.

192. Imai, T., et al., *Peroxisome proliferator-activated receptor gamma is required in mature white and brown adipocytes for their survival in the mouse.* Proc Natl Acad Sci U S A, 2004. **101**(13): p. 4543-7.

193. Sinha, R., et al., *Assessment of Skeletal Muscle Triglyceride Content by 1H Nuclear Magnetic Resonance Spectroscopy in Lean and Obese Adolescents: Relationships to Insulin Sensitivity, Total Body Fat, and Central Adiposity.* Diabetes, 2002. **51**(4): p. 1022-1027.

194. Yamauchi, T., et al., *Adiponectin stimulates glucose utilization and fatty-acid oxidation by activating AMP-activated protein kinase.* Nat Med, 2002. **8**(11): p. 1288-95.

195. Wellen, K.E. and G.S. Hotamisligil, *Inflammation, stress, and diabetes.* J Clin Invest, 2005. **115**(5): p. 1111-9.

196. Odegaard, J.I., et al., *Macrophage-specific PPARgamma controls alternative activation and improves insulin resistance.* Nature, 2007. **447**(7148): p. 1116-20.

197. Febbraio, M., et al., *Targeted disruption of the class B scavenger receptor CD36 protects against atherosclerotic lesion development in mice.* J Clin Invest, 2000. **105**(8): p. 1049-56.

198. Glass, C.K., *Potential roles of the peroxisome proliferator-activated receptor-gamma in macrophage biology and atherosclerosis.* J Endocrinol, 2001. **169**(3): p. 461-4.

199. Chinetti, G., et al., *PPAR-alpha and PPAR-gamma activators induce cholesterol removal from human macrophage foam cells through stimulation of the ABCA1 pathway.* Nat Med, 2001. **7**(1): p. 53-8.

200. Chawla, A., et al., *A PPARγ-LXR-ABCA1 Pathway in Macrophages Is Involved in Cholesterol Efflux and Atherogenesis.* Molecular Cell, 2001. **7**(1): p. 161-171.

201. Ricote, M., et al., *The peroxisome proliferator-activated receptor-gamma is a negative regulator of macrophage activation.* Nature, 1998. **391**(6662): p. 79-82.

202. Jiang, C., A.T. Ting, and B. Seed, *PPAR-gamma agonists inhibit production of monocyte inflammatory cytokines.* Nature, 1998. **391**(6662): p. 82-6.

203. Delerive, P., et al., *Peroxisome proliferator-activated receptor alpha negatively regulates the vascular inflammatory gene response by negative cross-talk with transcription factors NF-kappaB and AP-1.* J Biol Chem, 1999. **274**(45): p. 32048-54.

204. Szatmari, I., et al., *PPARgamma controls CD1d expression by turning on retinoic acid synthesis in developing human dendritic cells.* J Exp Med, 2006. **203**(10): p. 2351-62.

205. Szanto, A., et al., *STAT6 transcription factor is a facilitator of the nuclear receptor PPARgamma-regulated gene expression in macrophages and dendritic cells.* Immunity, 2010. **33**(5): p. 699-712.

206. Nobs, S.P., et al., *PPARgamma in dendritic cells and T cells drives pathogenic type-2 effector responses in lung inflammation.* J Exp Med, 2017. **214**(10): p. 3015-3035.

207. Lee, S.H., P.M. Starkey, and S. Gordon, *Quantitative analysis of total macrophage content in adult mouse tissues. Immunochemical studies with monoclonal antibody F4/80.* J Exp Med, 1985. **161**(3): p. 475-89.

208. Hume, D.A. and S. Gordon, *Mononuclear phagocyte system of the mouse defined by immunohistochemical localization of antigen F4/80. Identification of resident macrophages in renal medullary and cortical interstitium and the juxtaglomerular complex.* J Exp Med, 1983. **157**(5): p. 1704-9.

209. Hume, D.A., et al., *The mononuclear phagocyte system of the mouse defined by immunohistochemical localization of antigen F4/80. Relationship between macrophages, Langerhans cells, reticular cells, and dendritic cells in lymphoid and hematopoietic organs.* J Exp Med, 1983. **158**(5): p. 1522-36.

210. Gordon, S., *The macrophage: past, present and future.* Eur J Immunol, 2007. **37 Suppl 1**: p. S9-17.

211. Murray, P.J. and T.A. Wynn, *Protective and pathogenic functions of macrophage subsets.* Nat Rev Immunol, 2011. **11**(11): p. 723-37.

212. Parkhurst, C.N., et al., *Microglia promote learning-dependent synapse formation through brain-derived neurotrophic factor.* Cell, 2013. **155**(7): p. 1596-609.

213. Chow, A., et al., *Bone marrow CD169+ macrophages promote the retention of hematopoietic stem and progenitor cells in the mesenchymal stem cell niche.* J Exp Med, 2011. **208**(2): p. 261-71.

214. Jakubzick, C., et al., *Minimal differentiation of classical monocytes as they survey steady-state tissues and transport antigen to lymph nodes.* Immunity, 2013. **39**(3): p. 599-610.

215. Glass, C.K. and G. Natoli, *Molecular control of activation and priming in macrophages.* Nat Immunol, 2016. **17**(1): p. 26-33.

216. Lavin, Y., et al., *Regulation of macrophage development and function in peripheral tissues.* Nat Rev Immunol, 2015. **15**(12): p. 731-44.

217. Butovsky, O., et al., *Identification of a unique TGF-beta-dependent molecular and functional signature in microglia.* Nat Neurosci, 2014. **17**(1): p. 131-43.

218. Takayanagi, H., et al., *Induction and activation of the transcription factor NFATc1 (NFAT2) integrate RANKL signaling in terminal differentiation of osteoclasts.* Dev Cell, 2002. **3**(6): p. 889-901.

219. Kurotaki, D., T. Uede, and T. Tamura, *Functions and development of red pulp macrophages.* Microbiol Immunol, 2015. **59**(2): p. 55-62.

220. Aziz, M.H., et al., *The Upregulation of Integrin alphaDbeta2 (CD11d/CD18) on Inflammatory Macrophages Promotes Macrophage Retention in Vascular Lesions and Development of Atherosclerosis.* J Immunol, 2017. **198**(12): p. 4855-4867.

221. Clausen, B.E., et al., *Conditional gene targeting in macrophages and granulocytes using LysMcre mice.* Transgenic Res, 1999. **8**(4): p. 265-77.

222. Caton, M.L., M.R. Smith-Raska, and B. Reizis, *Notch-RBP-J signaling controls the homeostasis of CD8- dendritic cells in the spleen.* J Exp Med, 2007. **204**(7): p. 1653-64.

223. de Boer, J., et al., *Transgenic mice with hematopoietic and lymphoid specific expression of Cre.* Eur J Immunol, 2003. **33**(2): p. 314-25.

224. Ruzankina, Y., et al., *Deletion of the developmentally essential gene ATR in adult mice leads to age-related phenotypes and stem cell loss.* Cell Stem Cell, 2007. **1**(1): p. 113-26.

225. Luche, H., et al., *Faithful activation of an extra-bright red fluorescent protein in "knock-in" Cre-reporter mice ideally suited for lineage tracing studies.* Eur J Immunol, 2007. **37**(1): p. 43-53.

226. Picelli, S., et al., *Full-length RNA-seq from single cells using Smart-seq2.* Nat Protoc, 2014. **9**(1): p. 171-81.

227. Hatakeyama, M., et al., *SUSHI: an exquisite recipe for fully documented, reproducible and reusable NGS data analysis.* BMC Bioinformatics, 2016. **17**(1): p. 228.

228. Dobin, A., et al., *STAR: ultrafast universal RNA-seq aligner.* Bioinformatics, 2013. **29**(1): p. 15-21.

229. Liao, Y., G.K. Smyth, and W. Shi, *The Subread aligner: fast, accurate and scalable read mapping by seed-and-vote.* Nucleic Acids Res, 2013. **41**(10): p. e108.

230. Robinson, M.D., D.J. McCarthy, and G.K. Smyth, *edgeR: a Bioconductor package for differential expression analysis of digital gene expression data.* Bioinformatics, 2010. **26**(1): p. 139-40.

231. Subramanian, A., et al., *Gene set enrichment analysis: a knowledge-based approach for interpreting genome-wide expression profiles.* Proc Natl Acad Sci U S A, 2005. **102**(43): p. 15545-50.

232. Mootha, V.K., et al., *PGC-1alpha-responsive genes involved in oxidative phosphorylation are coordinately downregulated in human diabetes.* Nat Genet, 2003. **34**(3): p. 267-73.

233. Shannon, P., et al., *Cytoscape: a software environment for integrated models of biomolecular interaction networks.* Genome Res, 2003. **13**(11): p. 2498-504.

234. Merico, D., et al., *Enrichment map: a network-based method for gene-set enrichment visualization and interpretation.* PLoS One, 2010. **5**(11): p. e13984.

235. Kierdorf, K., et al., *Microglia emerge from erythromyeloid precursors via Pu.1- and Irf8-dependent pathways.* Nat Neurosci, 2013. **16**(3): p. 273-80.

236. Barak, Y., et al., *PPARγ Is Required for Placental, Cardiac, and Adipose Tissue Development.* Molecular Cell, 1999. **4**(4): p. 585-595.

237. Siersbaek, R., R. Nielsen, and S. Mandrup, *PPARgamma in adipocyte differentiation and metabolism--novel insights from genome-wide studies.* FEBS Lett, 2010. **584**(15): p. 3242-9.

238. Gautier, E.L., et al., *Systemic analysis of PPARgamma in mouse macrophage populations reveals marked diversity in expression with critical roles in resolution of inflammation and airway immunity.* J Immunol, 2012. **189**(5): p. 2614-24.

239. Lefterova, M.I., et al., *Cell-specific determinants of peroxisome proliferator-activated receptor gamma function in adipocytes and macrophages.* Mol Cell Biol, 2010. **30**(9): p. 2078-89.

240. Menendez-Gutierrez, M.P., et al., *Retinoid X receptors orchestrate osteoclast differentiation and postnatal bone remodeling.* J Clin Invest, 2015. **125**(2): p. 809-23.

241. Yakubenko, V.P., et al., *The role of integrin alpha D beta2 (CD11d/CD18) in monocyte/macrophage migration.* Exp Cell Res, 2008. **314**(14): p. 2569-78.

242. Lee, C.Z.W., T. Kozaki, and F. Ginhoux, *Studying tissue macrophages in vitro: are iPSC-derived cells the answer?* Nat Rev Immunol, 2018. **18**(11): p. 716-725.

243. Takata, K., et al., *Induced-Pluripotent-Stem-Cell-Derived Primitive Macrophages Provide a Platform for Modeling Tissue-Resident Macrophage Differentiation and Function.* Immunity, 2017. **47**(1): p. 183-198 e6.

244. Seymour, J.F. and J.J. Presneill, *Pulmonary alveolar proteinosis: progress in the first 44 years.* Am J Respir Crit Care Med, 2002. **166**(2): p. 215-35.

245. Trapnell, B.C., J.A. Whitsett, and K. Nakata, *Pulmonary alveolar proteinosis.* N Engl J Med, 2003. **349**(26): p. 2527-39.

246. Mucci, A., et al., *Murine iPSC-Derived Macrophages as a Tool for Disease Modeling of Hereditary Pulmonary Alveolar Proteinosis due to Csf2rb Deficiency.* Stem Cell Reports, 2016. **7**(2): p. 292-305.

247. Mucci, A., et al., *iPSC-Derived Macrophages Effectively Treat Pulmonary Alveolar Proteinosis in Csf2rb-Deficient Mice.* Stem Cell Reports, 2018. **11**(3): p. 696-710.

248. Suzuki, T., et al., *Pulmonary macrophage transplantation therapy.* Nature, 2014. **514**(7523): p. 450-4.

249. Happle, C., et al., *Pulmonary transplantation of macrophage progenitors as effective and long-lasting therapy for hereditary pulmonary alveolar proteinosis.* Sci Transl Med, 2014. **6**(250): p. 250ra113.

250. Fejer, G., et al., *Nontransformed, GM-CSF-dependent macrophage lines are a unique model to study tissue macrophage functions.* Proc Natl Acad Sci U S A, 2013. **110**(24): p. E2191-8.

251. Schneider, C., et al., *Frontline Science: Coincidental null mutation of Csf2ralpha in a colony of PI3Kgamma-/- mice causes alveolar macrophage deficiency and fatal respiratory viral infection.* J Leukoc Biol, 2017. **101**(2): p. 367-376.

252. Bachmann, M.F., B. Ecabert, and M. Kopf, *Influenza virus: a novel method to assess viral and neutralizing antibody titers in vitro.* J Immunol Methods, 1999. **225**(1-2): p. 105-11.

253. Ramkumar, C., R.M. Gerstein, and H. Zhang, *Serial Transplantation of Bone Marrow to Test Self-renewal Capacity of Hematopoietic Stem Cells In Vivo*, in *Stem Cells and Aging: Methods and Protocols*, K. Turksen, Editor. 2013, Humana Press: Totowa, NJ. p. 17-24.

254. Lachmann, N., et al., *Gene correction of human induced pluripotent stem cells repairs the cellular phenotype in pulmonary alveolar proteinosis.* Am J Respir Crit Care Med, 2014. **189**(2): p. 167-82.

255. Varol, C., A. Mildner, and S. Jung, *Macrophages: development and tissue specialization.* Annual review of immunology, 2015. **33**: p. 643-75.

256. Buchrieser, J., W. James, and M.D. Moore, *Human Induced Pluripotent Stem Cell-Derived Macrophages Share Ontogeny with MYB-Independent Tissue-Resident Macrophages.* Stem Cell Reports, 2017. **8**(2): p. 334-345.

257. Lee, S., et al., *Macrophage-based cell therapies: The long and winding road.* J Control Release, 2016. **240**: p. 527-540.

258. Byrne, A.J., T.M. Maher, and C.M. Lloyd, *Pulmonary Macrophages: A New Therapeutic Pathway in Fibrosing Lung Disease?* Trends Mol Med, 2016. **22**(4): p. 303-316.

259. Subach, F.V., et al., *Monomeric fluorescent timers that change color from blue to red report on cellular trafficking.* Nat Chem Biol, 2009. **5**(2): p. 118-26.

260. Bending, D., et al., *A timer for analyzing temporally dynamic changes in transcription during differentiation in vivo.* J Cell Biol, 2018. **217**(8): p. 2931-2950.

261. Sauvageau, G., et al., *Overexpression of HOXB4 in hematopoietic cells causes the selective expansion of more primitive populations in vitro and in vivo.* Genes Dev, 1995. **9**(14): p. 1753-65.

262. Antonchuk, J., G. Sauvageau, and R.K. Humphries, *HOXB4-induced expansion of adult hematopoietic stem cells ex vivo.* Cell, 2002. **109**(1): p. 39-45.

8 Appendix

8.1 Abbreviations

13-HODE - 13-hydroxyoctadecadienoic acid

15-dPGJ2 - 15-deoxy-D12,14-prostaglandin J2

5-FU - 5-fluorouracil

9-HODE - 9-hydroxyoctadecadienoic acid

ABC - ATP-binding cassette transporter

AE2C - alveolar epithelial cell type 2

AF - activation function

AGM - aorta, gonads and mesonephros

ALR - AIM2-like receptor

AM - alveolar macrophage

aP2 - adipocyte protein 2

APC - antigen-presenting cell

AQP7 - glycerol transporter aquaporin 7

Bach1 - BTB Domain and CNC homolog 1

Bach2 - BTB Domain and CNC homolog 2

BAL - bronchoalveolar lavage

BAT - brown adipose tissue

BM - bone marrow

BMC - bone marrow cells

BMEIM - bone marrow erythroid island macrophage

BMM - bone marrow macrophages

C/EBP - CCAAT/enhancer-binding protein

CBP - cycling-AMP responsive element binding protein (CREB)-binding protein

CCR - CC chemokine receptor

cDC - classical DC

Cdk - cyclin-dependent kinase

CDP - common DC precursor

ChIP-seq - chromatin immunoprecipitation sequencing

CLR - C-type lectin receptor

cMOP - common monocyte progenitor

CNS - central nervous system

CO - carbon monoxide

COX - cyclooxygenase

CRISPR/Cas9 - clustered regularly interspaced short palindromic repeats/CRISPR associated protein 9

Csf1r - colony-stimulating factor 1 receptor

CSF2-cFLiMo - CSF2-dependent cultured fetal liver monocyte

Csf2ra - colony-stimulating factor 1 receptor alpha subunit

Csf2rb - colony-stimulating factor 1 receptor beta subunit

DAMP - damage-associated molecular pattern

DBD - DNA-binding domain

DC - dendritic cell

DN - double negative

DNA - deoxyribonucleic acid

DP - double positive

EBI - erythroblastic island

EMP - erythro-myeloid precursor

ER - endoplasmic reticulum

FATP - fatty acid transport protein

FDR - false discovery rate

FFA - free fatty acid

FLiMo - fetal liver monocyte

Flt3 - fms-like tyrosine kinase 3

Fpn1 - ferroportin-1

FT - fluorescent timer

Fth - ferritin heavy chain

GFP - green fluorescent protein

Glut4 - glucose transporter type 4

GM-CSF - granulocyte-macrophage colony stimulating factor

GO - gene ontology

gRNA - guide RNA

GSEA - gene set enrichment analysis

HAT - histone acetyltransferase

HDAC - histone deacetylase

herPAP - hereditary pulmonary alveolar proteinosis

HO-1; Hmox1 - heme oxygenase 1

HoxB4 - homeobox B4

HSC - hematopoietic stem cell

i.n. - intranasal

i.p. - intraperitoneal

i.t. - intratracheal

i.v. - intravenous

IL - interleukin

IM - interstitial macrophage

iMac - induced pluripotent stem cell-derived macrophages

IRES - internal ribosome entry site

IRF4 - interferon regulatory factor 4

IRF8 - interferon regulatory factor 8

KC - Kupffer cells

KO - knockout

LBD - ligand-binding domain

LDL - low-density lipoprotein

LDTF - lineage-determining transcription factor

LN - lymph node

LP - lymphoid precursor

LPL - lipoprotein lipase

LPM - large peritoneal macrophage

LPS - lipopolysaccharide

LRR - leucine-rich repeat

LXRα - liver X receptor

M-CSF - macrophage colony-stimulating factor

MAPK - mitogen-activated protein kinase

MDP - monocyte, macrophage, and DC precursor

MFGE8 - milk fat globule-epidermal growth factor 8

MHC - major histocompatibility complex

MMM - marginal metallophilic macrophage

moDC - monocyte-derived DC

MP - myeloid precursor

MPS - mononuclear phagocyte system

mRNA - messenger RNA

MZ - marginal zone

MZM - marginal zone macrophage

NCoR - nuclear receptor corepressor

NFκB - nuclear factor kappa-light-chain-enhancer of activated B cells

NK - natural killer cell

NLR - NOD-like receptor

NOX2 - NADPH oxidase 2

Nrf2 - nuclear factor E2-related factor-2

NTD - N-terminal domain

PALS - periarteriolar lymphoid sheath

PAMP - pathogen-associated molecular pattern

PAP - pulmonary alveolar proteinosis

PCR - polymerase chain reaction

pDC - plasmacytoid DC

PEPCK - phosphoenolpyruvate carboxykinase

PGC-1α - PPARg coactivator 1

pMo-FLi - primary fetal liver monocyte

PPARγ - peroxisome proliferator-activated receptor gamma

PPRE - PPAR-responsive element

PRDM16 - PR/SET Domain 16

PRR - pattern-recognition receptor

PU.1 - E26 transformation specific (Ets) family transcription factor

RA - retinoic acid

RANKL - receptor activator of NFκB ligand

RARβ - retinoic acid receptor beta

RBC - red blood cell

RLR - RIG-I-like receptor

RNA - ribonucleic acid

RNAseq - RNA sequencing

RNS - reactive nitric species

ROS - reactive oxygen species

RPM - red pulp macrophage

Runx1 - runt-related transcription factor 1

RV - retrovirus

RXR - retinoid X receptor

SDTF - signal-driven transcription factor

Siglec-1 - sialic-acid-binding immunoglobulin-like lectin 1

SIRPα - signal-regulatory protein alpha

SMRT - silencing mediator of retinoid and thyroid hormone receptor

SOCS - suppressor of cytokine-signaling

SP - surfactant protein

Spi-C - Spi-1/PU.1-related transcription factor

SPM - small peritoneal macrophage

SRC - steroid receptor coactivator

STAT6 - transducer and activator of transcription 6

TBP - TATA-box-binding protein

TGFβ - transforming growth factor beta

TGFβR - transforming growth factor beta receptor

TGM - tangible body macrophage

TIR - Toll/IL-1 receptor

TLR - Toll-like receptor

TM - transmembrane

TNFα - tumor necrosis factor alpha

TSS - transcription start site

TZD - thiazolidinedione

WAT - white adipose tissue

WS - WSXWS motif

WT - wild-type

YFP - yellow fluorescent protein

YS - yolk sac

8.2 Acknowledgements

I would like to thank following people:

Manfred Kopf for allowing me to be a part of his team and work on demanding projects which helped me develop my character and skills. For constant support and always open door for discussion.

Florent Ginhoux and **Gerald Schwank**, for their time, constructive criticism during my committee meetings, and for agreeing to be co-supervisors of my PhD thesis.

All the current lab members:

Lea Pohlmeier for being there always for me, even if I didn't want to share my troubles. For becoming a good friend and making the next 'last heat-map' every time I asked for it and for substantial contribution to this thesis by writing "Zusammenfassung".

Fengqi Li for extremely efficient team-work, many discussions (not only about the projects), for her great effort to make the cFLiMo story ready before my thesis submission.

Christoph Schneider and **Peter Nielsen**, for great engagement in my projects, support and help.

Jan Kisielow for all trouble-shooting we did together in my CRISPR project, for guidance and constant curiosity.

Gosia Kisielow for answering all FACS-related questions and help during sorts but also for making my start in a new country much easier. The whole **Kisielow family** for my beloved orange sofa, Christmas cookie baking, and time spent together.

Jonathan Muri for sharing his protocols with me, being a great SOLA team organizer and a friend also outside the lab.

Irini Vgenopoulou for facilitating our lab work in any possible way, for her contagious cheerfulness and positive attitude, for all support I have received and meetings after hours.

Patrizia Diethelm for guarding supplies in module 3 so efficiently, that we never had to worry about it, for being a great contact person to the EPIC team and lab closest neighbor (although back turned).

Esther Rosenwald for keeping everything in order and correct place, organizing many lab events and Christmas dinners, for expertise in cloning and retroviral production.

Federica Piattini for being extremely independent student, multi-tasking and hard-working.

Luigi Tortola for always making jokes, which only chosen people can laugh at, for scientific curiosity and knowledge, the involvement and advice concerning my projects.

Sophie Braverman for enriching our team, taking care of gifts for round birthdays and other significant occasions, sharing sesame paste and great hummus recipes.

Qian Feng for her optimism, kindness and love to music.

Franziska Ampenberger for help with experiments, sharing her knowledge on mouse techniques and evening chats.

Anette Schütz and **Hong-Ying Teh** for help with sorts and many nice chats about travels, plants and life in general.

Franz Obermair for cool sense of humor and offering me coffee during my first visit in the lab.

Helen Thut Emiko and **Robin Wuigk** for doing great job as master students, so their supervisors can really trust them and use their help.

All the former lab members, in particular:

Mareike Schmid (Bindszus) for constant support, endless creativity, similar taste not only in shoes and clothes but also backpacks, ceramics, music, outdoor and more. For becoming a great soulmate and hopefully staying a life-long friend.

Sam Nobs for an amazing attitude towards life, modesty, his excitement and constant willingness to discuss projects and search for solutions when I got stuck.

Sebastian Heer for great cakes and hiking trips.

Merve Kayhan for being a really easy-going person and not giving up.

I would like to thank also mouse care takers, especially **Theresia Heuberger** who helped me practice my German and encouraged to speak it, also **Aretussa Apladas**, **Dominique Flota**, **André Mund** and **Paul Hauswirth**.

Thanks to **Rolf Huber**, **Claudia Stucki**, **Giorgio Giordano** and **Ruth Henneberger** for infrastructural, IT and administrative support.

My friends, especially:

Maxime Bodak for always willing to help even if he could get into troubles. For introducing me to IMHS network and many many shared bottles of Gewürztraminer.

Daniel Spies for listening at anytime and anywhere, for being an artistic soul encapsulated in IT skin, enjoying photo exhibits, hiking and wine.

All members of **Polish Alliance** established once by an American, for making the time of PhD a time of great fun.

Jagoda Lasota, **Malgorzata Osiecka** and **Paulina Rybakowska** for being great friends, regardless of the distance.

My family:

Kuba Jagielski for enormous support from the very first moment. I cannot imagine my life without you.

Marzena Kubiczek-Jagielska and **Janusz Jagielski** for coming all the way to participate and support me during the defense day and for all the love I have received.

My sister, **Kinga** for teaching me how to be tough and not give up easily.

My parents, **Bozena** and **Jozef**, for always believing in me and letting me develop on my own terms.